27
3/22/78

ORNL/TM-6174

Actinide Partitioning and Transmutation Program Progress Report for Period July 1 to September 30, 1977

D. W. Tedder
J. O. Blomeke

MASTER

OAK RIDGE NATIONAL LABORATORY
OPERATED BY UNION CARBIDE CORPORATION · FOR THE DEPARTMENT OF ENERGY

DISTRIBUTION OF THIS DOCUMENT IS UNLIMITED

DISCLAIMER

This report was prepared as an account of work sponsored by an agency of the United States Government. Neither the United States Government nor any agency Thereof, nor any of their employees, makes any warranty, express or implied, or assumes any legal liability or responsibility for the accuracy, completeness, or usefulness of any information, apparatus, product, or process disclosed, or represents that its use would not infringe privately owned rights. Reference herein to any specific commercial product, process, or service by trade name, trademark, manufacturer, or otherwise does not necessarily constitute or imply its endorsement, recommendation, or favoring by the United States Government or any agency thereof. The views and opinions of authors expressed herein do not necessarily state or reflect those of the United States Government or any agency thereof.

DISCLAIMER

Portions of this document may be illegible in electronic image products. Images are produced from the best available original document.

Printed in the United States of America. Available from
National Technical Information Service
U.S. Department of Commerce
5285 Port Royal Road, Springfield, Virginia 22161
Price: Printed Copy $9.25; Microfiche $3.00

This report was prepared as an account of work sponsored by an agency of the United States Government. Neither the United States Government nor any agency thereof, nor any of their employees, contractors, subcontractors, or their employees, makes any warranty, express or implied, nor assumes any legal liability or responsibility for any third party's use or the results of such use of any information, apparatus, product or process disclosed in this report, nor represents that its use by such third party would not infringe privately owned rights.

ORNL/TM-6174

Contract No. W-7405-eng-26

CHEMICAL TECHNOLOGY DIVISION

ACTINIDE PARTITIONING AND TRANSMUTATION PROGRAM

PROGRESS REPORT FOR PERIOD JULY 1 TO SEPTEMBER 30, 1977

Compiled by:

D. W. Tedder

J. O. Blomeke

NOTICE

This report was prepared as an account of work sponsored by the United States Government. Neither the United States nor the United States Department of Energy, nor any of their employees, nor any of their contractors, subcontractors, or their employees, makes any warranty, express or implied, or assumes any legal liability or responsibility for the accuracy, completeness or usefulness of any information, apparatus, product or process disclosed, or represents that its use would not infringe privately owned rights.

Date Published: February 1978

NOTICE This document contains information of a preliminary nature. It is subject to revision or correction and therefore does not represent a final report.

OAK RIDGE NATIONAL LABORATORY
Oak Ridge, Tennessee 37830
operated by
UNION CARBIDE CORPORATION
for the
DEPARTMENT OF ENERGY

DISTRIBUTION OF THIS DOCUMENT IS UNLIMITED

THIS PAGE

WAS INTENTIONALLY

LEFT BLANK

CONTENTS

FOREWORD

This is the third in a series of progress reports to be issued on the Actinide Partitioning and Transmutation Program, which is a multi-site effort coordinated at the Oak Ridge National Laboratory. Previous reports in this series were issued as ORNL/TM-5888 and ORNL/TM-6056. The overall program objective is to evaluate the feasibility and incentives for partitioning (separating) the long-lived biologically significant isotopes from fuel cycle wastes and transmuting (burning) them to shorter-lived or stable isotopes in power reactors.

During FY 1977 and 1978, the principal emphasis will be on the experimental evaluation of partitioning actinides, followed by their recovery in forms suitable for fabrication into transmutation targets. Detailed computer analyses will be undertaken to determine the effects on reactor and fuel cycle operations of recycling the partitioned actinides and to further verify the feasibility of transmutation itself. In FY 1979 the major effort will be directed toward a detailed assessment of the costs, risks, and benefits associated with this concept. The program is expected to produce: (1) realistic reprocessing and refabrication flowsheets which have been at least partly verified by experimental work, (2) several realistic transmutation schemes based on sophisticated reactor physics calculations, (3) an evaluation of partitioning and transmutation impacts on all phases of the nuclear fuel cycle, (4) a meaningful risk-cost-benefit analysis, and (5) a program plan for future development and demonstration requirements for eventual implementation in commercial operations. This analysis should constitute a reasonably firm technical basis for determining whether partitioning-transmutation represents a viable waste management alternative for managing long-lived waste nuclides that are generated by a nuclear power economy.

The program consists of 16 major tasks. This report summarizes the work done on those that were active during the period July 1-September 30, 1977.

THIS PAGE

WAS INTENTIONALLY

LEFT BLANK

SUMMARY

In PUREX PROCESS MODIFICATIONS, two cold runs with mixer-settlers were made on the extraction and stripping of ruthenium and zirconium without the presence of uranium. Two percent of the ruthenium and 7% of the zirconium were extracted using 8 extraction and 8 scrubbing stages. After 16 stages of stripping with 0.1 M HNO_3, about 1% of the ruthenium and 4% of the zirconium remained in the organic phase. The use of 0.1 M nitrite in the 3 M HNO_3 reduced the extent of ruthenium extraction from 2% to 1%. The poor stripping behavior of plutonium reported in ORNL/TM-6056 last quarter in batch countercurrent tests apparently resulted from radiolytically generated dibutyl phosphoric acid in the aged (>2-day) organic feeds.

Efforts in ACTINIDE RECOVERY FROM SOLIDS this quarter were directed toward the determination of dissolution parameters in various reagents for ^{241}Am and ^{239}Pu oxide mixtures, ^{233}U oxide, ^{237}Np oxide, ^{244}Cm oxide, ^{232}Th oxide, and PuO_2. The reagents used were various concentrations of: HNO_3-HF-H_2SO_4, HNO_3-$(NH_4)_2Ce(NO_3)_6$, HNO_3-HF, and HNO_3. Tests were conducted using both simulated contaminated HEPA filter media and actual glove-box filter media from spent filters. The maximum decontamination factor achieved was 833 using a six-stage dissolution process. Fusion tests were also completed using PuO_2 and Na_2CO_3 at various elevated temperatures.

Studies in AMERICIUM-CURIUM RECOVERY WITH OPIX, TALSPEAK, and CEC focused on the feasibility of forming oxalate precipitates in continuous systems, the effects of zirconium on Talspeak, and methods for removing solvent degradation products of the Talspeak system. In oxalate precipitation, it appears that the oxalate yields increase with the residence time in a stirred precipitator; by using two stirred tank reactors in series, product yields of 90 wt % of the feed were obtained. Results of the Talspeak studies showed that the rare earths could be effectively extracted in the first cycle; no entrainment in the product streams was observed when zirconium concentrations of 10^{-4} M or less were present in the feed, but interfacial crud formed in the first stage of the stripping bank. The reference flowsheet was changed to show 0.4 M HDEHP where flow ratios of extractant:feed:scrub of 2:1:1 could be employed. Scoping tests showed

that Dowex-1 anion exchange resin was effective in removing H_2MEHP from ethylene glycol scrub liquid, thus permitting its recycle.

In studies of AMERICIUM-CURIUM RECOVERY USING BIDENTATE EXTRACTANTS, additional distribution coefficients for actinides and other key elements between reduced synthetic LWR waste solution and 30% dihexyl-N,N-diethylcarbamylmethylene phosphonate (DHDECMP) in diisopropylbenzene (DIPB) were measured. Distribution coefficients for extraction, scrub, and strip contacts for americium between cadmium-modified synthetic HAW and 30% DHDECMP in DIPB were also obtained. Distribution coefficients for Cf(III) between 30% DHDECMP in DIPB and various concentrations of nitric acid have been determined. Diluent scoping studies indicate that kerosene mixtures with p-DIPB are slightly better diluents for DHDECMP compared with technical-grade DIPB. Further efforts to obtain pure (>99%) DHDECMP have been made using preparative liquid chromatography.

Studies in AMERICIUM-CURIUM RECOVERY USING INORGANIC ION EXCHANGE MEDIA to determine the pH dependence of lanthanide ion affinity for niobate, titanate, and zirconate ion exchange materials have been completed. The affinities of europium, gadolinium, and promethium (in addition to lanthanum as previously reported) for the inorganic ion exchangers show dramatic increases with increases in pH. Lanthanides deposited on inorganic ion exchangers at relatively high pH may be desorbed by reducing the pH. The affinity of curium for niobate ion exchangers was found to be greater than that of the lanthanides studied, suggesting the possibility of an actinide-lanthanide ion exchange separation by pH control. The large affinities that these inorganic ion exchangers display for lanthanides and, presumably, actinides suggest their use in scavenging radionuclides from low-level waste streams.

A modified flowsheet for the extraction of uranium, neptunium, plutonium, americium, and curium from high-level liquid waste is presented under RECOVERY ALTERNATIVES APPLICABLE TO WASTE STREAMS. The process involves two basic parts: first, the extractions of uranium, neptunium, plutonium, americium, and curium, together with fission product zirconium, niobium, molybdenum, yttrium, and rare earths, using 0.5 M dihexoxyethyl phosphoric acid (HDHoEP) in diethylbenzene (DEB) followed by stripping of americium,

curium, and rare earths with 6 M HNO_3, stripping of neptunium, plutonium, zirconium, niobium, molybdenum, and iron with oxalate, and stripping of uranium, yttrium, and zirconium with 8 M H_3PO_4; and second, the purification of neptunium and plutonium from the zirconium, niobium, molybdenum, iron, and oxalate using 0.25 M tricaprylmethylammonium nitrate ($TCMA \cdot NO_3$) in DEB. The process has been studied using synthetic exhaustively-extracted waste. Data are presented for batch countercurrent extraction studies. These data were used to calculate the number of stages required for the desired separation.

Evaluation of methods for measuring actinides from incinerator ash is continuing in ACTINIDE RECOVERY FROM COMBUSTIBLE WASTE. Two promising recovery methods are: (1) reaction with cerium(IV) in HNO_3 to solubilize carbon and actinide oxides, and (2) fusion with carbonate-nitrate mixtures. Silica proved to be a problem; if dissolved, it interferes with subsequent actinide recovery by forming polysilicic acid upon acidification. If not solubilized, silica-encapsulated actinide oxides are not contacted by the dissolvent. Pretreatment of ash by refluxing with $\geq$6 M NaOH appears to remove silica, simplifying subsequent recovery steps.

A preliminary evaluation of methods for treatment of salt waste and waste waters was completed in ACTINIDE RECOVERY AND RECYCLE PREPARATION FOR WASTE STREAMS. These studies indicated that bidentate systems can remove 99.98% of the plutonium and 99% of the americium from salt wastes. They also suggested that a combination of Amberlite XAD-4 (nonionic resin for organics) and Amberlite IRA-900 (strong base resin for anions) would be an effective preparatory step in the recycle of a waste-water stream.

The study of the RADIATION EFFECTS on ion exchange materials is near completion, and the results will be published as a Brookhaven National Laboratory report.

The FUEL AND TARGET FABRICATION STUDIES were not active during this period.

Scoping studies on LMFBR TRANSMUTATION were terminated at the end of this quarter, and a final report of this work will be issued in the near future.

In THERMAL REACTOR TRANSMUTATION STUDIES, waste actinides from an LWR lattice containing mixed uranium-plutonium assemblies were recycled in separate target assemblies. When an actinide concentration was chosen such that the specific power of the target was equal to that of the regular fuel assemblies, the transmutation rate of the waste actinides was about 10% per fuel cycle. Waste actinides from plutonium-enriched fuel contained about eight times the americium and 20 times the curium as actinides from regular uranium-enriched LWR fuel.

The FUEL CYCLE IMPACT STUDIES were not active during this quarter.

Planning activities were initiated for the RISK-COST/BENEFIT ANALYSIS subtask to better define the important considerations that will be involved in performing this analysis. The approach taken is to first identify each individual contribution to the risk-cost/benefit analysis. Subsequently, the comparison of these individual contributions leading to a determination of the incentives for partitioning is discussed. Finally, each of the individual contributions to the overall risk-cost/benefit analysis is assigned a priority based on its amenability to calculation, importance to the overall analysis, and compatibility with the overall analysis.

The ECONOMIC ANALYSIS of this concept was not active during this quarter.

Under ANALYSIS, COORDINATION, AND EVALUATION, the development of a generalized solvent extraction code, GENEX, proceeded. The model can consider different chemical mixtures and stoichiometric relationships between the chemical species without major revisions in the code itself.

1. PUREX PROCESS MODIFICATIONS

W. D. Bond, F. A. Kappelmann, and F. M. Scheitlin
(Oak Ridge National Laboratory)

This task focuses on modifications to the Purex process which should result in higher recoveries of uranium, neptunium, and plutonium. Modifications to the process operations are considered, as well as alternatives in cleanup systems which result in smaller waste volumes and actinide losses.

1.1 Introduction

Experiments are being carried out on the Purex process relative to the countercurrent extraction and stripping of actinides using both continuous mixer-settlers and batch equipment. The purpose of these experiments is to determine the effects on actinide losses by either including additional stages of extraction and stripping or using an additional Purex cycle to remove actinides from the high-level waste stream. The effects of the increased extraction of the zirconium and ruthenium fission products are also being evaluated. It is not known whether the increased radiation damage caused by the additional extraction stages (or cycles) will result in interfacial precipitates and cruds. Zirconium compounds formed with degradation products are reported to be of limited solubility in both the organic and the aqueous phases and have been observed to impair operability when high-burnup fuels are processed.

All laboratory work to date has been carried out using simulated, nonradioactive fuel dissolver and high-level waste solutions as feeds. Plutonium work is performed at the tracer level.

1.2 Studies Using Mixer-Settlers

1.2.1 Experimental

The equipment used in these studies consists of two 16-stage stainless steel mixer-settler banks of Belgian design; one bank is

for extraction-scrubbing and the other for stripping. All experimental runs were conducted at 43°C. Both the virgin and the recycled extractants (30% TBP-70% n-dodecane) were purified by scrubbing with 0.5 M sodium carbonate and washed three times with 0.01 M HNO_3 to remove the entrained sodium carbonate.

Basically, the reference Purex flowsheet (Fig. 1.1) was used for the ruthenium and the zirconium experimental runs. Uranium was absent in the feed solution for each of the runs.

1.2.2 Ruthenium behavior

Last quarter we reported[1] that attempts to measure distribution coefficients for ruthenium were unsuccessful due to the low levels of ruthenium in the presence of appreciable amounts of uranium. Therefore, during this report period, a run, R-8, was made using a feed solution containing ruthenium at a concentration of 1 g/liter but no uranium. Standard Purex flow conditions were used as shown in Table 1.1; note that the feed and scrub solution contained 0.1 M $NaNO_2$. The behavior of ruthenium exiting in the end streams during the run (see Fig. 1.2) suggests that the system was at steady state after 1.5 to 2.5 hr.

Table 1.1. Flowsheet conditions for run R-8

Process stream	Flow rate (liters/hr)	Composition
Feed	0.5	0.98 g Ru/liter; 0.1 M $NaNO_2$; 2.5 M HNO_3
Solvent	1.75	30% TBP-n-dodecane
Scrub	0.2	0.1 M $NaNO_2$; 3 M HNO_3
Strip	2.0	0.1 M HNO_3

Measurements of the distribution coefficients for ruthenium in each stage of both mixer-settler banks were made after withdrawing samples at the completion of the run. The aqueous concentrations and

ORNL DWG 77-1105

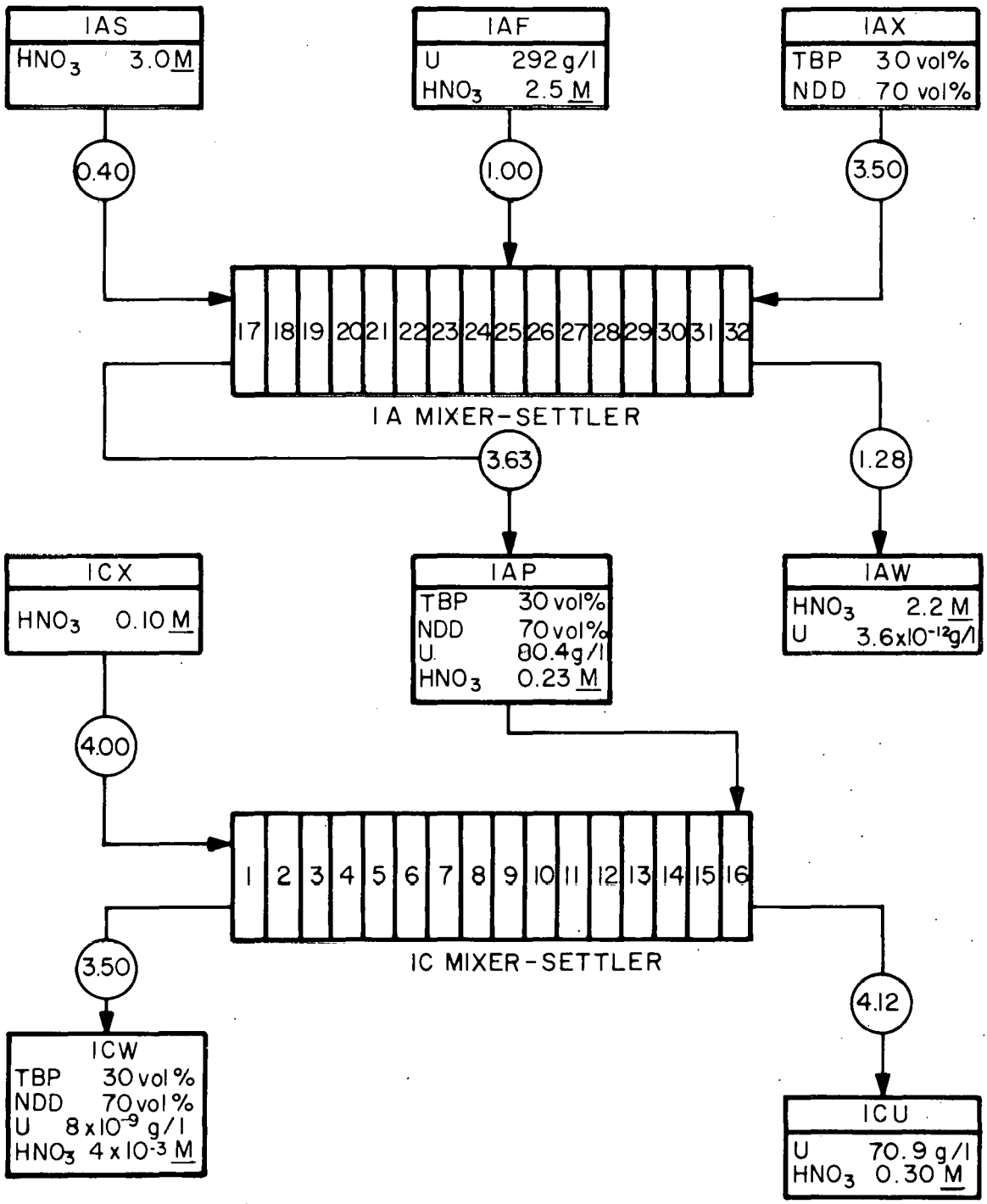

Fig. 1.1. Purex flowsheet using 0.1 M HNO_3 in stripping (S series).

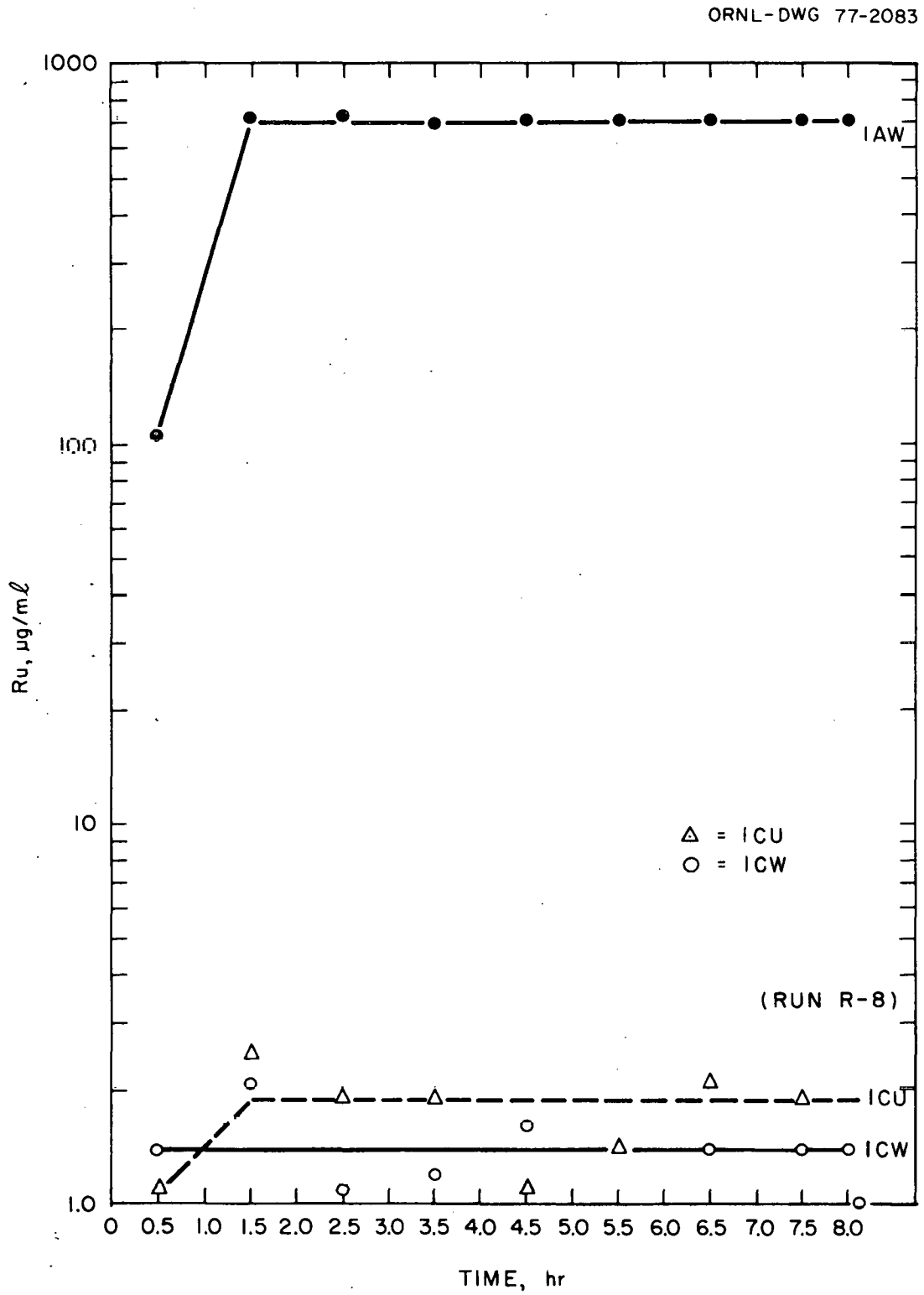

Fig. 1.2. Ruthenium concentrations of end streams as a function of time.

distribution coefficients for ruthenium in the extraction-scrubbing and stripping banks are given in Table 1.2. It should be noted that only a small amount of ruthenium was stripped out of the organic phase in the stripping bank. A profile of the ruthenium in each stage of the extraction-scrubbing bank is presented in Fig. 1.3. Stage efficiencies were 89 to 91% for the extraction-scrubbing bank. Measurements were unreliable in the stripping bank because of the small volume of sample and the low level of the ruthenium concentration in the sample (2 μg/ml or less).

The effect of the addition of sodium nitrite on ruthenium behavior is shown in Table 1.3. Results indicate that, with the addition of 0.1 M $NaNO_2$ in the feed and scrub solutions, 98% of the ruthenium exited from the extraction-scrubbing bank via the IAW stream and the ruthenium contamination was reduced in the end streams from the stripping bank.

After the profile samples had been taken, the mixer-settler system was run for an additional 4 hr (run R-8C) in order to flush the ruthenium from the system. The composition of the feed solution was 0.1 M $NaNO_2$-2.5 M HNO_3. At the end of the 4-hr period, only a low concentration of ruthenium (1.5 μg/ml) was exiting via the IAW waste stream (see Fig. 1.4).

When the mixer-settler banks were at steady state for run R-8, ~0.5 g of ruthenium was held up in both mixer-settler units; 96% of this amount was in the extraction-scrubbing bank. The material balance for ruthenium (output/input x 100) was 95% (analytical samples not included).

1.2.3 Zirconium behavior

In our previous work,[1] attempts to measure distribution coefficients for zirconium were unsuccessful due to the low levels of zirconium in the presence of appreciable amounts of uranium; therefore, during this report period, a run, R-9, was made using a feed solution containing zirconium at a concentration of 1.2 g/liter. Standard Purex flow conditions were used, as shown in Table 1.4. The concentrations of

Table 1.2. Aqueous concentrations and distribution coefficients for ruthenium in the extraction-scrubbing and stripping banks for run R-8

Extraction-scrubbing bank			Stripping bank		
Stage number	Aqueous Ru concentration (μg/ml)	D_A^o (Ru)[a]	Stage number	Aqueous Ru concentration (μg/ml)	D_A^o (Ru)[a]
17	11.6	0.24	1	0.2	6.0
18	22.9	0.174	2	0.4	4.5
19	-	-	3	0.5	3.8
20	58.9	0.136	4	0.6	2.7
21	84.4	0.118	5	0.6	3.0
22	136.0	0.098	6	0.4	4.75
23	229	0.083	7	0.5	4.0
24	314	0.082	8	0.6	3.83
25	766	0.051	9	0.5	4.6
26	801	0.051	10	0.6	2.3
27	804	0.056	11	0.6	2.8
28	841	0.065	12	0.8	2.5
29	923	0.07	13	0.9	2.1
30	974	0.08	14	1.0	1.9
31	934	0.103	15	1.0	2.0
32	724	0.105	16	1.0	1.9

[a] D_A^o is defined as the concentration of a species in the organic phase divided by its concentration in the aqueous phase when the system is at chemical equilibrium.

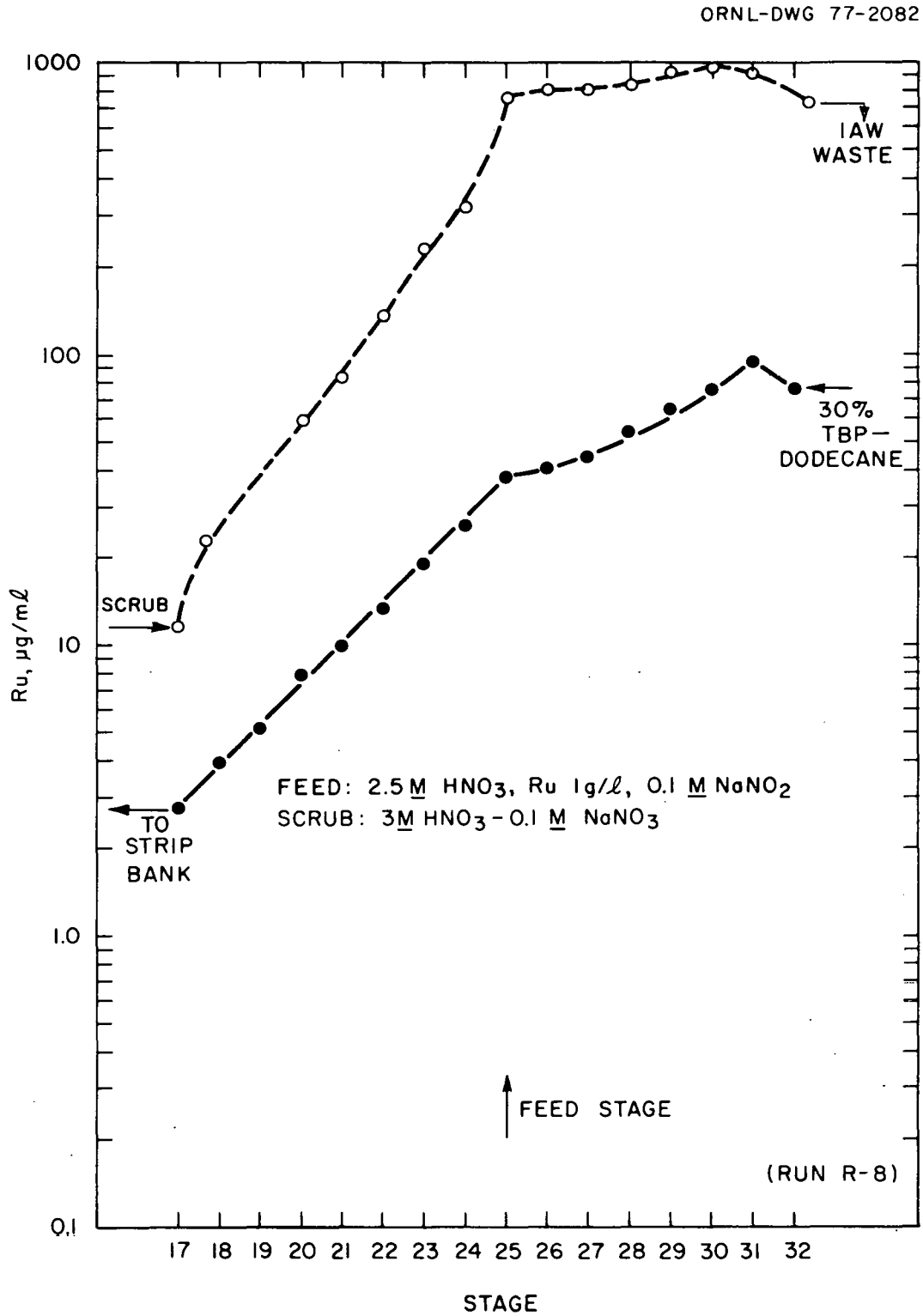

Fig. 1.3. Profile of ruthenium concentrations in the extraction-scrubbing bank.

Table 1.3. Ruthenium in the exiting process streams and the effect of sodium nitrite addition

	Run number		
	R-2	R-7	R-8
Feed	Ru - 0.69 g/liter	Ru - 0.65 g/liter	Ru - 0.98 g/liter
	U - 300 g/liter	U - 17.0 g/liter	
	Cold fission products	0.1 M $NaNO_2$	0.1 M $NaNO_2$
	2.5 M HNO_3	2.5 M HNO_3	2.5 M HNO_3
Scrub	3.0 M HNO_3	3.0 M HNO_3	3.0 M HNO_3;
			0.1 M $NaNO_2$
Extraction-scrubbing bank, % Ru			
Raffinate waste (1AW)	88.5	96.7	98.078
Stripping bank, % Ru			
Uranium aqueous product (1CU)	1.3	2.0	0.957
Stripped organic (1CW)	9.5	1.3	0.965

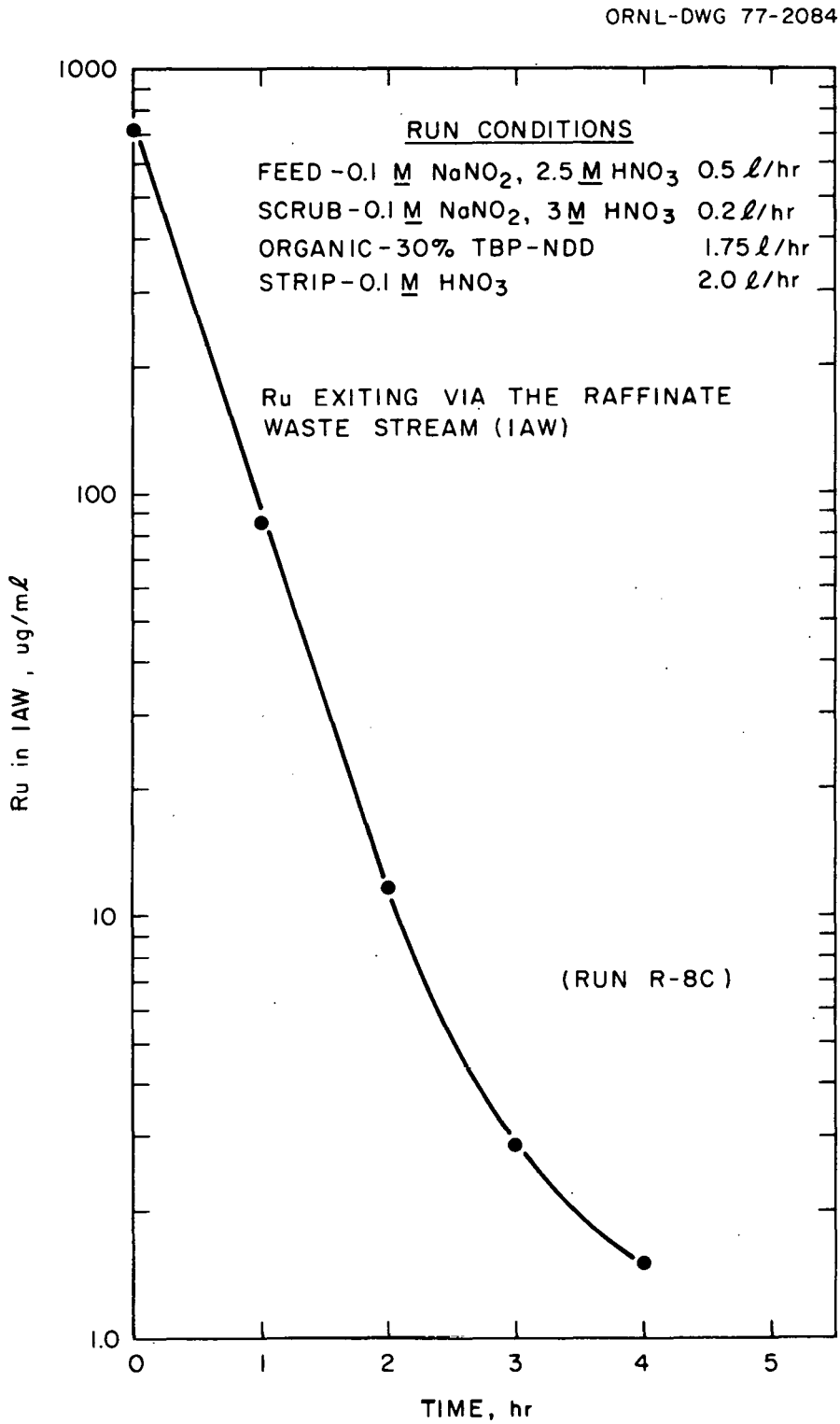

Fig. 1.4. Cleanout of extraction-scrubbing bank during run R-8C.

zirconium exiting in the end streams during the 8-hr run are shown in Fig. 1.5. Apparently, steady-state conditions for the zirconium in both mixer-settler banks were reached after 5 to 6 hr.

Table 1.4. Flowsheet conditions for run R-9

Process stream	Flow rate (liters/hr)	Composition
Feed	0.5	1.2 g Zr/liter; 2.5 M HNO_3
Solvent	1.75	30% TBP-n-dodecane
Scrub	0.2	3 M HNO_3
Strip	2.0	0.1 M HNO_3

Profile samples were taken from stages in both mixer-settler units at the completion of the run. Table 1.5 gives the organic and aqueous concentrations along with the distribution coefficients for zirconium in the extraction-scrubbing and stripping banks. A profile of the zirconium concentration in each stage of the extraction-scrubbing bank is shown in Fig. 1.6. The high zirconium concentration (23 μg/ml) in the aqueous phase of stage 16 is probably due to aqueous entrainment in the extractant that is flowing from the extraction-scrubbing bank into the 16th stage of the stripping bank. In stages 1 through 13, only a small amount of zirconium was stripped out of the organic extractant. Stage efficiencies calculated from equilibrium shake-outs of samples taken from individual stages in the extraction-scrubbing bank were 62 and 90% in the scrub and extraction sections respectively. Stage efficiencies for the stripping bank were unreliable because of the small volume of sample and the low zirconium concentration in each case.

At the completion of the run, each catch tank for the exiting process streams was stirred and sampled. As shown in Table 1.6, the IAW stream leaving the extraction scrubbing bank contained 93% of the

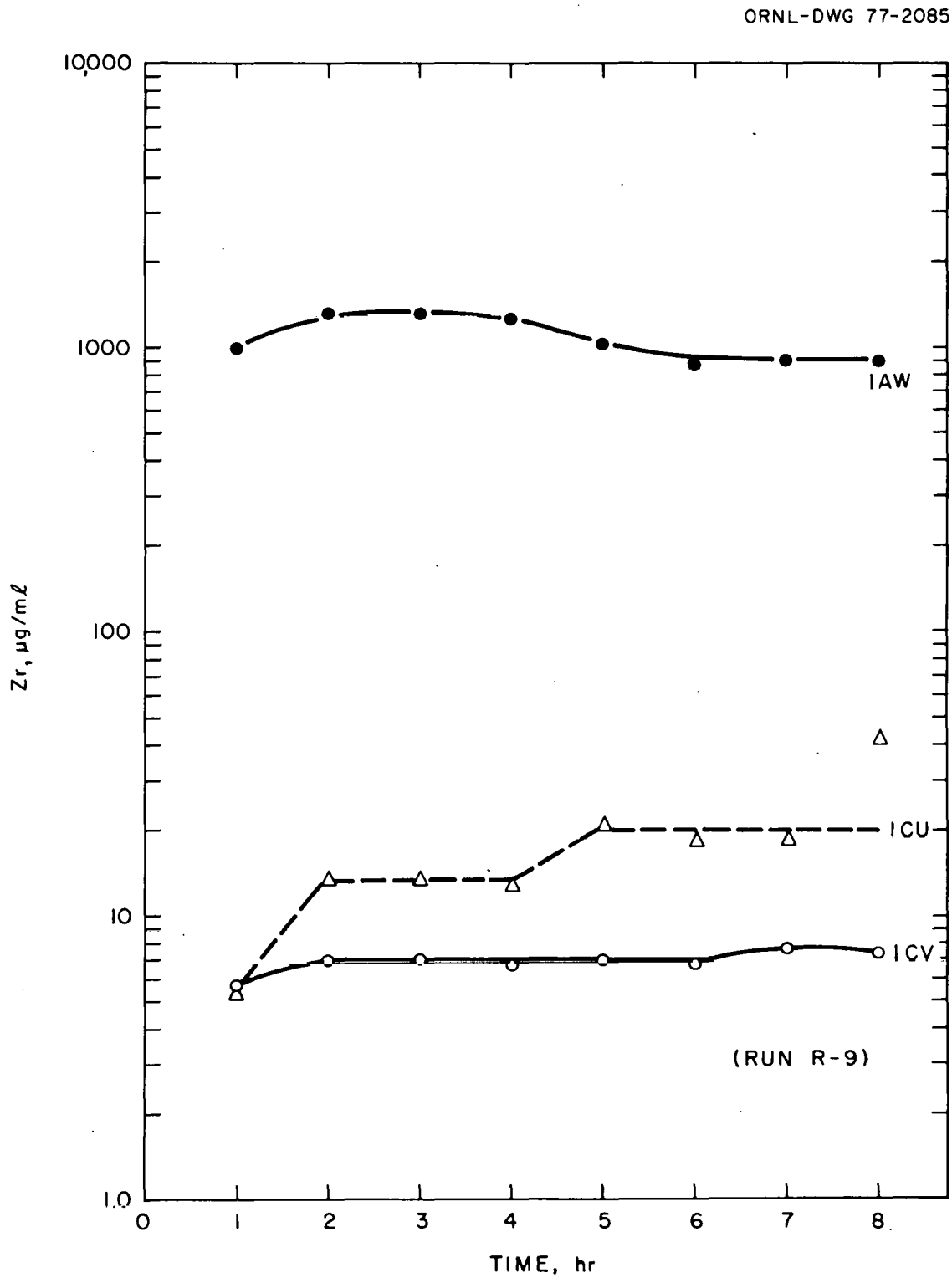

Fig. 1.5. Zirconium concentrations in end streams as a function of time (run R-9).

Table 1.5. Profile of the zirconium concentrations and distribution coefficients in the extraction-scrubbing and stripping banks for run R-9

Extraction-scrubbing bank				Stripping bank			
Stage number	Zr conc. (μg/ml) Organic	Aqueous	D_A^o (Zr)	Stage number	Zr conc. (μg/ml) Organic	Aqueous	D_A^o (Zr)
17	17.5	65	0.27	1	3.0	<2	-
18	18.0	108	0.17	2	2.9	<2	-
19	21.2	148	0.14	3	3.1	<2	-
20	18.5	203	0.09	4	4.7	<2	-
21	20.8	244	0.09	5	2.8	<2	-
22	20.0	323	0.06	6	7.3	<2	-
23	26.9	504	0.05	7	3.3	<2	-
24	51.1	646	0.08	8	3.4	<2	-
25	-	1,240	-	9	4.7	<2	-
26	89	1,180	0.08	10	3.2	<2	-
27	103	1,130	0.09	11	3.9	<2	-
28	72	1,110	0.065	12	4.2	<2	-
29	58	1,040	0.06	13	4.4	<2	-
30	50	970	0.05	14	4.9	2.1	2.33
31	27.5	910	0.03	15	7.0	4.0	1.75
32	12.1	910	0.01	16	8.4	23.0	0.37

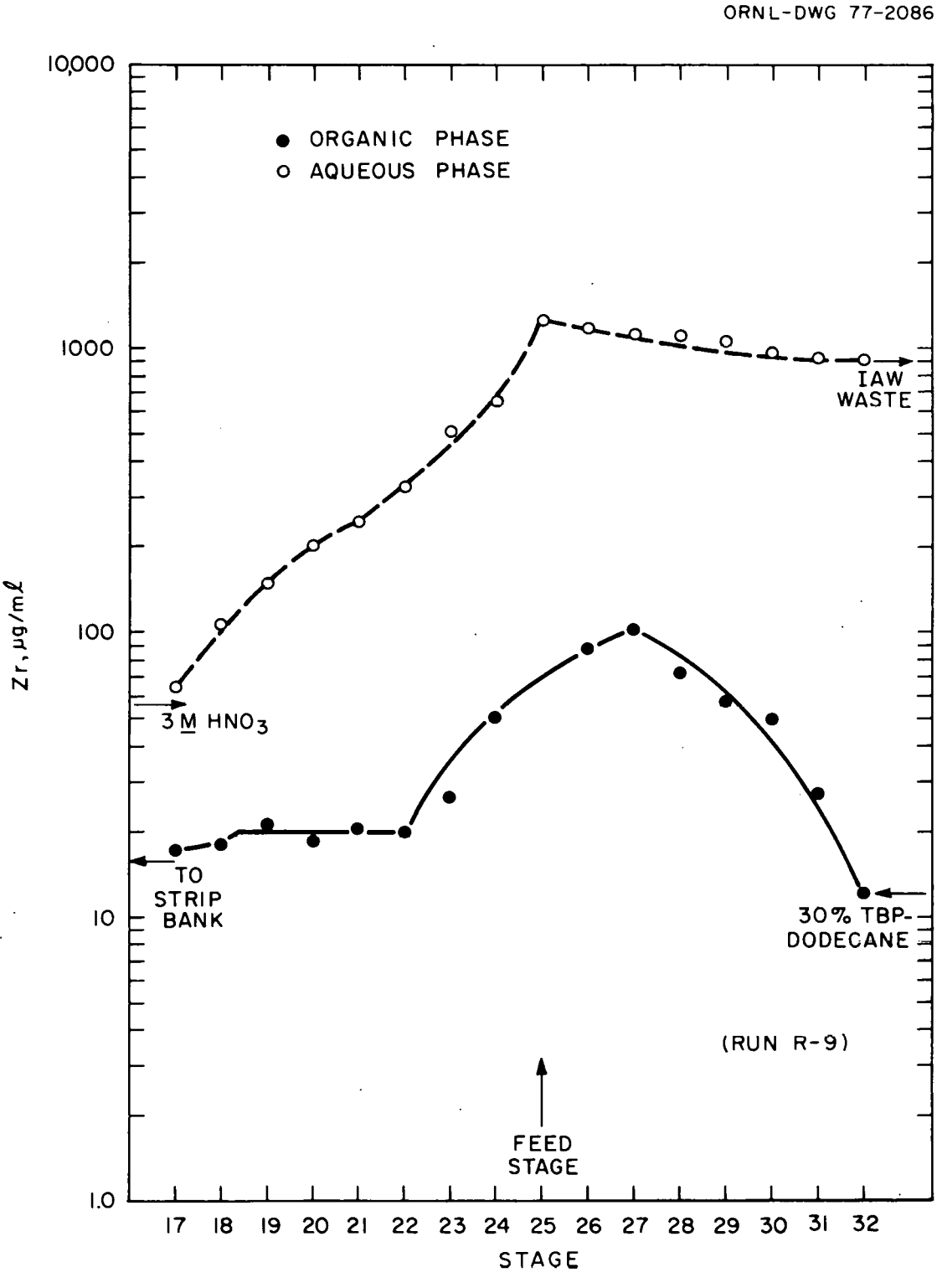

Fig. 1.6. Profile of the zirconium concentrations in the extraction-scrubbing bank for run R-9.

Table 1.6. Zirconium concentrations in the exiting process streams

	Run number	
	R-2	R-9
Feed	1.3 g Zr/liter 288 g U/liter 2.5 M HNO_3	1.2 g Zr/liter 2.5 M HNO_3
Extraction-scrubbing bank, % Zr		
Raffinate waste (IAW)	96.5	93.3
Stripping bank, % Zr		
Uranium aqueous product (ICU)	3.0	3.14
Stripped organic (ICW)	0.5	3.6

total accountable zirconium entering the mixer-settler system during the run. The amounts of zirconium in the IAW and the IAP catch tanks compare favorably with the results obtained previously in run R-2. However, 3% more zirconium was present in the stripped organic catch tank (ICW) in run R-9 than in run R-2. This disagreement occurred because the feed solution for run R-2 had a high uranium concentration (288 g/liter), which caused the organic entering the stripping bank to be loaded with uranium; this, in turn, resulted in a smaller amount of zirconium being extracted into the organic solvent in the extraction-scrubbing bank.

After the sampling for run R-9 had been completed, the mixer-settler system was run for an additional 4 hr (run R-9C) to flush the zirconium from the system (no zirconium in the feed solution). At the end of this period, low levels of zirconium were still exiting via the IAW waste stream (see Fig. 1.7).

Measurements indicate that approximately 0.107 g of zirconium was held up in both mixer-settler units during steady-state operations for run R-9. The material balance for zirconium (output/input x 100) was 96% (analytical samples not included).

1.3 Batch Countercurrent Studies

No batch countercurrent runs were made this quarter because Talspeak studies were emphasized. The poor stripping observed for plutonium from aged organic phases last quarter[1] was found to be the result of radiolytically generated dibutyl phosphoric (DBP) and monobutyl phosphoric acids (MBP). With the plutonium concentrations of $\sim$1 g/liter and a specific heat of $\sim$0.003 W/g, exposures were sufficient after a few days to yield significant amounts of the powerful extractants DBP and MBP. Irradiation at 1 W-hr/liter yields about 10^{-3} M DBP and 10^{-4} M MBP. Spectrophotometric studies of the organic phases showed that the unstripped plutonium was held by the DBP.

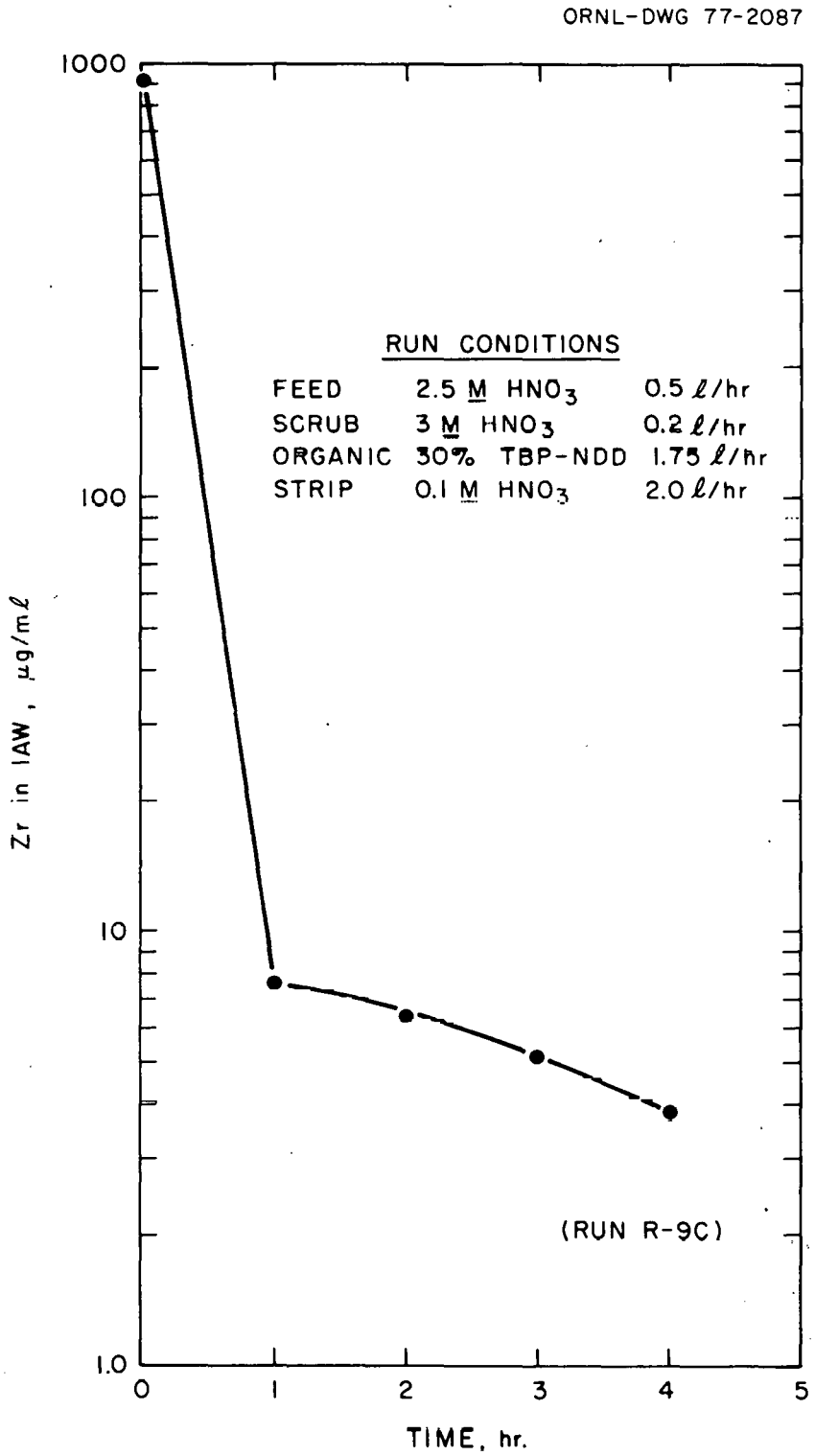

Fig. 1.7. Cleanout of extraction-scrubbing bank during run R-9C.

1.4 Reference for Section 1

1. D. W. Tedder and J. O. Blomeke (compilers), Actinide Partitioning and Transmutation Program Progress Report for Period April 1 to June 30, 1977, ORNL/TM-6056 (October 1977).

2. ACTINIDE RECOVERY FROM SOLIDS

E. L. Lewis and D. F. Luthy (Mound Laboratory)

The objective of this task is to measure the ability to decontaminate solids using reagents which are compatible with the reprocessing and refabrication flowsheets. The initial studies focus on the ability to decontaminate HEPA filters.

2.1 Experimental

2.1.1 Americium and plutonium* mixed oxide dissolution studies

Contaminated filter media were prepared by mixing AmO_2-PuO_2 powder with shredded filter media. Small samples of this mixture were then treated with various leaching reagents, including 4 N HNO_3-0.1 M $(NH_4)_2Ce(NO_3)_6$, 12 N HNO_3-0.05 N HF-0.01 N H_2SO_4, and 8 N HNO_3. A sample of filter media was placed in a beaker, 250 ml of the leaching reagent was added, and the temperature was increased to the boiling point of the solution. Samples were withdrawn periodically and filtered through a 4- to 5-μ glass filter. The ^{241}Am and ^{239}Pu concentrations were determined by alpha spectrometry. The volume and concentration of the solution were kept constant by adding acid of the proper concentration to replace that lost by evaporation. As can be seen in Table 2.1, the 4 N HNO_3-0.1 M $(NH_4)_2Ce(NO_3)_6$ was an effective leachant, dissolving greater than 90% of both AmO_2 and PuO_2 in 11.75 hr. On the other hand, the 8 N HNO_3 was not satisfactory since it dissolved only 36% of the PuO_2 in 13.5 hr (even though it dissolved 97% of the AmO_2 during this time). The HNO_3-HF-H_2SO_4 mixture was effective in dissolving the AmO_2 (90% in 11.25 hr) but not as effective in dissolving the PuO_2 (80% in 11.25 hr). Of the three reagents tested, the 4 N HNO_3-0.1 M $(NH_4)Ce(NO_3)_6$ is the recommended leaching reagent for AmO_2-PuO_2 mixtures.

---

*This material contained approximately three parts of ^{239}Pu oxide mixed with one part of ^{241}Am oxide, by weight. It had been fired for 2 hr at 1000°C.

Table 2.1. Results of AmO_2-PuO_2 dissolution tests

Acid test number	Reagent composition	Time heated (hr)	Amount of PuO_2 dissolved (wt %)	Amount of AmO_2 dissolved (wt %)
Am-Pu-1A	4 N HNO_3-0.1 M CAN[a]	5.75	72.9	63.3
Am-Pu-1B	4 N HNO_3-0.1 M CAN[a]	11.75	93.7	111.8
Am-Pu-2A	12 N HNO_3-0.05 N HF-0.01 N H_2SO_4	5.75	68.9	72.4
Am-Pu-2B	12 N HNO_3-0.05 N HF-0.01 N H_2SO_4	11.25	80.2	90.4
Am-Pu-4A	8 N HNO_3	7.25	37.2	88.9
Am-Pu-4B	8 N HNO_3	13.5	36.3	96.7

[a]CAN is abbreviation for ceric ammonium nitrate.

2.1.2 Uranium oxide dissolution studies

These studies were conducted using U_3O_8 mixed with filter media. The oxide had been fired at 950°C for 2 hr. A small sample of the prepared filter media (∿3.2 g) was placed in a beaker containing 250 ml of boiling reagent. Three reagents were used: 8 N HNO_3, 4 N HNO_3-0.1 M $(NH_4)_2Ce(NO_3)_6$, and 12 N HNO_3-0.05 N HF-0.01 N H_2SO_4. Samples were withdrawn periodically for alpha analysis. All samples were filtered through 4- to 5-μ glass filters. The volume and concentration of the solution were kept constant by adding acid of the proper concentration to replace that lost by evaporation. As can be seen from Table 2.2, the dissolution was very rapid and exceeded 90% in all cases. Thus, each of the reagents evaluated would be an acceptable dissolvent for ^{233}U oxide.

2.1.3 Sodium carbonate fusions of PuO_2*

Two fusion tests were conducted in order to determine the effect of temperature on fusion efficiency. Small samples were prepared by mixing 64 mg of PuO_2 with 2.25 g of Na_2CO_3. The PuO_2-Na_2CO_3 mixture was then added to a platinum crucible, which in turn was placed in a resistance tube furnace. The crucible and contents were subsequently heated to the desired operating temperature and maintained there for 1 hr. Finally, the crucible and melt were cooled to room temperature, and the melt was removed from the crucible and dissolved in 4 N HNO_3. The difference (4.6%) between the dissolution percentages obtained in the two tests (see Table 2.3) is not significant and is thought to be due to experimental error. Therefore, it can be concluded that the fusion efficiency is ∿58% (average value) within the temperature range under investigation.

---

*The PuO_2 was a fine powder composed of 80 wt % ^{238}Pu, 16 wt % ^{239}Pu, 2.5 wt % ^{240}Pu, 0.8 wt % ^{241}Pu, and 0.2 wt % ^{242}Pu, plus small amounts of other actinides. It was calcined for 2 hr at 950°C.

Table 2.2. Results of ^{233}U oxide dissolution tests

Acid test number	Reagent composition	Time heated (min)	Amount of ^{233}U oxide dissolved (wt %)
U-3-1	8 N HNO_3	5	97.4
U-3-2	8 N HNO_3	20	106.1
U-3-3	8 N HNO_3	65	93.8
U-3-4	8 N HNO_3	255	95.9
U-4-1	4 N HNO_3-0.1 M CAN[a]	5	89.7
U-4-2	4 N HNO_3-0.1 M CAN[a]	15	104.8
U-4-3	4 N HNO_3-0.1 M CAN[a]	60	95.2
U-4-4	4 N HNO_3-0.1 M CAN[a]	360	95.7
U-5-1	12 N HNO_3-0.05 N HF-0.01 N H_2SO_4	5	100.9
U-5-2	12 N HNO_3-0.05 N HF-0.01 N H_2SO_4	15	106.2
U-5-3	12 N HNO_3-0.05 N HF-0.01 N H_2SO_4	50	100.1
U-5-4	12 N HNO_3-0.05 N HF-0.01 N H_2SO_4	240	102.5

[a]CAN is abbreviation for ceric ammonium nitrate.

Table 2.3. Sodium carbonate fusions of PuO_2

Fusion test number	Time heated (hr)	Operating temperature (°C)	Amount of PuO_2 solubilized (wt %)	Dissolution reagent
Pu-44	1	1300	56.4	4 N HNO_3
Pu-45	1	1200	61.0	4 N HNO_3

2.1.4 Neptunium oxide dissolution studies

The NpO_2 was fired for 2 hr at 950°C. Samples of contaminated filter media were prepared by mixing 0.2 g of NpO_2 with 3 g of filter media. The procedure was identical to that used in the ^{233}U oxide dissolution studies (see Sect. 2.1.2). Three leaching reagents, namely 8 N HNO_3, 4 N HNO_3-0.1 M $(NH_4)_2Ce(NO_3)_6$, and 12 N HNO_3-0.05 N HF-0.01 N H_2SO_4, were tested. Table 2.4 lists the results for these experiments. As can be seen, the 8 N HNO_3 was rather ineffective, dissolving only 32% of the NpO_2 in 8 hr. On the other hand, each of the other two reagents effected rapid dissolution; that is, greater than 90% of the NpO_2 was dissolved after 0.5 hr of boiling. Therefore, both the 4 N HNO_3-0.1 M $(NH_4)_2Ce(NO_3)_6$ and the 12 N HNO_3-0.05 N HF-0.01 N H_2SO_4 acid mixtures would be recommended as reagents for dissolving NpO_2 from filter media.

2.1.5 Curium oxide* dissolution studies

Contaminated filter media were prepared by mixing 13 mg of CmO_2 with 3 g of filter media. The experimental procedure was identical to that used for the U_3O_8 dissolution studies (Sect. 2.1.2). Two leaching reagents, namely 12 N HNO_3-0.05 N HF and 4 N HNO_3-0.1 M $(NH_4)_2Ce(NO_3)_6$, were tested. The results from these tests are found in Table 2.5. As can be seen, each of the reagents dissolved the CmO_2 very rapidly (essentially 100% dissolution was achieved in 10 min). Therefore, both are recommended for dissolution of CmO_2 from contaminated filter media.

2.1.6 Thorium oxide dissolution tests

Contaminated filter media were prepared by mixing 0.24 g of ThO_2 with 3 g of filter media. The experimental procedure was identical to that used in the uranium oxide studies. The ThO_2 was a fine powder

---

*This was a powder which was ~94% ^{244}Cm and 4% ^{246}Cm, with the remainder being ^{245}Cm, ^{247}Cm, and ^{248}Cm.

Table 2.4. Results of ^{237}Np oxide dissolution tests

Acid test number	Reagent composition	Time heated (min)	Amount of NpO_2 dissolved (wt %)
Np-3-1	8 N HNO_3	10	1.3
Np-3-2	8 N HNO_3	25	1.9
Np-3-3	8 N HNO_3	45	4.1
Np-3-4	8 N HNO_3	75	6.1
Np-3-5	8 N HNO_3	480	32.3
Np-4-1	4 N HNO_3-0.1 M CAN[a]	10	93.7
Np-4-2	4 N HNO_3-0.1 M CAN[a]	25	97.2
Np-4-3	4 N HNO_3-0.1 M CAN[a]	40	88.9
Np-4-4	4 N HNO_3-0.1 M CAN[a]	60	89.1
Np-5-1	12 N HNO_3-0.05 N HF-0.01 N H_2SO_4	10	64.7
Np-5-2	12 N HNO_3-0.05 N HF-0.01 N H_2SO_4	25	105.2
Np-5-3	12 N HNO_3-0.05 N HF-0.01 N H_2SO_4	45	107.4
Np-5-4	12 N HNO_3-0.05 N HF-0.01 N H_2SO_4	100	102.3

[a]CAN is abbreviation for ceric ammonium nitrate.

Table 2.5. Results of curium oxide dissolution tests

Acid test number	Reagent composition	Time heated (min)	Amount of CmO_2 dissolved (wt %)
Cm-2A	12 N HNO_3-0.05 N HF	10	103.3
Cm-2B	12 N HNO_3-0.05 N HF	25	100.8
Cm-2C	12 N HNO_3-0.05 N HF	60	105.0
Cm-2D	12 N HNO_3-0.05 N HF	120	99.1
Cm-2E	12 N HNO_3-0.05 N HF	180	104.5
Cm-2F	12 N HNO_3-0.05 N HF	540	93.3
Cm-2G	12 N HNO_3-0.05 N HF	540	99.0
Cm-3A	4 N HNO_3-0.1 M CAN[a]	10	112.1
Cm-3B	4 N HNO_3-0.1 M CAN[a]	25	110.0
Cm-3C	4 N HNO_3-0.1 M CAN[a]	60	109.0
Cm-3D	4 N HNO_3-0.1 M CAN[a]	120	107.6
Cm-3E	4 N HNO_3-0.1 M CAN[a]	330	110.5

[a]CAN is abbreviation for ceric ammonium nitrate.

that had been fired at 600°C. The purpose of this experiment was to determine whether ThO_2 would dissolve in 4 N HNO_3-0.1 M $(NH_4)_2Ce(NO_3)_6$ similarly to other actinide oxides tested previously (PuO_2, CmO_2, AmO_2, U_3O_8, and NpO_2). As can be seen from the data in Table 2.6 and Fig. 2.1, the dissolution rate was slow at first (0 to 7 hr), rapid from 7 to 9 hr, and slow again from 9 to 20 hr. The reason for this change in rates is not known at present; however, it is thought that the first 7 hr was required to attack the surface of the ThO_2 and open the pores so that rapid dissolution could begin. Therefore, 4 N HNO_3-0.1 M $(NH_4)_2Ce(NO_3)_6$ appears to be an acceptable leaching reagent for ThO_2, although the dissolution time is longer than for other actinides. A point of interest is that, in a similar experiment performed using ThO_2 alone (no filter media), only 25% dissolution was achieved after 20 hr of boiling. This difference in dissolution percentages (25% vs 100%) cannot presently be explained.

2.1.7 Dissolution of PuO_2 from actual glove-box filters using 4 N HNO_3 plus various concentrations of $(NH_4)_2Ce(NO_3)_6$

These tests were conducted using samples of filter media removed from actual spent glove-box filters. The PuO_2 on the filters was the same type as that used in the fusion experiments (Sect. 2.1.3).

In experiment A, a 9.5-g sample of filter media containing 0.18 g of PuO_2 was dissolved in a six-stage procedure. The volume of leaching solution was based on that stipulated by the flowsheet submitted in the previous quarterly report,[1,2] namely, 18 ml of solution per gram of filter media. The amount of ceric ammonium nitrate required was based on the initial moles of PuO_2 present in the filter media (60 moles of Ce^{4+} per mole of PuO_2). Using these criteria, the leaching reagent in the first five stages was 4 N HNO_3-0.23 M $(NH_4)_2Ce(NO_3)_6$, while the sixth stage contained 12 N HNO_3-0.1 N HF. The 12 N HNO_3-0.1 N HF was used because the 4 N HNO_3-0.23 M $(NH_4)_2Ce(NO_3)_6$ had proved to be ineffective in the fifth stage of dissolution. The volume of 12 N HNO_3-0.1 N HF used in each case was 250 ml; all studies were done at boiling temperature. The solution was sampled periodically for plutonium concentration, and all samples were filtered through 4- to

Table 2.6. Data for dissolution of ThO_2 in the presence of HEPA filter

Acid test number	Reagent composition	Time heated (min)	Amount of ThO_2 dissolved (wt %)
Th-1	4 N HNO_3-0.1 M CAN[a]	5	0.6
Th-2	4 N HNO_3-0.1 M CAN[a]	10	0.4
Th-3	4 N HNO_3-0.1 M CAN[a]	20	1.4
Th-4	4 N HNO_3-0.1 M CAN[a]	35	2.4
Th-5	4 N HNO_3-0.1 M CAN[a]	60	5.1
Th-6	4 N HNO_3-0.1 M CAN[a]	180	4.7
Th-7	4 N HNO_3-0.1 M CAN[a]	300	12.5
Th-8	4 N HNO_3-0.1 M CAN[a]	440	31.7
Th-9	4 N HNO_3-0.1 M CAN[a]	440	29.3
Th-10	4 N HNO_3-0.1 M CAN[a]	470	42.1
Th-11	4 N HNO_3-0.1 M CAN[a]	545	82.3
Th-12	4 N HNO_3-0.1 M CAN[a]	905	100.5
Th-13	4 N HNO_3-0.1 M CAN[a]	1205	104.3
Th-14[b]	4 N HNO_3-0.1 M CAN[a]	1200	25.0

[a]CAN is abbreviation for ceric ammonium nitrate.

[b]No HEPA filter was present during test.

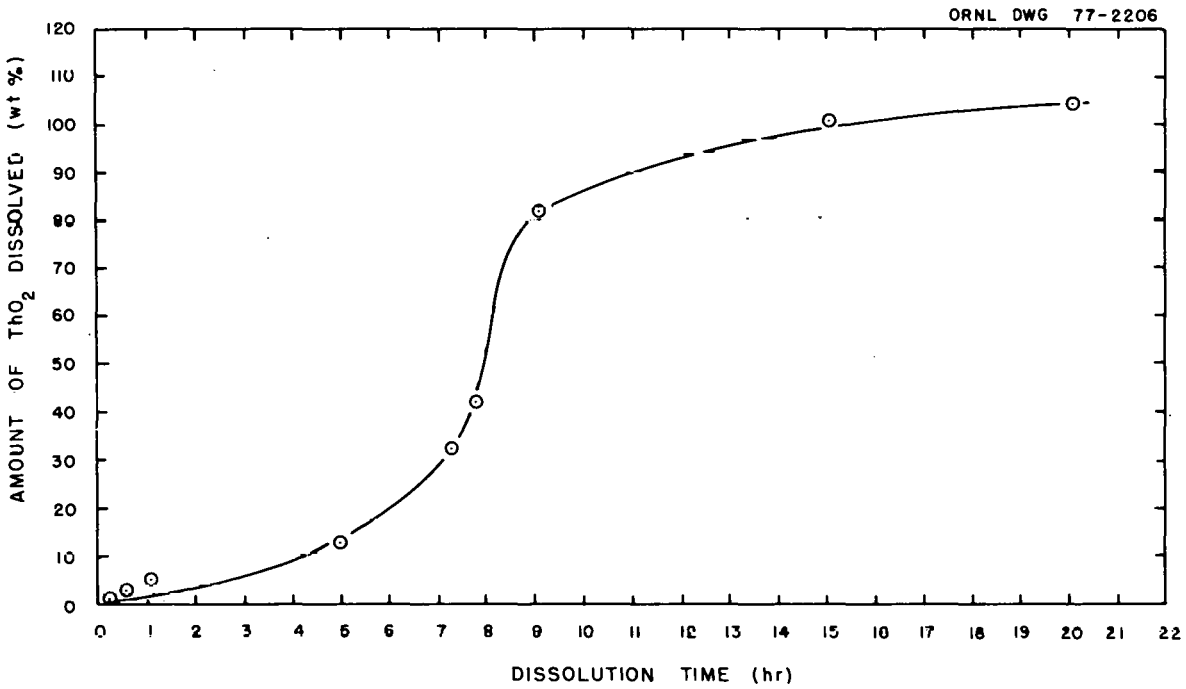

Fig. 2.1. Dissolution of ThO_2 in the presence of HNO_3, ceric ammonium nitrate, and HEPA filter material.

5-μ glass filters. When the dissolution rate for a particular stage had become very slow (as indicated by alpha analysis of the solution), the filter material was separated from the leaching solution by filtration and subjected to the next stage of dissolution. Results for this experiment are given in Table 2.7. Figure 2.2 shows the observed cumulative weight percentage dissolved as a function of time for stages 2 and 3. It should be noted that the final cumulative percentage dissolved was 99.88% (equivalent to a decontamination factor of 833). This result, which was determined by gamma-ray spectrometry of the residual filter media, is in good agreement with the final value as determined by alpha counting of the solution samples (99.80%). It should also be noted that the 12 N HNO_3-0.1 N HF solution used in the sixth stage was more than twice as effective as the 4 N HNO_3-0.1 M $(NH_4)_2Ce(NO_3)_6$ used in the fifth stage (0.079% dissolved vs 0.031%). The reason for this is not presently understood. Additional studies will have to be made to investigate this phenomenon.

In experiment B, a 25.6-g sample of filter media containing 0.31 g of PuO_2 was dissolved in a four-stage dissolution process. The leaching reagent used in the test was 4 N HNO_3-0.30 M $(NH_4)_2Ce(NO_3)_6$. The volume of solution was again based on the flowsheet submitted last quarter (i.e., 18 ml of solution per gram of filter media), while the amount of ceric ammonium nitrate was increased to 120 times the initial moles of PuO_2 present in the filter media. The experimental procedure was identical to that used in experiment A. The results are given in Table 2.8. The dissolution percentages in Table 2.8 were determined by alpha counting, but the cumulative percentages as calculated by gamma-ray spectrometry showed a final value of 98.24% dissolved. As one can see, this value compares favorably with that (i.e., 97.62%) obtained by alpha counting. The value obtained by gamma spectrometry is, however, considered to be more accurate than the total obtained by simple addition of the individual alpha count values. The decontamination factor (DF) obtained using this gamma-spectrometry value is ∿57. The DF obtained after four stages for experiment A was 417.

Table 2.7. PuO_2 dissolution data[a] obtained in experiment A

Acid test number	Reagent Composition	Time heated (min)	Amount of PuO_2 dissolved (wt %)	Process stage
256-1 A	4 N HNO_3-0.23 M CAN[a]	10	82.0	1
256-2 A	4 N HNO_3-0.23 M CAN[a]	20	79.5	1
256-3 A	4 N HNO_3-0.23 M CAN[a]	40	87.3	1
256-4 A	4 N HNO_3-0.23 M CAN[a]	60	80.9	1
256-5 A	4 N HNO_3-0.23 M CAN[a]	120	85.8	1
256-6 A	4 N HNO_3-0.23 M CAN[a]	210	90.6	1
256-1 B	4 N HNO_3-0.23 M CAN[a]	10	0.41	2
256-2 B	4 N HNO_3-0.23 M CAN[a]	20	1.17	2
256-3 B	4 N HNO_3-0.23 M CAN[a]	45	2.50	2
256-4 B	4 N HNO_3-0.23 M CAN[a]	65	2.97	2
256-5 B	4 N HNO_3-0.23 M CAN[a]	120	4.75	2
256-6 B	4 N HNO_3-0.23 M CAN[a]	360	7.30	2
256-7 B	4 N HNO_3-0.23 M CAN[a]	510	7.47	2
256-1 C	4 N HNO_3-0.23 M CAN[a]	30	0.29	3
256-2 C	4 N HNO_3-0.23 M CAN[a]	75	0.55	3
256-3 C	4 N HNO_3-0.23 M CAN[a]	135	0.87	3
256-4 C	4 N HNO_3-0.23 M CAN[a]	315	1.06	3
256-5 C	4 N HNO_3-0.23 M CAN[a]	435	1.09	3
256-6 C	4 N HNO_3-0.23 M CAN[a]	675	1.31	3
256-7 C	4 N HNO_3-0.23 M CAN[a]	675	1.39	3
256-1 D	4 N HNO_3-0.23 M CAN[a]	20	0.029	4
256-2 D	4 N HNO_3-0.23 M CAN[a]	45	0.063	4
256-3 D	4 N HNO_3-0.23 M CAN[a]	60	0.079	4
256-4 D	4 N HNO_3-0.23 M CAN[a]	135	0.139	4
256-5 D	4 N HNO_3-0.23 M CAN[a]	330	0.213	4
256-6 D	4 N HNO_3-0.23 M CAN[a]	645	0.222	4
256-7 D	4 N HNO_3-0.23 M CAN[a]	645	0.228	4
256-1 E	4 N HNO_3-0.23 M CAN[a]	15	0.011	5
256-2 E	4 N HNO_3-0.23 M CAN[a]	30	0.012	5
256-3 E	4 N HNO_3-0.23 M CAN[a]	60	0.015	5
256-4 E	4 N HNO_3-0.23 M CAN[a]	135	0.023	5
256-5 E	4 N HNO_3-0.23 M CAN[a]	195	0.025	5
256-6 E	4 N HNO_3-0.23 M CAN[a]	465	0.029	5
256-7 E	4 N HNO_3-0.23 M CAN[a]	600	0.031	5
256-8 E	4 N HNO_3-0.23 M CAN[a]	780	0.032	5
256-9 E	4 N HNO_3-0.23 M CAN[a]	780	0.025	5
256-1 F	12 N HNO_3-0.1 N HF	30	0.016	6
256-2 F	12 N HNO_3-0.1 N HF	60	0.030	6
256-3 F	12 N HNO_3-0.1 N HF	240	0.047	6
256-4 F	12 N HNO_3-0.1 N HF	585	0.079	6
256-5 F	12 N HNO_3-0.1 N HF	945	0.075	6

[a]A 9.5-g sample was used in each test.

[b]CAN is abbreviation for ceric ammonium nitrate.

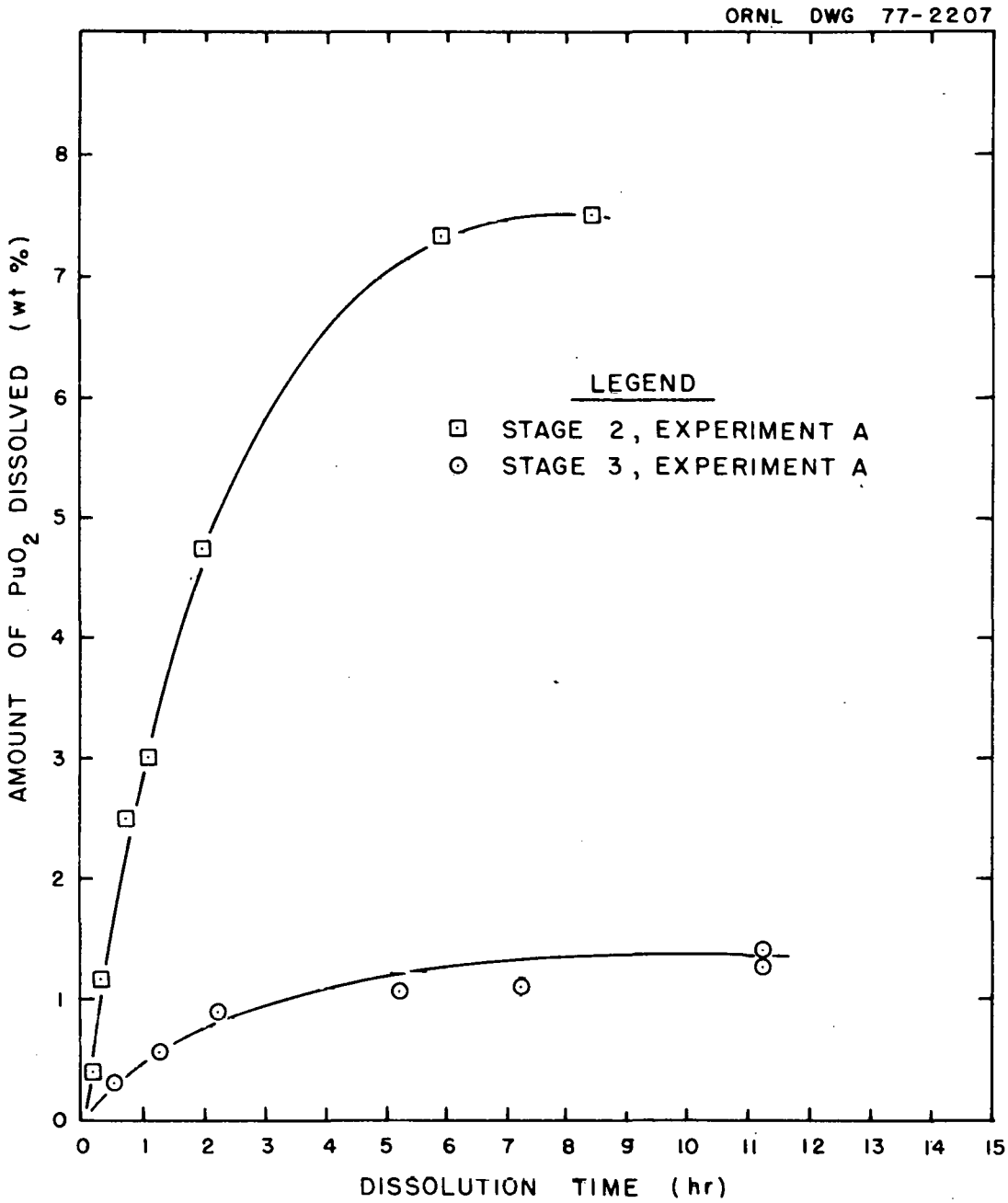

Fig. 2.2. Apparent decrease in the rate of PuO_2 dissolution with successive crosscurrent leaching stages.

Table 2.8. PuO_2 dissolution data[a] obtained in experiment B

Acid test number	Reagent composition	Stage	Time heated (hr)	Amount of PuO_2 dissolved	
				wt %	Cumulative wt %
12-1	4 N HNO_3-0.3 M CAN[b]	1	6.5	88.40	88.40
12-2	4 N HNO_3-0.3 M CAN[b]	2	15	4.04	92.44
12-3	4 N HNO_3-0.3 M CAN[b]	3	7.25	4.91	97.35
12-4	4 N HNO_3-0.3 M CAN[b]	4	7	0.27	97.62[c]

[a]A 25.6-g sample was used in each test.

[b]CAN is abbreviation for ceric ammonium nitrate.

[c]Gamma-ray analysis of remaining filter media indicated that 98.24% of the PuO_2 had been dissolved.

A logical question would be: Why was the decontamination factor in experiment B less than in experiment A when more ceric ammonium nitrate per mole of PuO_2 was used? It is known that the 25.6-g sample of filter media contained a greater percentage of pack-to-frame sealant* than the 9.5-g sample. It is also known (from the color change of the leaching solution) that the Ce^{4+} ions were reduced much more quickly during the dissolution of PuO_2 from the 25.6-g filter media sample. Therefore, it is surmised that the reason for the smaller DF (smaller percent dissolved) is that the Ce^{4+} ions were mainly used to oxidize the sealant, thus leaving fewer Ce^{4+} ions to oxidize the plutonium to Pu^{4+}. A simple solution to this problem might be to increase the amount of ceric ammonium nitrate when larger amounts of sealant are present with the filter media.

In experiment C, a 30-g sample of filter media containing 0.33 g of PuO_2 was dissolved in a four-stage dissolution process as shown on the flowsheet submitted in the last quarterly report.[1,2] The amount of ceric ammonium nitrate required for each step was based on the assumption that 0.01 mole of Ce^{4+} would oxidize 1 Ci (0.058 g) of ^{238}Pu oxide. Verification of this assumption was the purpose of the experiment. A 90% dissolution of the PuO_2 present was to be achieved in each of the four steps. As seen in Table 2.9, 95.28% of the PuO_2 was dissolved in the four-stage process. However, a more accurate gamma-ray spectrometry analysis showed that only 93.96% dissolved (a DF of 16.56). The results of this experiment confirm that the desired DF of 10,000 cannot be achieved using the above-mentioned basis for determining the amount of ceric ammonium nitrate required. As found in experiment B, the amount of ceric ammonium nitrate must be based on the total amount of material (PuO_2, sealant, and other organics) present. This total must be determined for each dissolution since the amount to be reacted varies with each batch.

---

*This material is used to seal the asbestos-glass filter pack to the wooden frame. It is a fire-retardant polyurethane foam and a rubber-base adhesive.

Table 2.9. PuO_2 dissolution data obtained in experiment C

Acid test number	Reagent composition	Stage	Time heated (hr)	Amount of PuO_2 dissolved	
				wt %	Cumulative wt %
13-1	4 N HNO_3-0.3 M CAN[a]	1	8.5	90.70	90.70
13-2	4 N HNO_3-0.3 M CAN[a]	2	12.25	1.08	91.78
13-3	4 N HNO_3-0.3 M CAN[a]	3	12.5	2.12	93.90
13-4	4 N HNO_3-0.3 M CAN[a]	4	8.75	1.38	95.28[b]

[a]CAN is abbreviation for ceric ammonium nitrate.

[b]Gamma-ray analysis showed that 93.96% of the PuO_2 had been dissolved.

The results from the multiple leaching tests were further analyzed in terms of relative stage efficiencies. That is, for each experiment, the percentage dissolved per stage was analyzed relative to the percentage dissolved during the first stage of leach during that series. A relative stage efficiency, η, was defined in terms of the first stage, which was arbitrarily assigned an efficiency of 100%. The definitions are then as follows:

$$Y_j^* = Y_1 X_{j-1}/100, \tag{2.1}$$

$$\eta = 100 Y_j / Y_j^*, \tag{2.2}$$

where

Y_j^* = wt % of actinide predicted to dissolve during the jth leach based on the wt % dissolved during the first-stage leach (assuming a constant DF per stage),

X_{j-1} = wt % of actinide remaining with the HEPA filter solids after the j-1 leach (originally 100%),

Y_j = wt % of actinide actually leached from the solids during the jth leach.

The relative stage efficiency as defined is partly analogous to the Murphree[3] stage efficiency, where the amount of dissolved actinide entering with the leachant, Y_{j-1}, is always zero. However, Y_j^* is not an equilibrium variable, but simply a measure of the fractional conversion per stage.

The observed relative efficiencies for the three crosscurrent leach experiments are presented in Fig. 2.3. The variability in efficiency is apparent; also, there appears to be a general trend downward with repeated leaching. The increase in efficiency between leach stages 5 and 6 in experiment A results from the use of fluoride in leach stage 6, as explained. The increases between stages 2 and 3 are probably due to the depletion of organic species by cerium oxidation. However, it is clear that a simple extrapolation of the leach results observed in a single-stage test to multiple stages is not generally valid under these conditions. In addition, the efficiencies observed in experiment C show that these leach conditions are not nearly as effective as originally assumed.

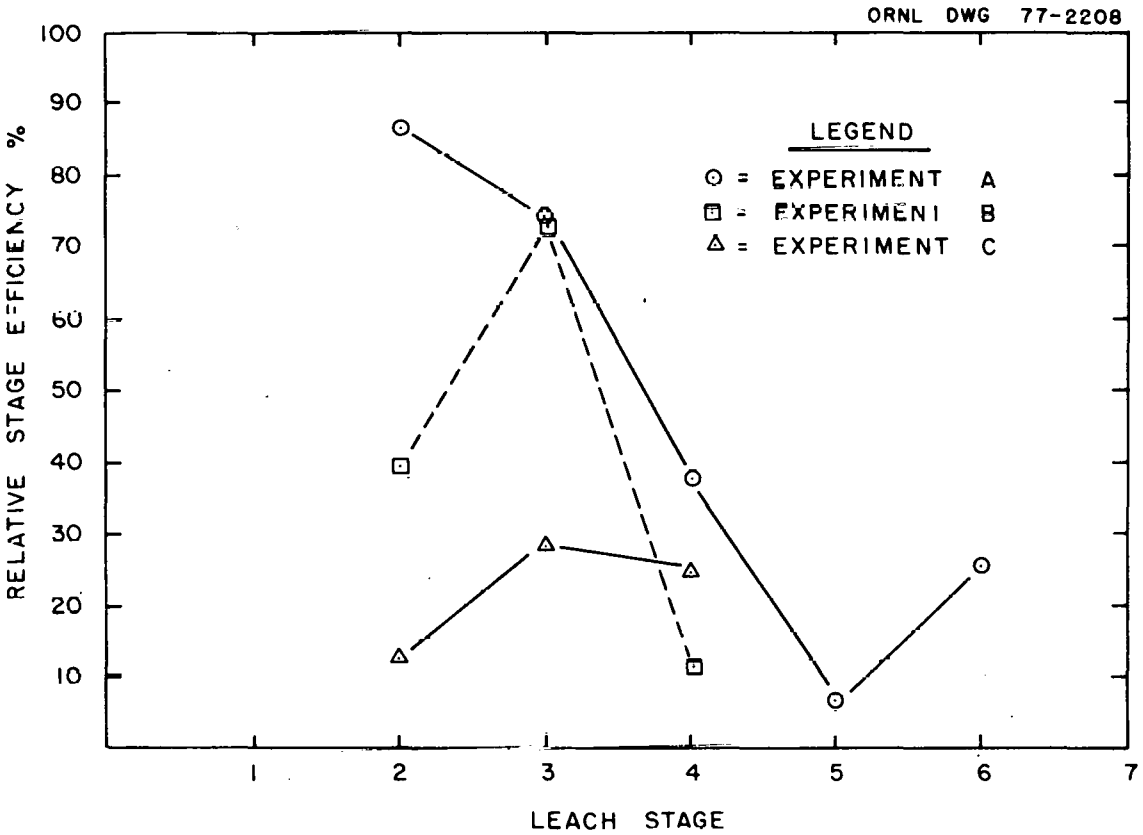

Fig. 2.3. Apparent decrease in relative stage efficiency with multiple leaching steps.

2.2 Summary

Filter media that were contaminated with ^{241}Am and ^{239}Pu oxides were treated with three different leaching reagents, 8 N HNO_3, 4 N HNO_3-0.1 M $(NH_4)_2Ce(NO_3)_6$, and 12 N HNO_3-0.05 N HF-0.01 N H_2SO_4, in order to determine the effectiveness of each in dissolving the actinide oxides. The best results were obtained with 4 N HNO_3-0.1 M $(NH_4)_2Ce(NO_3)_6$, which dissolved greater than 90% of the AmO_2 and the PuO_2.

Another series of tests was conducted in order to determine the most effective leaching reagent for uranium oxide (U_3O_8). Simulated samples of contaminated filter media were prepared by mixing 0.2 g of U_3O_8 powder with 3 g of shredded filter media. The reagents used in these tests were the same as those evaluated in the AmO_2-PuO_2 studies (see above). All three of the reagents were found to be successful in dissolving greater than 90% of the U_3O_8 in a very short time (i.e., 15 min).

Fusion studies were conducted using Na_2CO_3 and PuO_2. The purpose of these studies was to determine the effect of temperature on fusion efficiency. Results showed that there was not a significant difference in the percentage of PuO_2 solubilized ($\sim$59%) within the temperature range under investigation (1200 to 1300°C).

Experiments were conducted using filter media contaminated with neptunium oxide. The objective of these tests was to determine which of the three reagents (same as those used in the U_3O_8 and AmO_2-PuO_2 studies) would be most effective in dissolving the NpO_2. Results indicate that both the 4 N HNO_3-0.1 M $(NH_4)_2Ce(NO_3)_6$ and the 12 N HNO_3-0.05 N HF-0.01 N H_2SO_4 were successful in dissolving greater than 90% of the NpO_2 in 0.5 hr. The 8 N HNO_3, on the other hand, solubilized only 32% of the NpO_2 in 8 hr and hence would not be recommended as a leachant for NpO_2.

In other experiments, filter media contaminated with curium oxide were dissolved in leaching tests using both 4 N HNO_3-0.1 M $(NH_4)_2Ce(NO_3)_6$ and 12 N HNO_3-0.05 N HF. Each reagent dissolved essentially 100% of the CmO_2 in approximately 10 min and thus would be recommended for dissolving CmO_2 from filter media.

Filter media contaminated with thorium oxide were leached with a 4 N HNO_3-0.1 M $(NH_4)_2Ce(NO_3)_6$ solution in an attempt to dissolve the ThO_2. The rate of dissolution was slow at the beginning (0 to 7 hr) of the procedure, rapid from 7 to 9 hr, and slow again at the end (9 to 20 hr). Complete dissolution was achieved in 20 hr, a considerably longer period than for the other actinide oxides previously tested. A point of interest is that, in a similar experiment conducted using only 4 N HNO_3-0.1 M ceric ammonium nitrate and ThO_2 (no filter media), only 25% was dissolved after 20 hr. The reason for this difference is not presently understood. Therefore, it is concluded that 4 N HNO_3-0.1 M $(NH_4)_2Ce(NO_3)_6$ is an acceptable leaching reagent, even though the dissolution time was much longer for the ThO_2.

Several experiments were completed using PuO_2-contaminated filter media from spent glove-box filters in order to verify the flowsheet presented in the previous quarterly report[1] and to determine how much $(NH_4)_2Ce(NO_3)_6$ is required to dissolve PuO_2 from such filters. In one experiment, a 9.5-g sample of filter material was processed through a six-stage dissolution procedure. In the initial five stages, 4 N HNO_3-0.23 M $(NH_4)_2Ce(NO_3)_6$ was used; in the sixth stage, the leaching reagent was changed to 12 N HNO_3-0.1 N HF. An amount of $(NH_4)_2Ce(NO_3)_6$ equivalent to 60 times the initial moles of PuO_2 present in the filter media was used in each stage. The overall DF obtained for the process was 833. In a second experiment, a 25.6-g sample of filter material was processed through a four-stage dissolution procedure. The leaching solution was 4 N HNO_3-0.30 M $(NH_4)_2Ce(NO_3)_6$. An amount of ceric ammonium nitrate equivalent to 120 times the initial moles PuO_2 present in the filter media was used in each stage. The overall DF achieved in the process was 55.0.

In a third experiment, a 30-g sample of filter media was dissolved in a four-stage dissolution procedure. The amount of $(NH_4)_2Ce(NO_3)_6$ used in each stage of this process was based on the assumption that 0.01 mole of Ce^{4+} would oxidize 1 Ci (0.058 g) of ^{238}Pu. The overall DF achieved was 16.55. The flowsheet in the previous quarterly report[1] was based on the above assumption (0.01 mole of Ce^{4+} per curie of ^{238}Pu)

and an overall DF of 10,000. Since this degree of decontamination was not achieved, the flowsheet is not valid.

The amount of ceric ammonium nitrate required cannot be based exclusively on the amount of actinide present in the filter media because other reactants, such as the pack-to-frame sealant and other organic materials, are also present. A higher percentage of sealant was present in the 25.6-g sample, and this is perhaps why less PuO_2 was dissolved. In other words, even though more ceric ammonium nitrate was used per mole of PuO_2 present, a lower percentage of the PuO_2 was dissolved because a large percentage of the Ce^{4+} ions was depleted by the reaction with organics present. A formula for calculating the $(NH_4)_2Ce(NO_3)_6$ required per gram of filter media has not been developed. Additional experiments must be performed before this relationship can be established.

2.3 References for Section 2

1. D. W. Tedder and J. O. Blomeke (compilers), Actinide Partitioning and Transmutation Program Progress Report for Period April 1 to June 30, 1977, ORNL/TM-6056 (October 1977).
2. D. F. Luthy and E. L. Lewis, Decontamination of HEPA Filters: April-June 1977, MLM-2445, Fig. 6, p. 12 (September 1977).
3. W. L. McCabe and J. C. Smith, Unit Operations in Chemical Engineering, 2nd ed., McGraw-Hill, New York, 1967.

3. AMERICIUM-CURIUM RECOVERY WITH OPIX, TALSPEAK, AND CEC

W. D. Bond, C. W. Forsberg, F. A. Kappelmann, S. Katz, and F. M. Scheitlin
(Oak Ridge National Laboratory)

This work examines the use of oxalate precipitation and cation exchange (OPIX process) to remove the lanthanides and transplutonium actinides from the high-level liquid waste produced by the Purex solvent extraction process. Talspeak solvent extraction and cation exchange chromatography (CEC) are studied as methods of separating the lanthanides and trivalent actinides.

3.1 Introduction

The objectives of the work on oxalate precipitation and ion exchange (OPIX) during this period were to better understand the conditions and establish equipment requirements for separating the transplutonium actinides from the high-level waste by oxalate precipitation. In the conceptual flowsheets, the high-level raffinate from the first extraction cycle of Purex would be diluted with a mixture of oxalic and HNO_3 acids to achieve conditions favorable for the precipitation of the rare-earth and trivalent actinide oxalates. Following the dilution, this slurry would be centrifuged or, possibly, the precipitate could be separated by a gravity settler from the bulk of the fission products that do not form insoluble oxalates. The recovered precipitate would then be processed for a subsequent separation of the trivalent actinides from the rare earths. The oxalate supernate would be passed through an ion exchange bed for the removal of any residual actinides which did not precipitate. Experimentally, the goal is to find those conditions which maximize the desired separation with the minimum requirements of canyon space and equipment.

The reference Talspeak process flowsheet consists of two solvent extraction cycles for separating the trivalent actinides from the trivalent lanthanides. In the first cycle, the lanthanides are preferentially extracted into a 0.8 M solution of di(2-ethylhexyl)phosphoric acid (HDEHP) in diisopropylbenzene (DIPB) from an aqueous solution of

the trivalent elements in 1 M glycolic acid-0.025 M diethylenetriamine-pentaacetic acid (DTPA) at pH 3. In the second cycle, the aqueous raffinate from the first cycle is adjusted to pH 1.5 with HNO_3 and the actinides are recovered by extraction into 0.5 M HDEHP in normal dodecane (NDD). The separated actinides and lanthanides are then removed from their respective organic extracts by stripping with HNO_3.

Practical methods are not available for the purification of HDEHP from degradation products expected to be generated by radiation and hydrolysis, or from highly extractable elements which are likely to be present as impurities in the aqueous feed to the Talspeak process. The principal degradation product expected from HDEHP is mono-2-ethylhexylphosphoric acid (H_2MEHP). Highly extractable, difficult-to-strip elements that are expected to be impurities in Talspeak feeds include zirconium, molybdenum, plutonium, neptunium, and possibly ruthenium. In addition, the solubility limits of these elements in the extractant and aqueous phases may lead to the formation of precipitates or of a third organic phase. An aqueous oxalic acid solution has tentatively been selected in our reference flowsheet as the scrubbing reagent for elements that are difficult to strip from HDEHP, and ethylene glycol has been selected for the removal of H_2MEHP.

3.2 The OPIX Process

3.2.1 Previous work

Previous studies[1] have consisted of a few laboratory-scale batch precipitations of rare-earth and actinide mixtures from both synthetic* and actual high-level waste. The latter was produced by batch-extracting with TBP small amounts of dissolver solution generated by dissolving some spent LWR fuel. This fuel had been irradiated to 31,000 MWd per tonne of uranium in the Carolina Power and Light Company's H. B. Robinson Reactor and cooled 2 years. Gadolinium was added as a soluble poison, and conditions were adjusted to match those anticipated for the

*The composition of the synthetic waste is documented in ref. 2, p. 21.

operation of the Allied-General Nuclear Services (AGNS) plant at Barnwell, South Carolina. The raffinate had been evaporated to produce a waste concentrate which might be sent to HLLW storage. Under these conditions, the oxalate precipitation step appears favorable for removing actinides. Typical results, expressed as weight percent of the feed material precipitated, are presented in Table 3.1.

Additional experimental work was needed, however, to determine how effectively the precipitation and oxalate separation could be carried out in an open, continuous system where processing variables such as temperature, volumetric flow rates, and stirring speed for tank mixers can interact and affect the precipitation and recovery steps. Also, the flowsheet conditions[3] under consideration for partitioning purposes are different from those under consideration at AGNS.

3.2.2 Experimental techniques

Three sets of experiments, series A, B, and C, were conducted to establish some of the effects of various equipment configurations as well as those associated with a few of the operating variables. The equipment in series A consisted of a stirred tank (Fig. 3.1) with a paddle stirrer (Fig. 3.2) and a settler (Fig. 3.3) connected in series. The series B experiments utilized two stirred tanks with paddles identical to those used in series A. The effluent from the second stirred tank was then passed through the settler shown in Fig. 3.3. The equipment in series C consisted of a stirred tank and paddle (Figs. 3.1 and 3.2), followed by a settler (Fig. 3.4) consisting of two vertical, concentric columns. The waste slurry solution entered this latter settler through the smaller, cylindrical column at the top, traveled to the bottom of the inner column, and then proceeded up the outer, tapered column. Figures 3.5-3.7 further summarize the equipment configurations and show some of the other supporting apparatus as well.

Stirred tank reactors 4 in. in diameter and 8 in. high, with four equally sized baffles and a maximum capacity of 1600 ml (see Fig. 3.1) were used in each of the three series. During normal operation, the tanks were filled to 1 liter with solution.

Table 3.1. Hot-cell results[a,b,c] of actinide--rare-earth precipitation by oxalic acid

Isotope	Wt % in liquor	Wt % precipitated
^{242}Cm	0.42	94.4
^{244}Cm	0.38	94.1
^{137}Cs	94.3	0.09
^{106}Ru	93.9	0.99
^{144}Ce	2.73	89.0

[a]High yields difficult to measure; accuracy of yields may be ±30%.

[b]Numbers obtained through the courtesy of D. O. Campbell, ORNL.

[c]Results expressed as wt % of feed material.

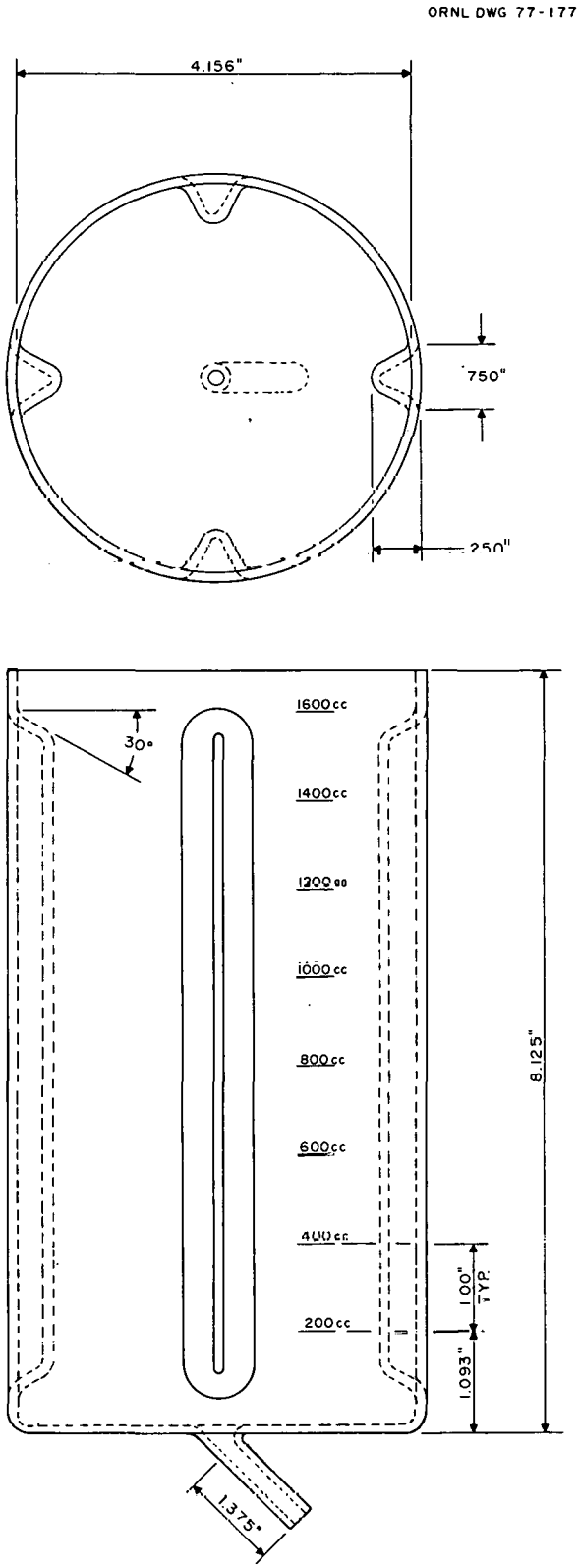

Fig. 3.1. Mixing tanks used in series A, B, and C experiments.

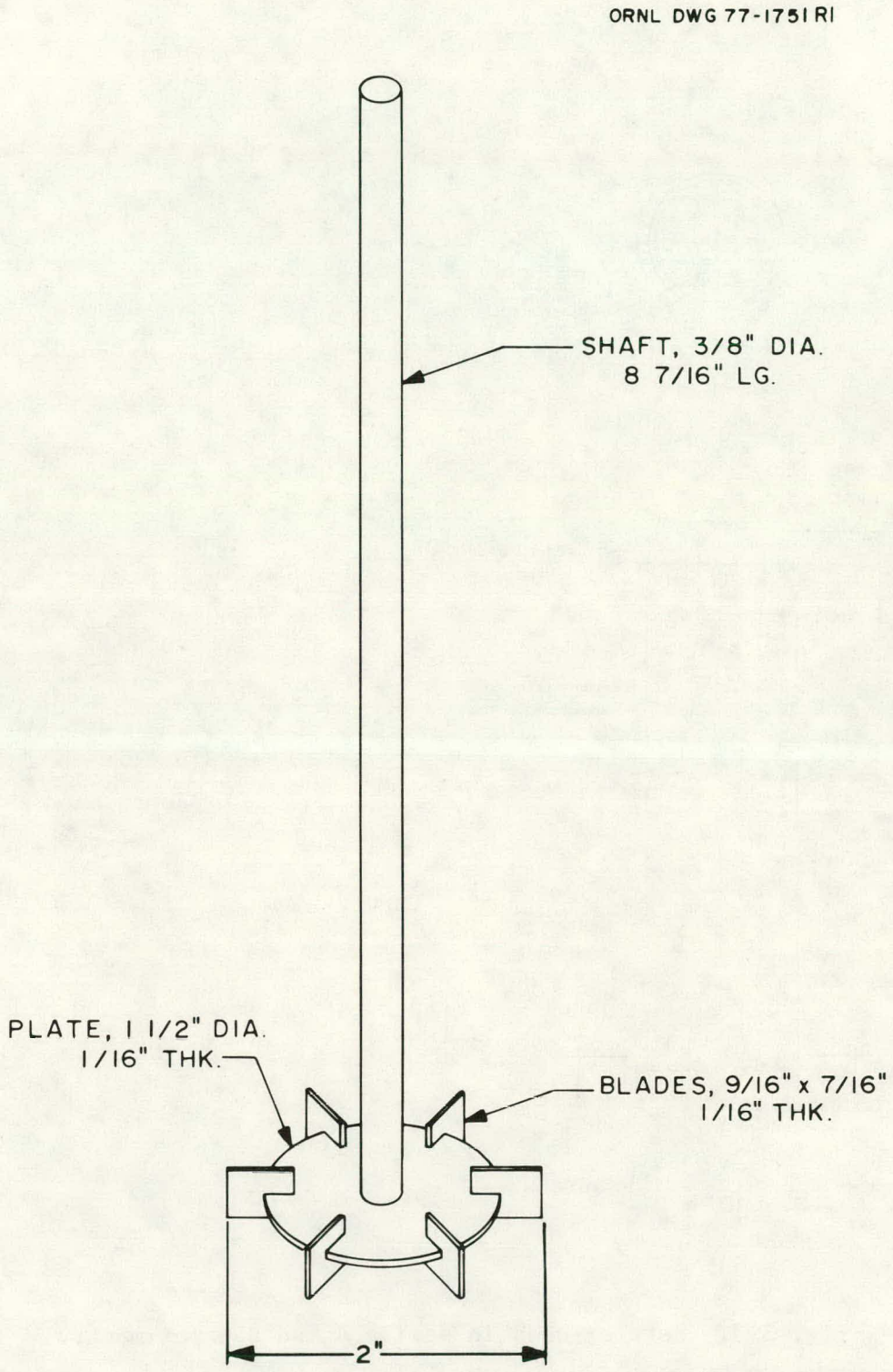

Fig. 3.2. Paddle stirrers used in series A, B, and C experiments.

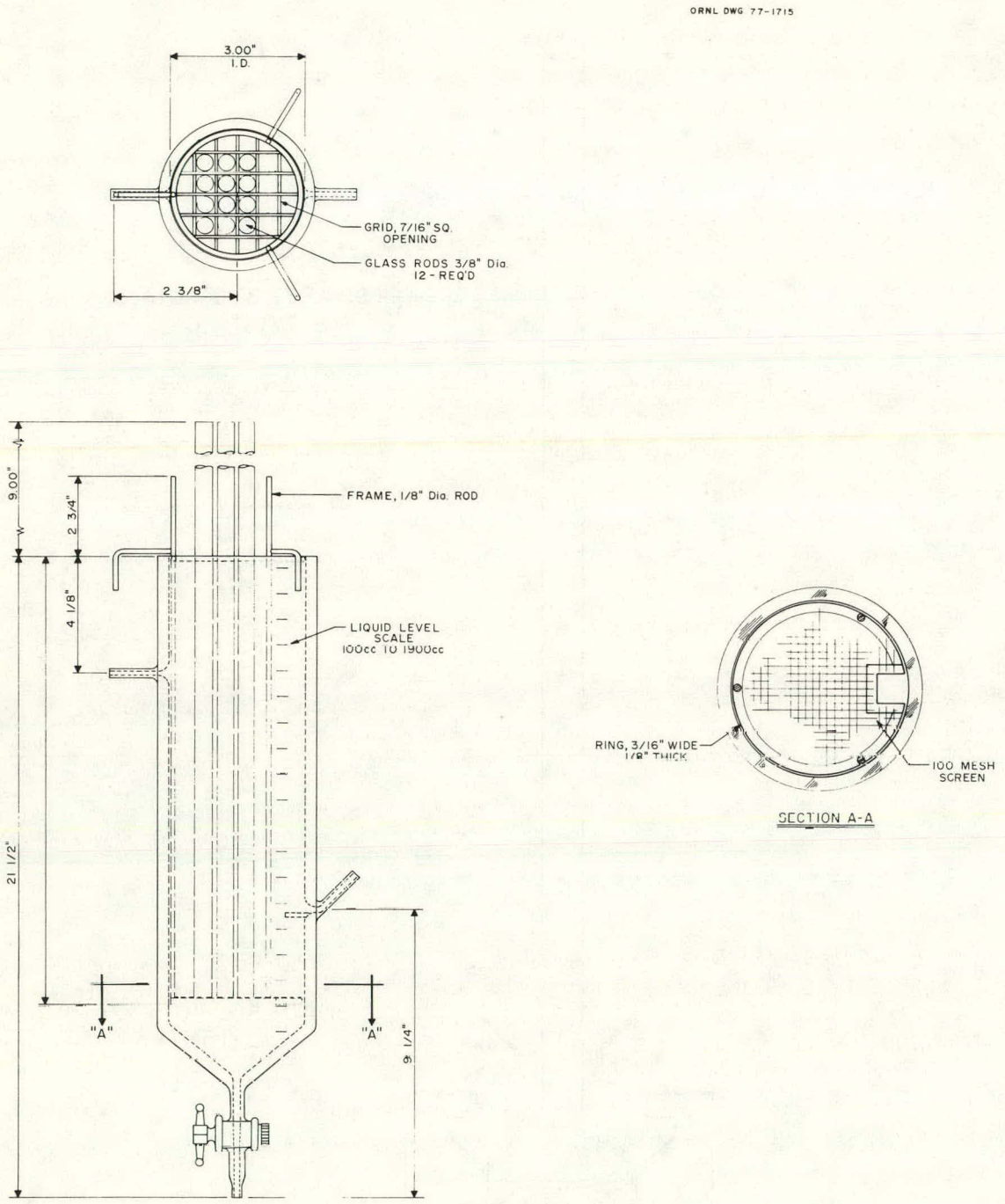

Fig. 3.3. Settler used in series A and B experiments.

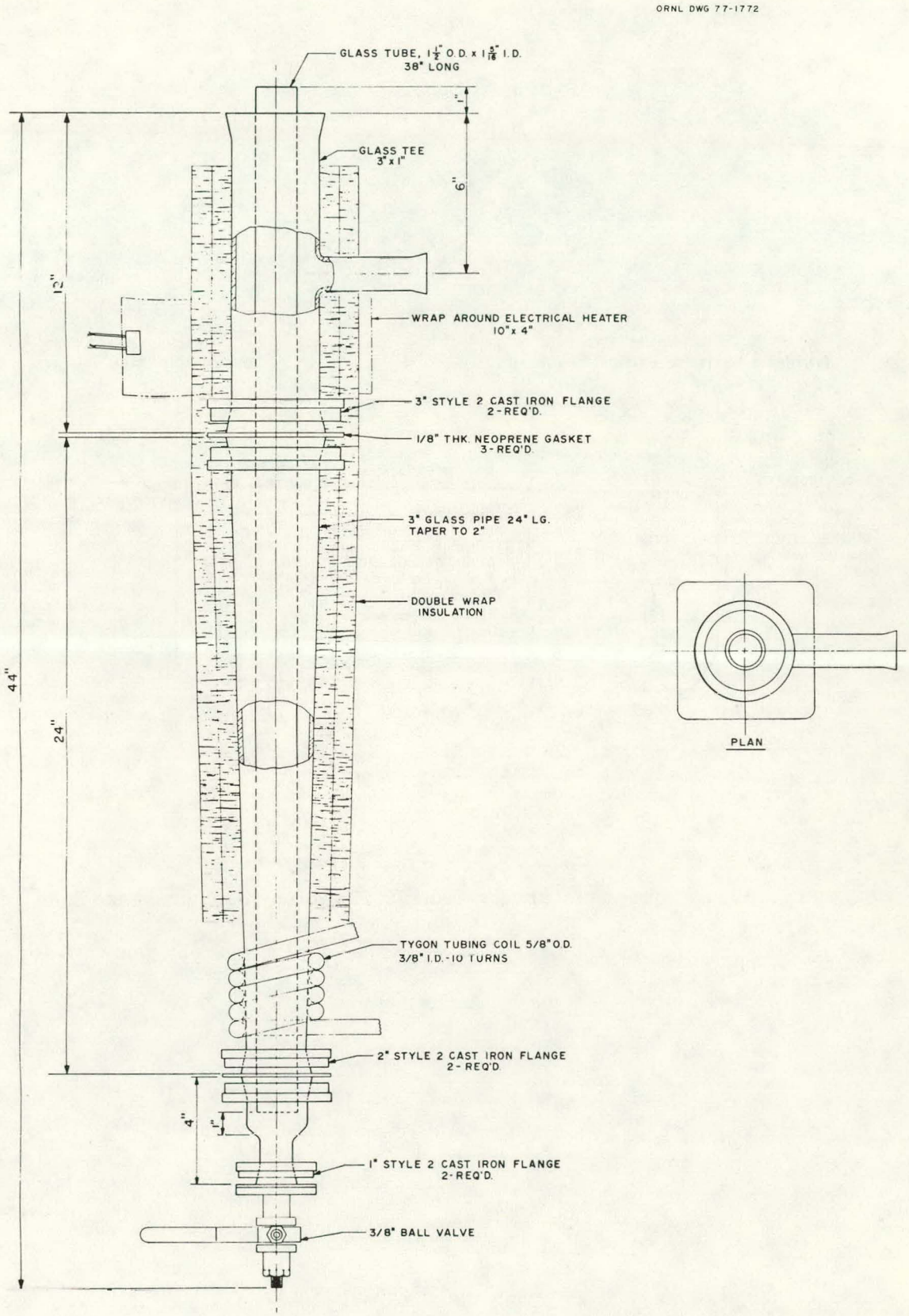

Fig. 3.4. Settler used in series C experiments.

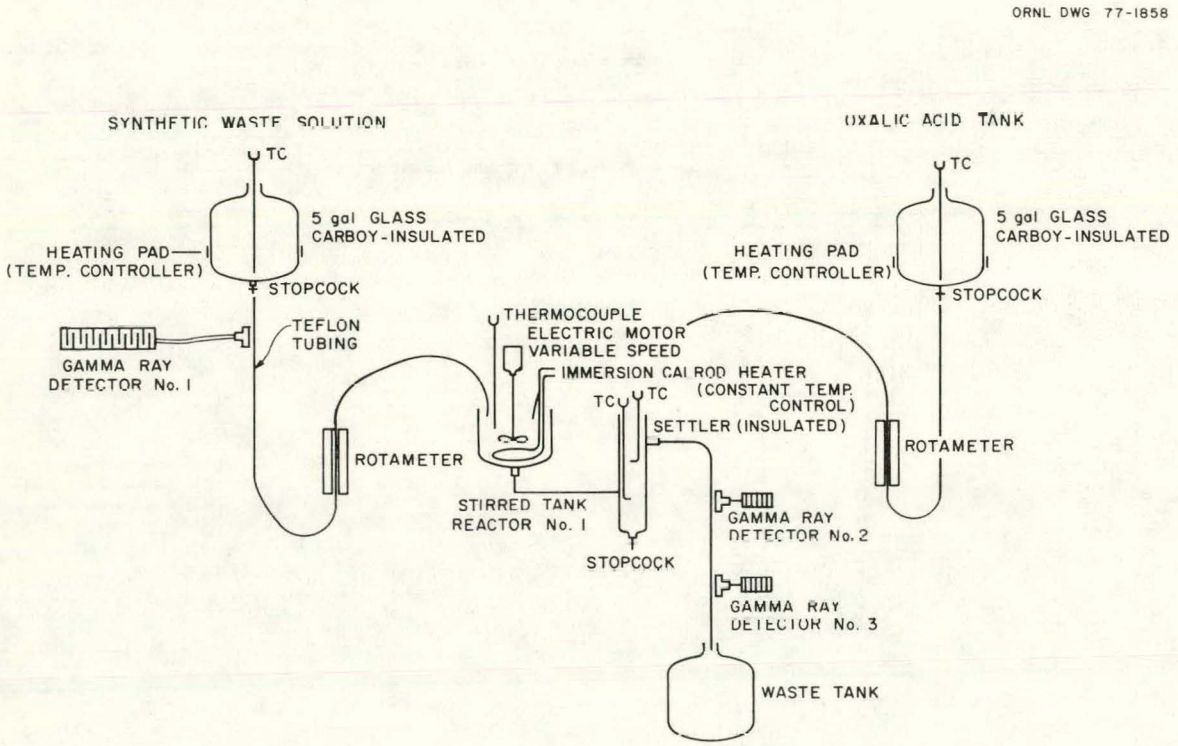

Fig. 3.5. Equipment arrangement for series A experiments.

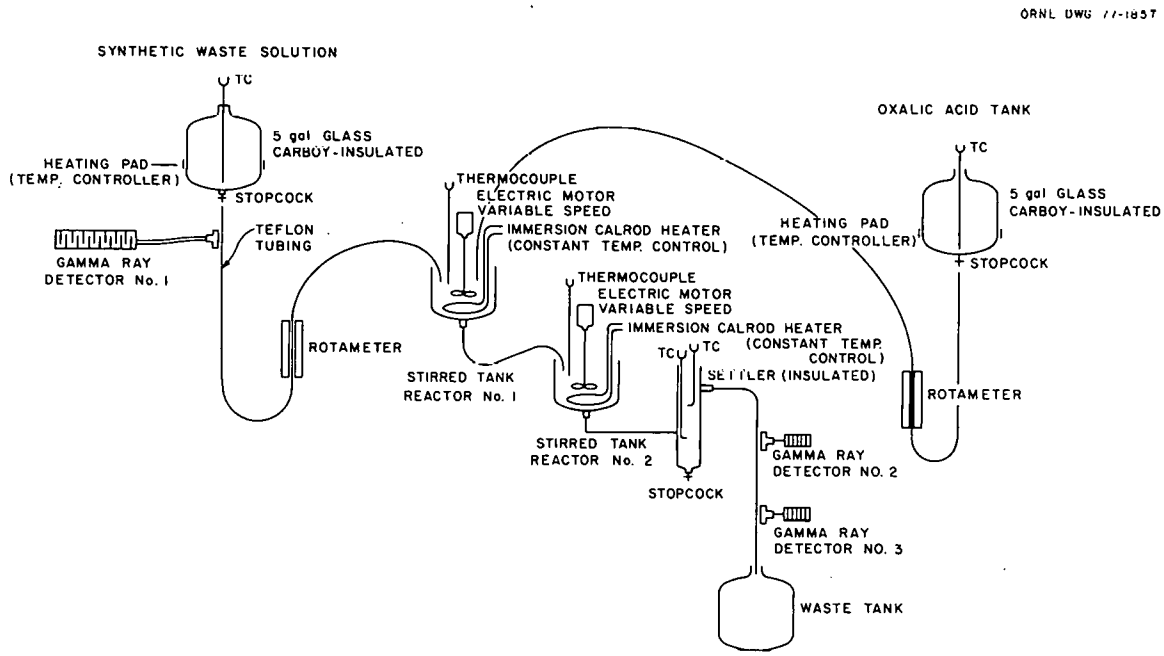

Fig. 3.6. Equipment arrangement for series B experiments.

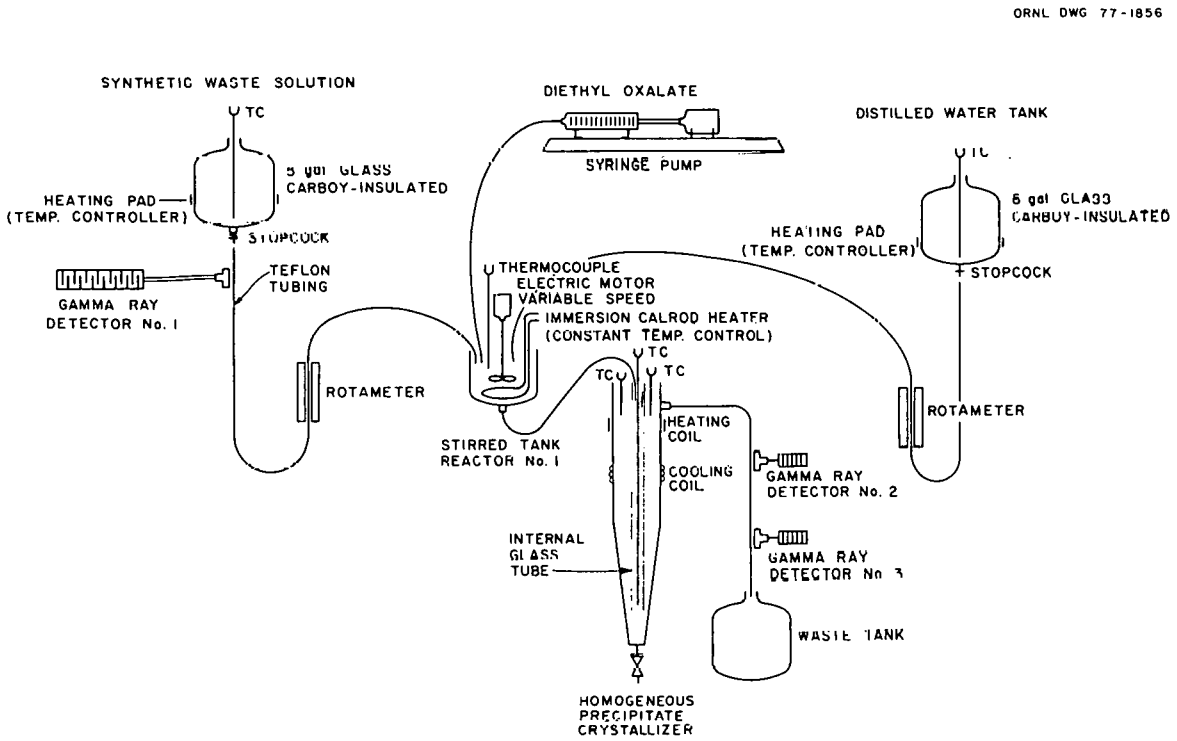

Fig. 3.7. Equipment arrangement for homogeneous precipitation in series C experiments.

The observations in these experiments were expressed as the calculated weight percent of ^{142}Pr tracer in the synthetic waste feed which was recovered as a precipitate. The praseodymium activity in the precipitates was measured by gamma-ray analysis. Since praseodymium is one of the more soluble of the rare-earth oxalates, the tracer measurements using ^{142}Pr are somewhat conservative when used as an indication of the total rare-earth removal from the waste solutions.

The estimation of the weight percents of actinides which would be precipitated under these conditions is more difficult since actinide tracers were not used experimentally, the solubilities of the actinide oxalates are generally lower than those of the rare earths, and carrier effects would be expected. The results in Table 3.1 suggest that the weight percent of curium precipitated, for example, would be greater than that of the cerium and probably the other rare earths as well. However, since gadolinium had been added to the waste to match the AGNS flowsheet conditions and the waste was evaporated first, the carrier effect in Table 3.1 is probably greater than that which would be observed under the flowsheet conditions examined here.

Two types of determinations were made during the experiments. The first type was that of the settler yield, which is simply the amount of precipitate removed from the flowing waste stream when the liquid leaves the settler used in a particular series. The other type was obtained by sampling the slurry in the stirred tank reactors and filtering the samples sequentially through 12-, 5-, and 1-μ filters. The data obtained in the latter type of determination are reported as a cumulative filter yield (i.e., the 1-μ yield equals the sum of the precipitates from the 12-, 5-, and 1-μ filters). During the experiments, the stirred tanks were maintained in a turbulent mixing mode so that the suspended slurry appeared to be completely uniform. If we assume that the slurry samples were representative, then the filter yields can be considered a measure of the particle size distribution of the precipitate.

The effects of four process variables on the precipitate yields were also investigated by performing half-factorial designs for series A and B experiments. The general 16-parameter model that results from

a full 2^4 factorial design is shown in Table 3.2, along with the definitions of variables for series A in the model. The definitions of the variables for series B are given in Table 3.3. Table 3.4 shows the confounding pattern for the parameters which results from the half-factorial designs used in these two experiments. Additional description of the factorial design method can be found elsewhere.[4]

3.2.3 Results of series A experiments

Series A experiments were carried out by mixing solutions of oxalic and HNO_3 acids with the synthetic high-level waste. The HNO_3 concentration was maintained at about 1 M in the stirred tank, but the oxalic acid concentration was varied* as the fourth independent variable (as defined in Table 3.2). The residence time in the stirred tank was the first independent variable, the temperature of the tank was the second, and the stirring speed in the tank was the third.

The precipitate yields, expressed as weight percents of the praseodymium in the feed, are summarized in Table 3.5 along with the process conditions. Table 3.6 summarizes the values of the confounded parameters that were calculated from the half-factorial design. As shown in Table 3.6, ∿56% of the rare earths (on the average) were recovered in the settler, whereas ∿72% (on the average) were recovered in the 1-μ filter. Apparently, ∿ % or more of the particulates were less than 12 μ in size and were not recovered by the settler. Ignoring any third-order interactions, the residence time and the oxalic acid concentration in the stirred tank appear to be the most important variables. Increasing these variables tends to increase the amount of precipitate recovered, presumably because of better crystal growth at the increased residence times and decreased oxalate solubilities due to higher concentrations of oxalic acid initially. The apparent temperature effect was also expected since the solubility of the oxalate increases with temperature. The effect apparently due to the change in stirring speed is less

*The oxalic acid concentration in the feed tank was varied, but the oxalic acid to waste flow rates were held constant at about 1.73:1 (see ref. 3, p. 35).

Table 3.2. General 16-parameter model and definitions of variables for series A experiments

General Model

$$\hat{y} = \beta_0 + \beta_1X_1 + \beta_2X_2 + \beta_3X_3 + \beta_4X_4 + \beta_{12}X_1X_2 + \beta_{13}X_1X_3 + \beta_{14}X_1X_4 + \beta_{23}X_2X_3 + \beta_{34}X_3X_4 + \beta_{123}X_1X_2X_3 + \beta_{124}X_1X_2X_4 + \beta_{134}X_1X_3X_4 + \beta_{234}X_2X_3X_4 + \beta_{1234}X_1X_2X_3X_4$$

Variables

$$X_1 = \frac{V_1 - 22.5}{7.5} \qquad X_2 = \frac{V_2 - 37.5}{12.5}$$

$$X_3 = \frac{V_3 - 187.5}{62.5} \qquad X_4 = \frac{V_4 - 0.38}{0.07},$$

where

V_1 = nominal stirred tank residence time, min;

V_2 = temperature of stirred tank, °C;

V_3 = stirrer speed, rpm;

V_4 = oxalic acid concentration in oxalic acid feed tank, M

Table 3.3. Definitions of variables for series B experiments

Variables
$X_1 = \frac{V_1 - 30}{10}$ $\quad X_2 = \frac{V_2 - 187.5}{62.5}$
$X_3 = \frac{V_3 - 187.5}{62.5}$ $\quad X_4 = \frac{V_4 - 0.38}{0.07}$,

where

V_1 = nominal stirred tank residence time, min;

V_2 = stirrer speed in tank 1, rpm;

V_3 = stirrer speed in tank 2, rpm;

V_4 = oxalic acid concentration in oxalic acid feed tank, M

Table 3.4. Confounding pattern of parameters resulting from half-factorial designs for series A and B experiments

Number	Calculated parameter	Confounding pattern in terms of the general model
1	γ_0	$\beta_0 + \beta_{1234}$
2	γ_1	$2(\beta_1 + \beta_{234})$
3	γ_2	$2(\beta_2 + \beta_{134})$
4	γ_3	$2(\beta_3 + \beta_{124})$
5	γ_4	$2(\beta_4 + \beta_{123})$
6	γ_{12}	$2(\beta_{12} + \beta_{34})$
7	γ_{13}	$2(\beta_{13} + \beta_{24})$
8	γ_{14}	$2(\beta_{14} + \beta_{23})$

Table 3.5. Initial experimental conditions and product yields for series A experiments

	Experiment number									
	15	16	17	18	19	20	21	22	23	24
Experimental Conditions										
Slurry residence time in reactor, min	15	30	30	15	30	15	15	30	22.5	22.5
Temperature of reactor, °C	25	25	50	50	25	25	50	50	37.5	37.5
Stirrer speed in reactor, rpm	125	250	125	250	125	250	125	250	187.5	187.5
Molarity of oxalic acid feed	0.31	0.31	0.31	0.31	0.45	0.45	0.45	0.45	0.38	0.38
Waste feed rate, cm^3/min	20.8	8.1	8.1	20.8	8.1	20.8	20.8	8.1	11.9	11.9
Oxalic acid feed rate, cm^3/min	41.6	19.6	19.6	41.6	20.7	40.8	40.8	20.7	27.0	27.0
Product Yield, %										
Settler	15.2	77.4	48.7	40.0	77.3	78.4	47.3	64.8	66.7	80.9
12-μm filter	30.7	77.9	38.7	36.2	77.3	78.2	35.5	76.7	76.0	76.5
5-μm filter	66.1	80.1	47.8	44.9	85.1	83.9	39.0	78.5	80.4	81.2
1-μm filter	76.1	82.6	57.0	49.8	88.0	88.2	45	86.2	84.7	84.9

Table 3.6. Confounded parameter values resulting from series A experiments

Confounded parameter	Parameter values			
	Settler	12-μ filter	5-μ filter	1-μ filter
γ_0	56.1	56.4	65.7	71.6
γ_1	21.9	22.5	14.4	13.7
γ_2	-11.9	-19.3	-26.3	-24.2
γ_3	18.0	21.7	12.3	10.1
γ_4	21.6	21.1	11.9	10.5
γ_{12}	-8.7	-0.6	6.8	10.6
γ_{13}	-9.9	-2.4	0.5	1.7
γ_{14}	-13.6	-2.4	6.0	6.8
95% confidence interval[a]	±90.6	±2.8	±5.0	±1.5

[a]One degree of freedom.

easily explained but may be attributable to decreased film resistance at the solid-liquid interface. It is not clear from these results whether any significant second-order interactions exist.

3.2.4 Results of series B experiments

Series B experiments were also carried out by mixing solutions of oxalic and HNO_3 acids with the synthetic high-level waste. Again, the HNO_3 concentration was held constant at 1 M, while the oxalic acid concentration was varied* over the same range as in series A. The residence times were varied as the first independent variable shown in Table 3.3; however, the center point was shifted upward to 30 min, although the range remained unchanged. Variables 2 and 3 in this series were the mixer speeds of the first and second tanks respectively. The ranges and center points for these variables were also the same as in the series A experiments; thus only the center point of the nominal tank residence time was shifted. The temperature in the series B experiment was held constant at 35°C, which was the temperature center point in series A.

The precipitate yields and operating conditions for this series of experiments are summarized in Table 3.7; the values of the confounded parameters are shown in Table 3.8. Comparison of the top row of Table 3.8 with that in Table 3.6 indicates that the conditions in the B series were more favorable. The average yield in the settler was almost 73%, nearly 17% higher on the average than achieved in series A. Moreover, the precipitates produced in series B were more nearly monosized, especially in the second stirred tank, since apparently only ∿5% of the precipitate was less than 12 μ in diameter.

In comparing Table 3.6 with Table 3.8, it is also apparent that the operating conditions used in the series B experiments are closer to those that maximize precipitate recovery since the major effects and interactions, in general, appear to be smaller in magnitude. It is also interesting to note that increasing the first tank stirrer speed

*See ref. 3, p. 35, for flowsheet.

Table 3.7. Initial conditions and product yields for series B experiments

	Experiment number										
	27	28	29	30	31	32	33	34	35	36	37
Experimental Conditions[a]											
Residence time per reactor, min	20	40	40	20	40	20	20	40	30	30	30
Stirrer speed in stirred tank reactor 1, rpm	125	250	125	250	125	250	125	250	187.5	187.5	187.5
Stirrer speed in stirred tank reactor 2, rpm	125	125	250	250	125	125	250	250	187.5	187.5	187.5
Oxalic acid concentration, M	0.31	0.31	0.31	0.31	0.45	0.45	0.45	0.45	0.38	0.38	0.38
Waste feed rate, cm^3/min	13	9.17	9.17	18	9.17	18	18	9.17	12.06	12.06	12.06
Oxalic acid feed rate, cm^3/min	32.33	15.77	15.77	32.33	16.50	32.08	32.08	16.50	21.83	21.83	21.83
Product Yield, %											
12-μm filter, STR 1	41.2	70.1	61.9	40.6	71.3	65.9	68.9	77.7	69.6	71.9	67.8
5-μm filter, STR 1	57.7	72.6	70.8	54.5	75.9	64.1	80.2	80.3	73.6	75.7	74.3
1-μm filter, STR 1	73.2	77.0	76.9	64.7	79.7	72.2	86.9	85.8	82.0	79.3	81.8
12-μm filter, STR 2	58.8	81.9	84.1	74.4	90.8	75.8	86.7	89.5	86.0	88.5	86.5
5-μm filter, STR 2	65.8	83.1	84.6	78.4	91.0	78.1	88.9	91.3	88.0	88.6	87.1
1-μm filter, STR 2	71.1	84.3	87.5	81.6	92.2	77.9	91.3	91.7	89.1	90.2	88.4
Settler	46.2	77.7	76.3	62.5	85.0	68.7	81.8	84.C	79.3	82.6	79.7

[a]Stirred tank temperatures were maintained at 35°C.

Table 3.8. Confounded parameter values resulting from series B experiments

Confounded parameter	Parameter values						
		Stirrer 1			Stirrer 2		
	Settler	12-μ filter	5-μ filter	1-μ filter	12-μ filter	5-μ filter	1-μ filter
γ_0	72.8	62.2	69.5	77.7	80.3	82.7	84.7
γ_1	15.0	16.1	10.8	4.4	12.7	9.7	8.5
γ_2	0.9	2.7	-3.3	-5.5	0.3	0.2	-1.7
γ_3	6.7	0.2	3.8	1.7	6.9	6.2	6.7
γ_4	14.2	17.5	11.2	6.9	10.9	9.4	7.1
γ_{12}	-0.7	4.6	5.4	8.6	-2.1	-0.8	-0.2
γ_{13}	-5.0	-1.0	-2.6	1.2	-6.4	-5.4	-5.3
γ_{14}	-6.7	-9.0	-4.8	-1.1	-3.8	-2.1	-1.1
95% confidence interval[a]	±5.5	±6.3	±3.2	±4.5	±4.0	±1.6	±2.8

[a]Two degrees of freedom.

appears to decrease the amounts of <5-μ particulates recovered. Comparison of the differences in the magnitudes of apparent primary effects (assuming that the third-order interactions are not important) between the two tables suggests that a small increase in residence time decreases the sensitivity of the process to the remaining variables. Hence the operating conditions for the series B experiments are somewhat more stable to perturbations than those for series A.

During these runs, the slurry in the downstream tank was noticeably clearer than that in the upstream tank. Since the feed to the second tank was taken from the bottom of the first tank, some preferential removal of the larger particles from the upstream tank occurred. Consequently, the smaller, more easily fluidized particles were retained in the first tank for longer periods on the average. Thus, the geometry of the two-tank system also appears to favor the formation of larger, more uniform particulates through this segregation effect.

3.2.5 Results of series C experiments

A few experimental runs were performed to determine the effects of homogeneous precipitation. In these runs, diethyl oxalate rather than oxalic acid was added to the stirred tank. Under the flowsheet conditions, diethyl oxalate slowly undergoes hydrolysis to form oxalic acid and ethanol. The slow release of oxalic acid favors the formation of larger, more perfect crystals.

The results of these experiments (summarized in Table 3.9) show that, whereas only moderate yields were obtained, the crystals collected from the bottom of the settler were about five times as large as those recovered from the stirred tank. Therefore, the crystals produced by the homogeneous precipitation technique were larger, but also fewer in number.

3.2.6 Summary and conclusions

The following conclusions can be drawn, based on the work completed to date:

Table 3.9. Initial conditions and product yields for series C experiments

	Experiment number				
	41	42	43	44	45
Experimental Conditions					
Residence time in reactor, min	60	90	90	60	120
Temperature of top of column, °C	60	60	79.45	79.45	60
Temperature of bottom of column, °C	30.2	28.8	30	32.6	26.9
Feed rate, cm^3/min	15.31	10.19	10.19	15.31	7.81
Water rate, cm^3/min	27.08	18.55	18.55	27.08	14.58
Diethyl oxalate rate, cm^3/min	1.67	1.08	1.08	1.67	0.85
Equivalent $(COOH)_2$ concentration, M	0.31	0.31	0.31	0.31	0.31
Product Yield, %					
12-μm filter	5.68	11.24	2.81	7.49	-15.11[a]
5-μm filter	21.84	51.17	34.39	60.24	71.27
1-μm filter	41.11	69.60	71.60	73.93	75.11
Exit stream	15.13	12.31	7.71	15.84	10.22

[a]The precipitation yields were calculated by differencing the feed and filtrate ^{141}Pr concentrations. The observed negative yield is attributable to experimental error since the minimum yield is 0%.

1. Because of the small particle size distribution and the problems caused by thermal gradients, centrifugation would probably be preferred over gravity settling to remove the solids from the high-level waste.
2. Two tanks in series appear to give a more monosized and uniform product than a single tank.
3. Precipitate recoveries in excess of 90 wt % can probably be achieved in a well-designed continuous system.

Although the amount of actinides (weight percent) precipitated by this process was not measured, it can be inferred from the data in Table 3.1 that this yield would probably be in excess of 90%. Consequently, the overall americium and curium removal from the high-level waste (99.9%) required for partitioning purposes could probably not be achieved by oxalate precipitation alone; however, it may be achievable when the oxalate supernate is subsequently passed through an ion exchange column.

Finally, it should be mentioned that small amounts of precipitate appeared to plate out on the stainless steel parts of the system during some of the runs. No significant plating-out was observed on the glass components. Although the plated-out material was easily removed with 3 M HNO_3, this occurrence could be indicative of significant scaling problems in a commercial-size system. Also, it was observed that, during the series B runs, this plating-out effect was strictly confined to the first stirred tank.

3.3 Talspeak Studies

During this quarter, the work on Talspeak encompassed three areas:

1. mixer-settler studies of the extraction of rare earths in the first Talspeak cycle and of the effects of zirconium impurity;
2. batch extraction tests on the effects of DTPA concentration, H_2MEHP impurity concentration, and extraction kinetics; and
3. an evaluation of solid sorbents for removing H_2MEHP from the ethylene glycol scrub liquid used for purification of HDEHP before recycle.

3.3.1 Mixer-settler studies

Experimental runs were made on the first cycle of Talspeak using the reference flowsheet[3] (Fig. 3.8). Table 3.10 shows the flow rates that were employed. Neodymium, the least extractable lanthanide, was used to simulate the extraction and stripping behavior of the lanthanides and to determine the overall performance of the flowsheet. The behavior of zirconium, a potential feed impurity, was observed by using a zirconium concentration of 10^{-4} M in some of the rare-earth feed solutions. All experimental runs were performed at 43°C. Variables in the runs included: (1) neodymium concentration in the feed solution, (2) pH of the aqueous feed and scrub solutions, and (3) HNO_3 concentration of the stripping solution.

Neodymium concentration in feed. Increasing the neodymium concentration from 4.8 g/liter to 6.3 g/liter had no effect on measured losses. For each concentration, the losses were ∿0.3% to the aqueous stream (1AP) and 0.06% to the stripped extractant (2AP). The 0.06% loss to the 2AP stream is the lower limit of detection of neodymium. Steady state was attained after about 4 hr of operation (Fig. 3.9). Concentrations in the 2AP stream were below the analytical limit of detection (<2 μg/ml) throughout the entire run. A profile of the steady-state neodymium concentration in the extraction-scrubbing bank for a typical run is shown in Fig. 3.10. These results indicate that the lanthanide contamination in an americium-curium product (1AP) would be very low.

Effect of pH. Increasing the pH of the feed and scrub solutions from 3.0 to 3.5 decreased the distribution coefficients, D_A^o (Nd),* of neodymium (Table 3.11). Under the flow conditions used, the losses of neodymium would be considerably greater using the higher pH as noted by the concentration profiles shown in Fig. 3.11.

Effects of zirconium impurity and DTPA concentration of the scrub solution. Two runs, TAL-4 and TAL-5, were made in which zirconium was present in the feed at a concentration of 10^{-4} M. Concentrations of

*The distribution coefficient, D_A^o, is defined as the organic-phase concentration divided by the aqueous-phase concentration when the two phases are at chemical equilibrium.

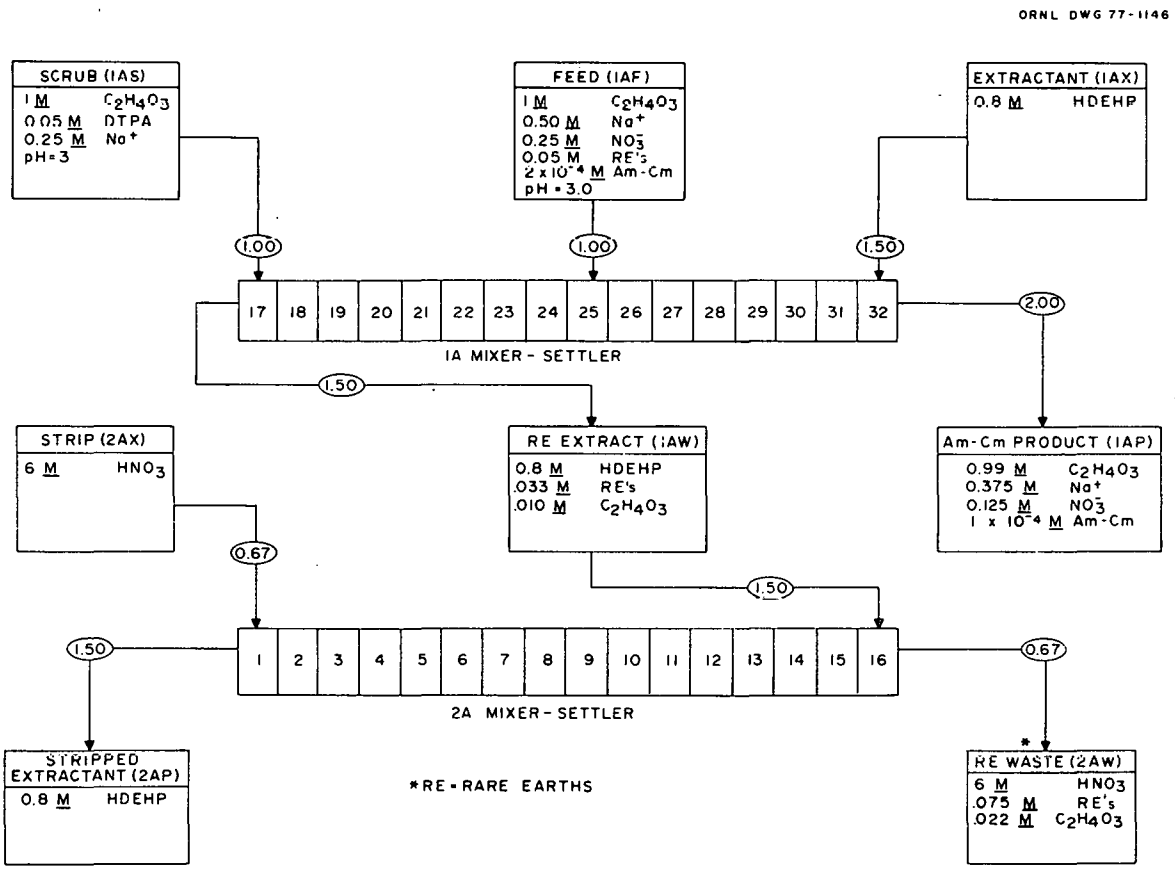

Fig. 3.8. Flowsheet for experimental run on first Talspeak cycle in 16-stage mixer-settlers.

Table 3.10. Reference flowsheet conditions for the first-cycle Talspeak experiments

Temperature: 43°C

Stirrer speed: 1000 rpm extraction scrubbing bank
1100 rpm stripping bank

Run time: 7.5-9.0 hr

Process stream	Flow rate (liters/hr)	Composition
Feed (IAF)	0.5	1 M $C_2H_4O_3$, 0.36 M Na, 4.8-6.5 g/liter Nd, pH 3.0
Solvent (IAX)	0.75	0.8 M HDEHP-DIPB
Scrub (IAS)	0.5	1 M $C_2H_4O_3$, 0.05 M DTPA, pH 3.0
Strip (2AX)	0.375	1 to 6 M HNO_3

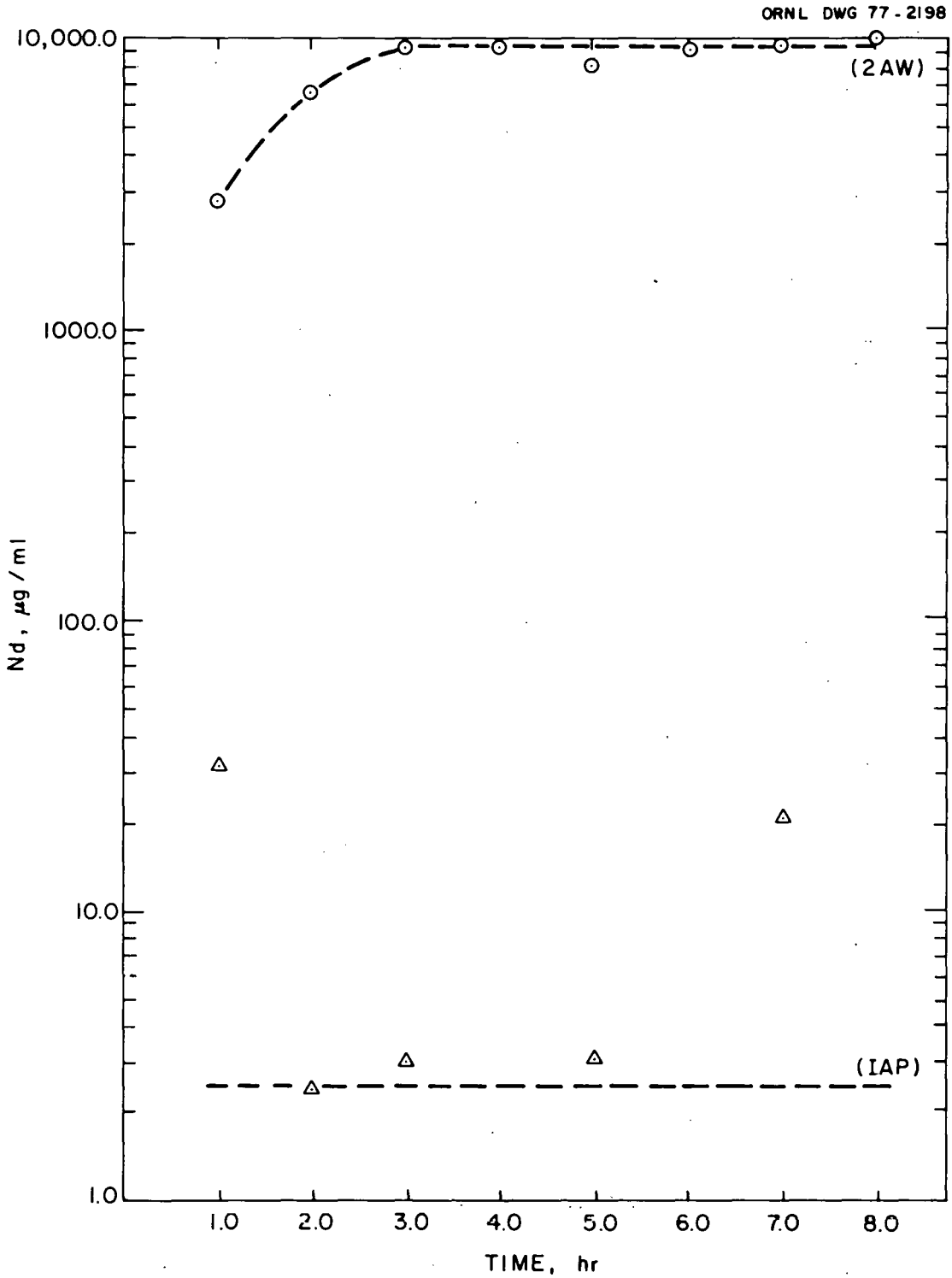

Fig. 3.9. Neodymium concentrations of end streams as a function of time (run TAL-2).

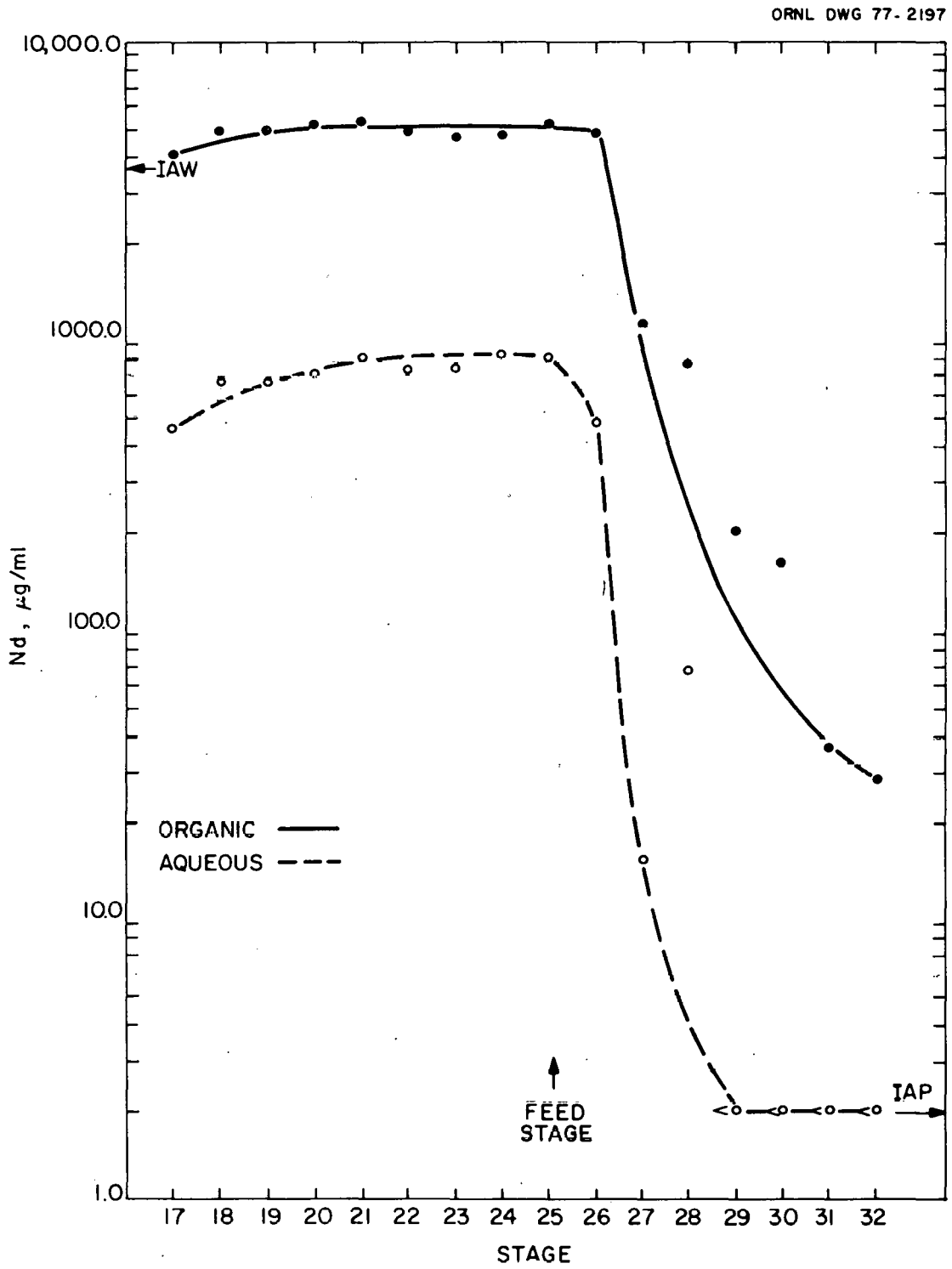

Fig. 3.10. Profile of neodymium concentrations in the extraction-scrubbing bank for run TAL-2.

Table 3.11. Neodymium concentrations and distribution coefficients in the extraction-scrubbing bank for runs TAL-2 and TAL-3

Nd concentration in feed: 6.3 g/liter, TAL-2; 6.1 g/liter, TAL-3

pH of feed and scrub solutions: 3.0, TAL-2; 3.5, TAL-3

TAL-2			TAL-3		
Stage number	Aqueous Nd conc. (μg/ml)	D_A^o (Nd)	Stage number	Aqueous Nd conc. (μg/ml)	D_A^o (Nd)
17	460	9.04	17	640	5.8
18	650	7.53	18	960	4.41
19	660	7.47	19	1250	3.64
20	700	7.43	20	1260	3.38
21	800	6.74	21	1460	3.27
22	720	6.89	22	1510	2.93
23	730	6.55	23	1510	3.33
24	830	5.76	24	1640	3.48
25	810	6.42	25	1460	3.98
26	480	10.02	26	1380	3.25
27	150	7.13	27	1220	3.99
28	69	11.3	28	1640	2.62
29	<2	-	29	982	4.20
30	<2	-	30	664	2.71
31	<2	-	31	256	3.16
32	<2	-	32	Sample lost	-

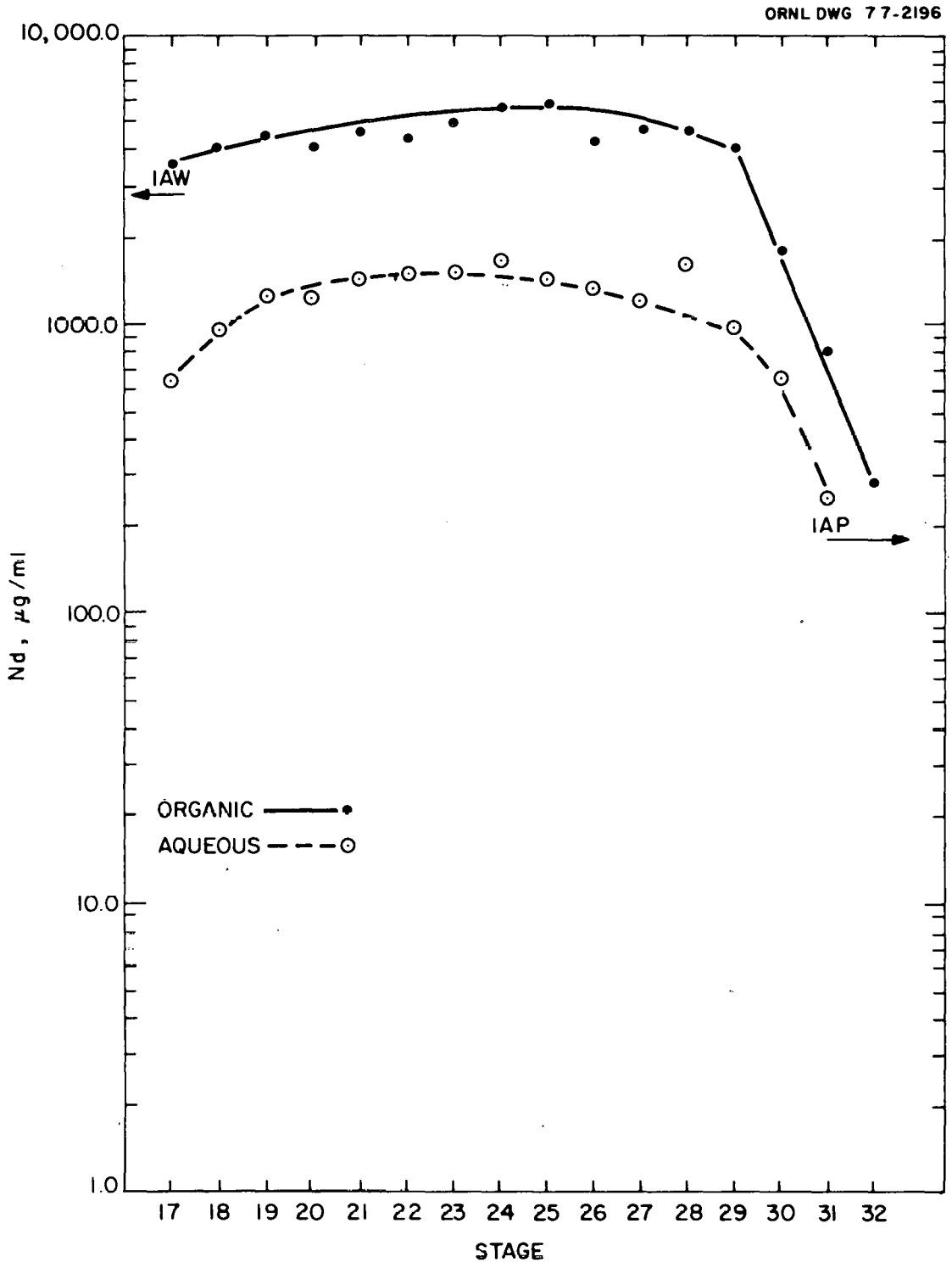

Fig. 3.11. Profile of neodymium concentrations in the extraction bank for run TAL-3.

0.05 and 0.1 M DTPA, respectively, were used in the runs. Flow conditions were the same as those stipulated in the reference flowsheet. Data from these runs are compared with those for runs TAL-1 and TAL-2 in Table 3.12. An unexpected result was the much higher neodymium losses when zirconium was present in the feed. Increasing the DTPA concentration increased the neodymium losses (from 3% to 4.5%). No emulsions or interfacial accumulation (sometimes called cruds) were observed in the extraction-scrubbing bank during runs TAL-4 and TAL-5. However, emulsions were formed in stages 10 through 16 in the stripping bank, and some crud accumulated at the interface of stage 16 where the lanthanide-loaded extractant enters.

It is difficult to see why the presence of 10^{-4} M zirconium in the feed would result in an order-of-magnitude increase in the loss of neodymium to the 1AP stream. The reproducibility of measured losses to the 1AP stream with no zirconium present was quite good: 0.32% for run TAL-2 and 0.43% for TAL-1 (which was reported last quarter). Further experiments will be required to determine the cause of the higher apparent losses of neodymium to the 1AW stream when zirconium is present. Analyses of end streams as a function of time (Fig. 3.12) indicated that steady state was attained in the 8-hr runs.

Figure 3.13 shows a profile of the neodymium throughout the extraction-scrubbing bank. Neodymium distribution coefficients for run TAL-5 are given in Table 3.13. Zirconium distribution coefficients were not measured because of the low concentrations of zirconium ($\leq 10^{-4}$ M).

Effect of HNO_3 concentration in stripping. Successful stripping runs were made using HNO_3 concentrations of 1, 2, 4, and 6 M. Very good phase separation was obtained at 2 M HNO_3. The aqueous neodymium concentrations and the distribution coefficients for the stripping bank using 2 M HNO_3 are listed in Table 3.14. The variation of D_A^o (Nd) values in stages 1 through 11 reflects the accuracy of the analytical method at these low levels of neodymium concentration. The neodymium concentration profile (Fig. 3.14) indicated that >95% of the neodymium was stripped from the extractant after five stages (i.e., stages 11-16).

Table 3.12. Effects of zirconium and DTPA concentrations on exiting process streams

	Run number			
	TAL-1	TAL-2	TAL-3	TAL-4
Feed concentrations				
Nd, g/liter	4.8	6.3	6.5	6.1
Zr, M	None	None	10^{-4}	10^{-4}
DTPA conc. in scrub, M	0.05	0.05	0.05	0.1
Nd content of stream, %				
1AP	0.43	0.32	3.0	4.3
2AW	93	99.6	96.9	95.6
2AP	0.06	<0.08	0.08	0.07

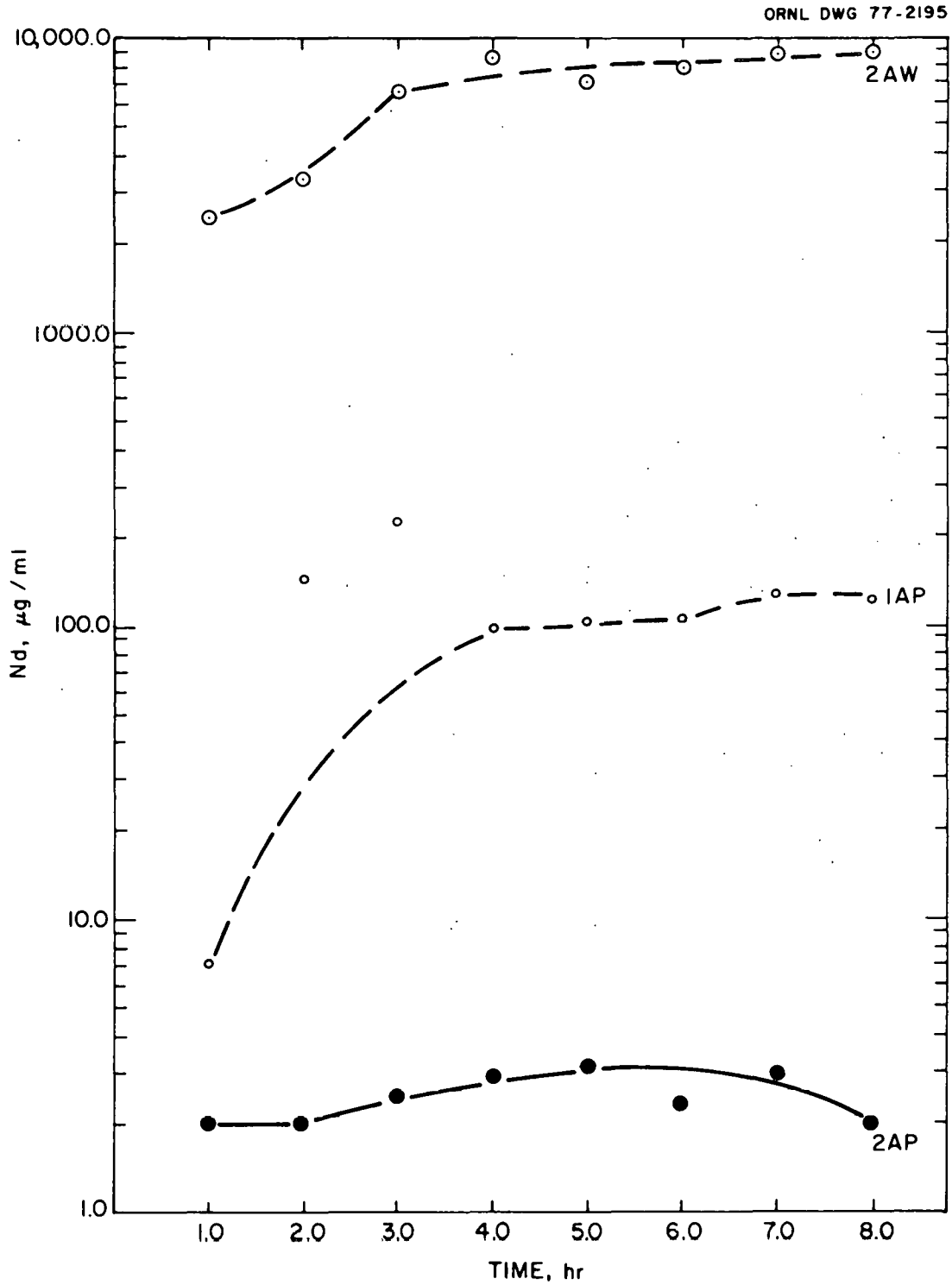

Fig. 3.12. Neodymium concentrations of end streams as a function of time (run TAL-5).

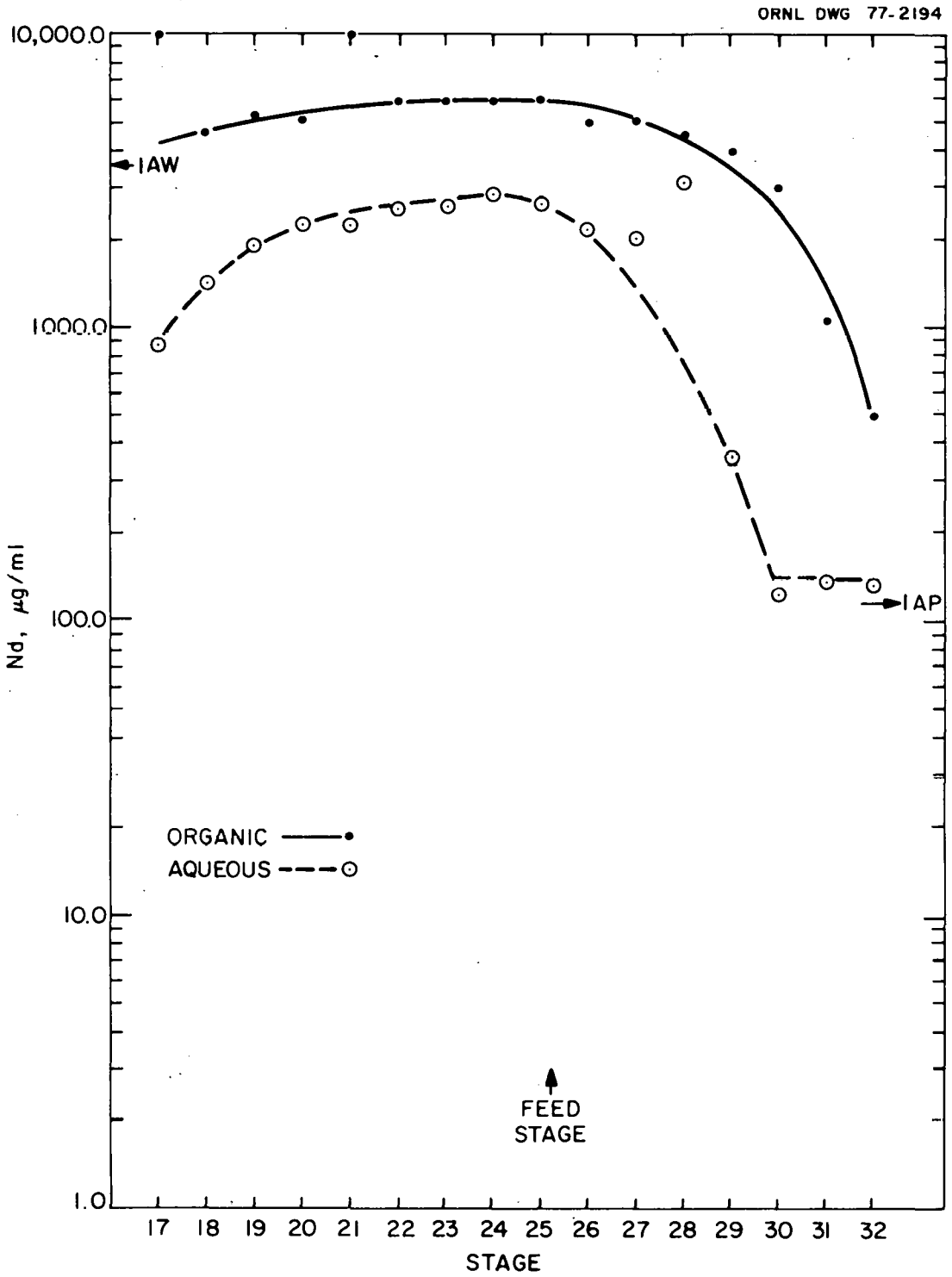

Fig. 3.13. Profile of neodymium concentrations in the extraction-scrubbing bank for run TAL-5.

Table 3.13. Neodymium concentrations and distribution coefficients in the extraction-scrubbing bank for run TAL-5

Feed: 6.1 g/liter Nd, 10^{-4} M Zr, 1 M glycolic acid, pH 3.0

Scrub: 1 M glycolic acid, 0.1 M DTPA, pH 3.0

Stage number	Aqueous Nd conc. (μg/ml)	D_A^o (Nd)
17	880	11.81
18	1430	3.30
19	1920	2.77
20	2240	2.12
21	2250	4.48
22	2570	2.24
23	2530	2.31
24	2880	2.07
25	2660	2.21
26	2140	2.32
27	2020	2.42
28	3170	1.42
29	360	1.1
30	-	-
31	139	7.76
32	135	3.60

Table 3.14. Neodymium concentrations and distribution coefficients in the stripping bank for run TAL-3

Strip solution (2AX): 2 M HNO_3

Stage number	Aqueous Nd conc. (μg/ml)	D_A^o (Nd)
1	<2	-
2	<2	-
3	2.0	8.5
4	3.0	2.33
5	6.8	0.88
6	3.0	3.66
7	3.0	-
8	3.0	1.66
9	3.0	2.0
10	24.0	0.25
11	8.0	1.25
12	56.0	0.089
13	204	0.083
14	515	0.018
15	2200	0.01
16	7810	0.096

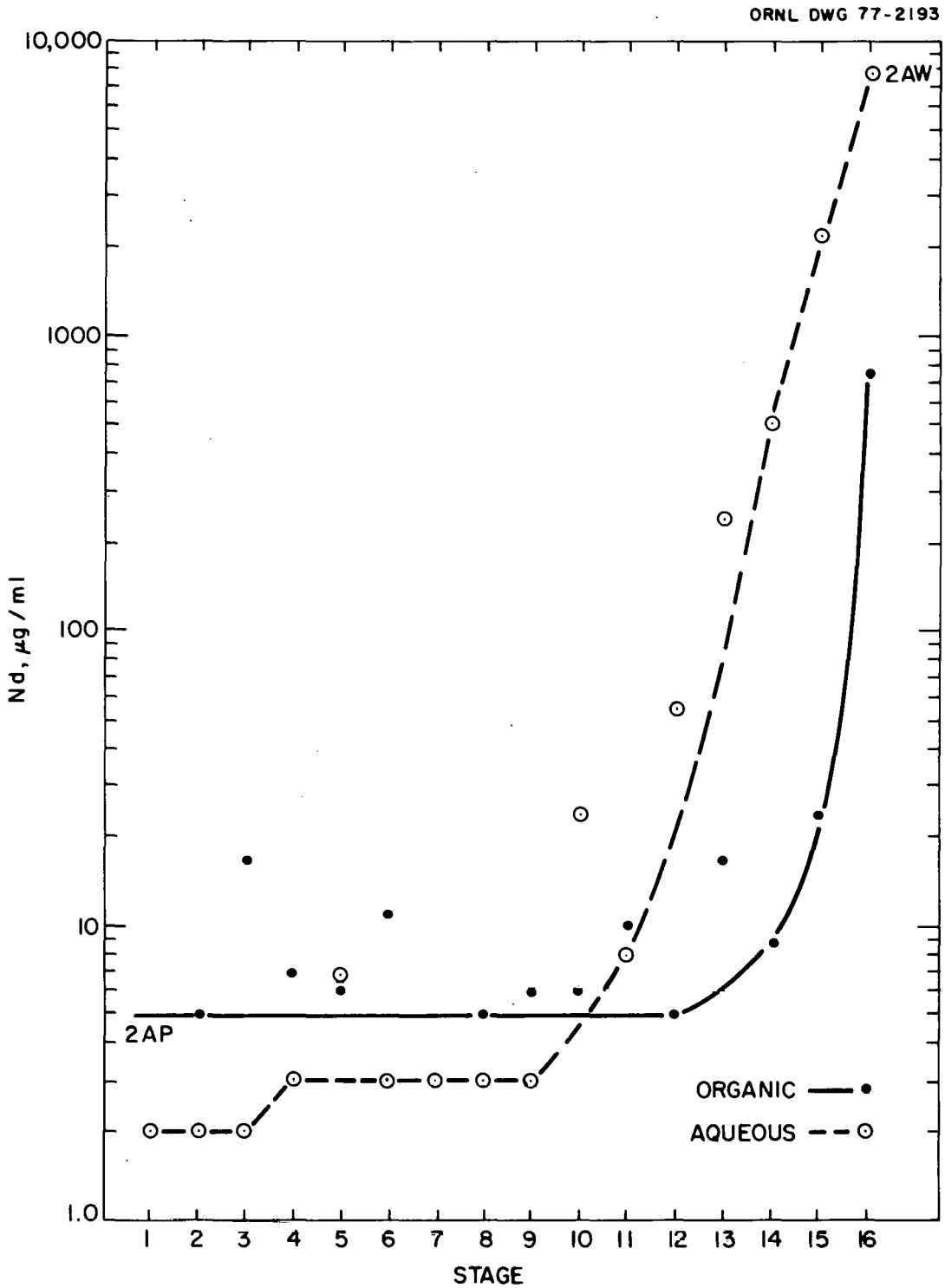

Fig. 3.14. Profile of neodymium concentrations in the stripping bank for run TAL-3.

3.3.2 Batch extraction experiments on Talspeak

Batch extraction experiments were carried out to determine the effects of H_2MEHP impurity, phase contact time, DTPA concentration, and metal loading on the D_A^o (Am) and D_A^o (Eu) in the extraction steps of the Talspeak process. Europium-152,154 and americium-241 tracers were utilized for analyses by radiometric assay. Compositions of the extractant phases were those of the reference flowsheet.[3] The composition of the extractant utilized for first-cycle preferential extraction of rare earths was 0.8 M HDEHP-DIPB. The extractant composition was 0.5 M HDEHP-NDD for the second-cycle extraction of americium. In most experiments, each extractant was purified of H_2MEHP impurity before use by making five equal-volume contacts of the extractant phase with 1 M glycolic acid-0.05 M DTPA at pH 3. However, in experiments on the effects of added H_2MEHP impurity, the extractants were not purified.

The effects of H_2MEHP impurity and DTPA concentration are shown in Tables 3.15 and 3.16. With 0.8 M HDEHP-DIPB, the D_A^o (Am) and D_A^o (Eu) increased with increasing H_2MEHP concentration when the DTPA concentration in the aqueous phase was 0.025 M. The separation factor was observed to decrease with the quantity of added H_2MEHP. However, when the DTPA concentration was 0.05 M, the D_A^o values generally decreased with increasing H_2MEHP impurity. With the 0.5 M HDEHP-NDD extractant and an aqueous-phase DTPA concentration of 0.05 M, the D_A^o values for americium increased and those for europium decreased when the H_2MEHP concentration was increased (Table 3.16).

The effects of contact time and rare-earth loading are shown in Table 3.17. The D_A^o for europium increased by a factor of about 2 when the contact time was increased from 2 min to 6 min. Slow kinetics for the extraction of europium have previously been observed.[5,6] When the europium concentration was increased by adding inactive europium to the tracer-level solutions, the D_A^o values decreased approximately in the manner expected for third-power dependence[5,6] on the free HDEHP concentration. This result would indicate that the rate of approach to equilibrium is not dependent on the initial europium concentration.

Table 3.15. Effects of H_2MEHP and DTPA concentrations on preferential extraction of lanthanides

Temperature: 25°C
Contact time: 2 min
Organic phase: 0.8 M HDEHP-DIPB
Aqueous phase: 1 M glycolic acid, pH 2.9

Added H_2MEHP (M)	0.025 M DTPA			0.05 M DTPA		
	D_A^o (Am)	D_A^o (Eu)	SF[a]	D_A^o (Am)	D_A^o (Eu)	SF[a]
0	1.53	86	56	1.54	21	13
0.002	1.64	83	50	0.31	3.3	11
0.006	1.88	110	59	0.35	3.8	11
0.019	2.56	110	43	0.43	4.8	11
0.056	5.41	169	31	0.48	11.6	24

[a]SF = separation factor, which is defined as D_A^o (Eu)/D_A^o (Am).

Table 3.16. Effect of H_2MEHP concentration on second-cycle extraction

Temperature: 25°C
Contact time: 2 min
Organic phase: 0.5 M HDEHP-NDD
Aqueous phase: 1 M glycolic acid-0.05 M DTPA, pH 1.3

H_2MEHP (M)	D_A^o	
	Am	Eu
0	34	554
0.002	26	-
0.006	46	171
0.019	115	186
0.056	99	260

Table 3.17. Effects of contact time and europium concentration on Talspeak extraction

Temperature: 25°C

Aqueous phase: 1 M glycolic acid; 0.05 M DTPA

Contact time (min)	pH	Inactive Eu (M)	D_A^o		D_A^o (Eu)
			Am	Eu	D_A^o (Am)
0.8 M HDEHP-DIPB					
2	3.0	A[a]		13.8	
6	3.0	A		25.6	
6	2.9	A	0.8	18.2	22.8
10	3.0	A		21.6	
6	1.3	A	10.3	73.3	7.1
2	3.0	0.015		10.1	
6	3.0	0.0015		35.5	
6	3.0	0.0072		32.9	
6	3.0	0.015		26.8	
6	3.0	0.029		22.1	
0.5 M HDEHP-NDD					
6	2.9	A	1.55	27.1	17.5
6	1.3	A	24.4	115	4.7

[a] A = inactive europium absent.

The distribution coefficients for americium using an aqueous-phase pH of 1.3 were sufficiently high to use either DIPB or NDD as the diluent for the second extraction cycle of Talspeak.

Conclusions from the results obtained during this report period may be summarized as follows:

1. An H_2MEHP impurity concentration of the order of 0.01 M will not significantly affect the actinide/lanthanide separation factor. On the other hand, it may have deleterious effects with regard to other ionic feed impurities such as zirconium.
2. The kinetics of europium extraction are relatively poor; however, the separation factor for europium/americium and the D_A^o for europium are still sufficiently high under nonequilibrium conditions for sharply defined separations.
3. The extraction coefficients of americium are too large ($D_A^o \sim 1$) with 0.8 M HDEHP-DIPB to permit a high recovery using operable flow ratios. Reducing the HDEHP concentration to 0.4 M, where D_A^o (Am) $\sim$0.1 and D_A^o (Re) $\sim$3, would permit more reasonable flow ratios. For example, with these D_A^o values about six extraction stages and four scrub stages using relative extractant:feed:scrub flows of 2:1:1 would recover >99.9% of the americium containing less than a few tenths percent of the rare earths. With the D_A^o (Am) $\sim$1 and 0.8 M HDEHP, extremely high flows of scrub relative to extractant would be required. Therefore, the reference flowsheet[3] based on 0.8 M HDEHP in the first cycle will be changed to 0.4 M HDEHP.

3.3.3 Removal of the degradation product H_2MEHP from ethylene glycol by sorption

The removal of H_2MEHP from Talspeak extractants by scrubbing with ethylene glycol would require that relatively large volumes of ethylene glycol be used. This is because the distribution coefficient values ($C_{glycol}/C_{extractant}$) are about 3 in the scrubbing of 0.8 M HDEHP-DIPB and about 1.5 for the scrubbing of 0.5 M HDEHP-NDD. A secondary step to cleanse the ethylene glycol of H_2MEHP is therefore desirable so that the glycol can be recycled.

Five solid sorbents were evaluated in gravity flow tests using 2 ml of each sorbent with a 1 wt % solution of H_2MEHP in ethylene glycol. Four of the test sorbents — Dowex 50 cation exchange resin, a neutral XAD resin, silica gel, and activated carbon — showed immediate breakthrough and poor holdup of the H_2MEHP. The hydroxyl form of Dowex 1 anion exchange resin (400 mesh) retained 94.60 of a total of 94.82 mg (99.77%) of H_2MEHP before rapid breakthrough. The loading breakthrough (assuming a sorbent density of 1) was 4.7%. These results indicate that it would be feasible to cleanse the ethylene glycol of H_2MEHP by passage through a bed of anion exchange resin.

3.4 References for Section 3

1. D. O. Campbell and S. R. Buxton, U.S. Patent 4,025,602.
2. J. O. Blomeke and D. W. Tedder (compilers), Actinide Partitioning and Transmutation Program Progress Report for Period October 1, 1976 to March 31, 1977, ORNL/TM-5888 (June 1977).
3. A. G. Croff, D. W. Tedder, J. P. Drago, J. O. Blomeke, and J. J. Perona, A Preliminary Assessment of Partitioning and Transmutation as a Radioactive Waste Management Concept, ORNL/TM-5808 (September 1977).
4. T. D. Murphy, "Design and Analysis of Industrial Experiments," Chem. Eng. 84(12), 180 (June 6, 1977).
5. B. Weaver and F. A. Kappelmann, "Preferential Extraction of Lanthanides or Trivalent Actinides by Monoacidic Organophosphonates from Carboxylic Acids and from Carboxylic and Aminopolyacetic Acids," J. Inorg. Nucl. Chem. 30, 263-72 (1968).
6. B. Weaver and F. A. Kappelmann, Talspeak: A New Method of Separating Americium and Curium from Lanthanides by Extraction from an Aqueous Solution of Aminopolyacetic Acid Complex with a Monoacidic Phosphate or Phosphonate, ORNL-3559 (August 1964).

4. AMERICIUM-CURIUM RECOVERY USING BIDENTATE EXTRACTANTS

L. D. McIsaac, J. D. Baker, J. F. Krupa, and N. C. Schroeder
(Allied Chemical Corporation-Idaho Chemical Programs)

The objective of this task is to study the usefulness of neutral bidentate extractants in recovering the transplutonium actinides from the HLLW. One phase of this study involves the development of flowsheets which describe the extraction of the actinides and lanthanides, their decontamination from other fission products, the stripping of the extractant, and the cleanup of the used solvent for recycle.

4.1 Studies Using Synthetic LWR Waste

Additional distribution coefficients for actinides and other elements between reduced synthetic commercial LWR waste solution and 30% dihexyl-N,N-diethylcarbamylmethylenephosphonate (DHDECMP) in diisopropylbenzene (DIPB) have been measured. These data are shown in Table 4.1, which is a composite of newly obtained results and values reported in the previous quarterly (ORNL/TM-6056). Experimental procedures for the reduced system, 0.01 M $Fe(SO_3NH_2)_2$-0.02 M HSO_3NH_2, were the same as those described last quarter (i.e., in ORNL/TM-6056). For comparison, values obtained using 0.1 M $NaNO_2$ are listed in the far right-hand column. Previous work[1] on oxidized synthetic LWR waste solution (0.1 M $NaNO_2$) showed similar trends in the distribution coefficients for groups or families of elements such as the alkali metals, alkaline earths, or lanthanides. For this reason, only representative elements from these various groups are listed in Table 4.1. In addition, other key elements from the actinides and transition elements are included. As expected, those elements whose oxidation states do not change between the two systems give similar distribution coefficients. The slight differences that occur are probably due to media effects or weak complexation by sulfamate anion. There is a marked difference in the distribution coefficients for elements such as neptunium and plutonium, whose oxidation states do change between systems.

Table 4.1. Distribution coefficients for key elements from reduced synthetic LWR waste solution

Element	Distribution coefficient	
	0.01 M $Fe(SO_3NH_2)_2$-0.02 M HSO_3NH_2	0.1 M $NaNO_2$
Np	98	2.2
Am	4.2	4.3
U	50	51
Pu	20	304
Ce	5.8	5.8
Eu	2.9	2.9
Mo	0.37	0.39
Nb	1.6	0.51
Tc	2.2	2.3
Zr	2.0	1.8
Pd	0.54	0.53
Ru	0.40	0.27
Ba	0.011	0.013
Cs	0.0004	0.0005
Rh	0.05	0.018
Sb	0.015	0.036

After extraction from reduced synthetic LWR waste solution, americium and plutonium were subjected to two 0.2-volume scrubs with 3.0 M HNO_3-0.05 M oxalic acid ($H_2C_2O_4$), followed by three strips with 0.05 M HNO_3-0.05 M hydroxylamine nitrate (HAN) and a final strip of 0.05 M HNO_3-0.05 M $H_2C_2O_4$. The distribution data in Table 4.2 show that americium and plutonium, once extracted from reduced waste solution, behave similarly to the oxidized system reported in the previous quarterly.

Table 4.2. Extraction, scrub, and strip distribution coefficients for americium and plutonium from reduced synthetic LWR waste solution

Element	Extraction	Scrub number		Strip number			
		1	9	1	2	3	4
Plutonium	20	134	26	0.54	0.04	0.18	0.05
Americium	4.2	4.3	5.3	0.71	0.12	0.10	0.13

4.2 Cadmium-Modified Synthetic HAW

The possibility of adding a neutron poison such as cadmium nitrate to HAW to prevent criticality problems during uranium reprocessing steps has been suggested.[2] The distribution coefficients for the extraction, scrub, and strip operations were measured for americium in order to determine what effect this modified HAW would have on actinide removal.

Synthetic HAW with contents reported earlier[3] but made 3.5 M in HNO_3 and 0.156 M in $Cd(NO_3)_2$ was tagged with ^{241}Am and extracted with 30% DHDECMP in DIPB. The extractant was the same as that used in earlier distribution studies. One scrub was made with 0.2 volume of 3.5 M HNO_3-0.05 M $H_2C_2O_4$, and the organic was then stripped with three successive equal-volume portions of 0.05 M HNO_3-0.05 M HAN. The results are given in Table 4.3. All runs were performed in duplicate. All contacts were made at 23°C for 5 min.

Table 4.3. Extraction, scrub, and strip distribution coefficients for americium from reduced synthetic LWR waste solution containing cadmium

Run number	Extraction	Scrub	Strip number 1	2	3
1	6.4	6.4	0.81	0.14	0.17
2	6.3	6.7	0.84	0.14	0.20

The extraction distribution coefficient observed for ^{241}Am is considerably higher than with synthetic HAW at 2.9 M HNO_3, where a coefficient of 4.2 was observed. Higher acidity and salting due to $Cd(NO_3)_2$ are responsible for the increase. Stripping is less efficient because of increased initial acidity in the organic phase.

4.3 Diluent Scoping Study

The type of solvent used to dilute the DHDECMP has been shown[4,5] to strongly influence the distribution of americium from acidic nuclear waste generated at the Idaho Chemical Processing Plant. Straight-chain aliphatic diluents produced a second organic phase from nitric acid solutions (i.e., 1.5 M HNO_3). Decalin, although marginally useful, produced a second phase when contacted with 6 M HNO_3.

We are conducting a diluent scoping study for the use of DHDECMP in synthetic HAW. All measurements are being made with the same batch of DHDECMP (~90% pure) and synthetic HAW tagged with americium. The data obtained thus far are shown in Table 4.4. When compared with technical-grade DIPB (50% meta, 40% para, and 10% ortho isomers), only kerosene mixtures with p-DIPB are found to be significantly better diluents. Preliminary results with decalin mixed with p-DIPB indicate increased americium distribution, but coalescence appears to be slow.

Table 4.4. Results of solvent effect studies of americium distribution between 30% DHDECMP and synthetic HAW

Solvent	D_{Am}[a]
Tech. Diisopropylbenzene	4.4
p-Diisopropylbenzene	4.7
Tert-Butylbenzene	4.1
n-Amylbenzene	4.6
1 part kerosene plus 1 part p-diisopropylbenzene	b
1 part kerosene plus 2 parts p-diisopropylbenzene	6.6
1 part kerosene plus 3 parts p-diisopropylbenzene	5.5
1 part kerosene plus 4 parts p-diisopropylbenzene	5.4
Amsco F65[c]	4.5
Isopropylcyclohexane	b
n-Propylcyclohexane	b
Tert-Butylcyclohexane	b
n-Butylcyclohexane	b
n-Amylcyclohexane	b

[a] Each value has an uncertainty of ±10%.

[b] Second organic phase was formed.

[c] Product of the Union Oil Company.

4.4 Preparation of Pure DHDECMP

Preparative liquid chromatography is being used to obtain pure DHDECMP. The liquid chromatograph is a Jobin Yvon "Chromatospac-Prep 100," which uses a gas-driven piston to vertically compact the column packing material. Parameters that have to be established for this system are column size, flow rates, loading, vertical column packing pressure, solvent strength, and type of column packing. Presently, a total of 800 g of silica gel (Merck H-60, 10- to 40-μ particle size) is being used for the column packing. A slurry of this packing in 1% methanol-dichloromethane is vertically compressed to 6.7 atm, resulting in a column approximately 7.5 cm in diameter and 40 cm long. Preparative runs, using loadings of up to 40 ml of various purities of DHDECMP have been attempted on this column. The eluent for these runs was 1% methanol in dichloromethane; flow rates were approximately 70 ml/min.

Figure 4.1 shows the percent purity of DHDECMP obtained vs fractions collected when 40 ml of 62% pure DHDECMP was loaded onto the column. Most of the DHDECMP comes off the column between fractions 15 and 20. The highest purity obtained in this run was 99% at fraction 19. Major impurities are also identified in Fig. 4.1. The dihexylhexylphosphonate, the dihexylmethylphosphonate, and the ester interfere with the leading edge of the DHDECMP peak. An unidentified compound starting at about fraction 21 interferes with the tailing DHDECMP peak. The octyl homolog is not a serious impurity since it is considered just as useful as DHDECMP for actinide partitioning.

Methods to improve this separation include increasing the column length, varying the methanol concentration in dichloromethane, and starting with DHDECMP of higher purity.

4.5 Extraction Studies

Distribution coefficients for Cf(III) between 30% DHDECMP (88% pure) and various concentrations of nitric acid have been determined. These data are shown in Table 4.5. Purified californium tracer[6] was

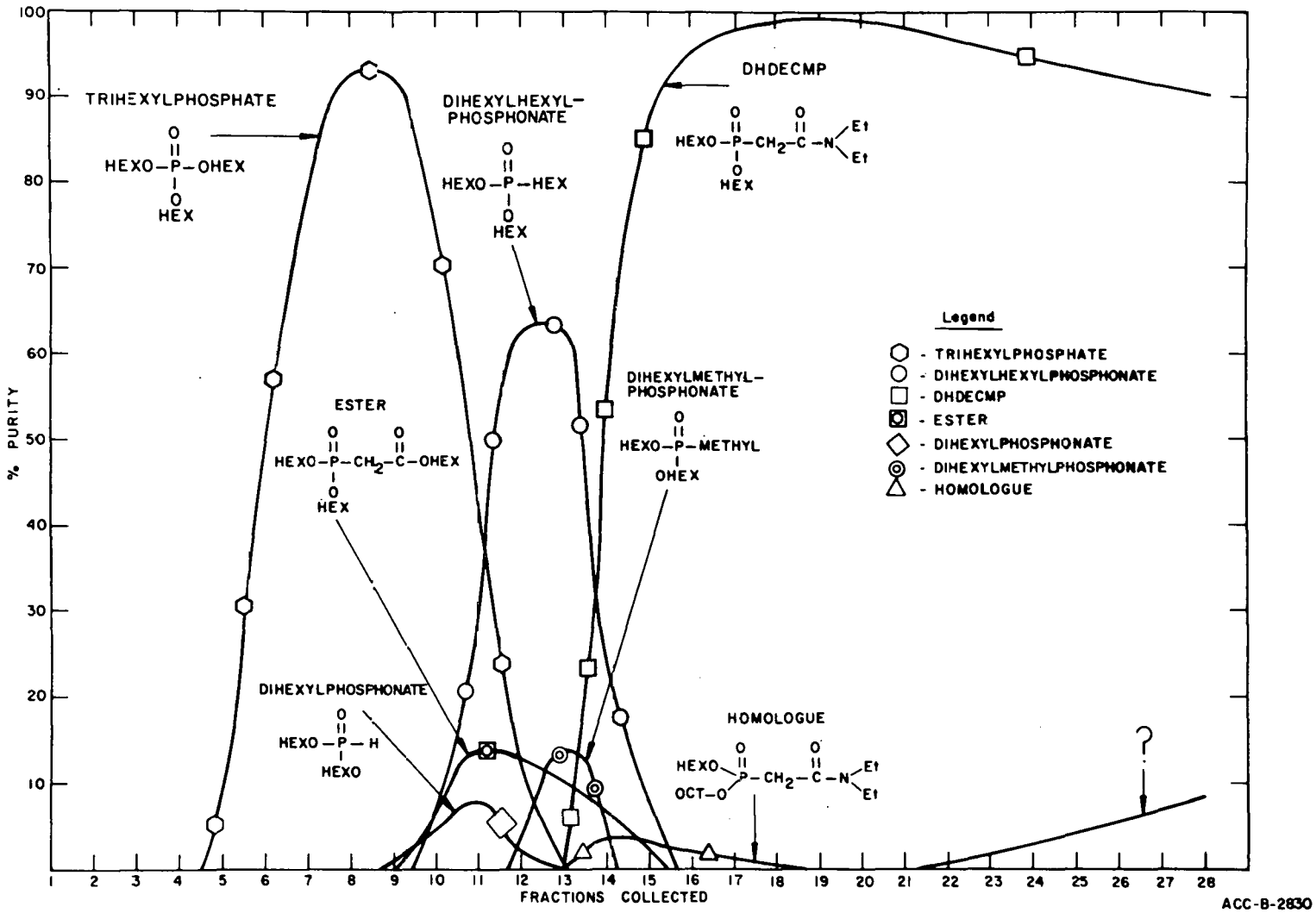

Fig. 4.1. Percent purity of DHDECMP obtained vs fractions collected by preparative liquid chromatography.

taken to incipient dryness in concentrated nitric acid. The resulting residue was then dissolved in a nitric acid solution of the particular concentration being studied and allowed to stand 1 hr. After this period, 1:1 extractions were performed in the manner described in previous reports. Aqueous and organic phases were counted by liquid scintillation spectroscopy.

Table 4.5. Distribution coefficients for Cf(III) between 30% DHDECMP in DIPB and nitric acid

HNO_3 (M)	0.1	0.5	1.0	3.0	6.0
Distribution coefficient	0.024	0.23	0.62	3.0	6.0

4.6 Future Work

Preparative liquid chromatography will be used to obtain pure (>99%) DHDECMP. This product will then be used to determine various physical and chemical properties of the compound. In addition, definitive distribution coefficients for key elements in synthetic LWR waste solution will be determined. Investigations of diluents for DHDECMP will be continued. Efforts will be continued to define the extraction, scrubbing, and stripping portions of an actinide partitioning flowsheet for both oxidized and reduced HAW.

4.7 Errata for Section 4 of ORNL/TM-6056

Table 4.2 on page 96 of the previous quarterly report[7] shows a distribution coefficient of 0.8 for palladium when the organic phase is contacted with a 0.05 M $H_2C_2O_4$-0.05 M HNO_3 aqueous phase. The correct distribution coefficient is 8.0 under these conditions.

4.8 References for Section 4

1. L. D. McIsaac, J. D. Baker, R. E. LaPointe, and N. C. Schroeder, Study of Bidentate Compounds for Separation of Actinides from Commercial LWR Reprocessing Wastes, ICP-1123 (July 1977).
2. D. W. Tedder, Oak Ridge National Laboratory, personnal communication (September 1977).
3. L. D. McIsaac, N. C. Schroeder, and R. E. LaPointe, Study of Bidentate Compounds for Separation of Actinides from Commercial LWR Reprocessing Wastes, ICP-1111 (March 1977).
4. L. D. McIsaac, J. D. Baker, and J. W. Thachyk, Actinide Removal from ICPP Waste, ICP-1080 (August 1975).
5. L. D. McIsaac, J. D. Baker, and D. H. Meikrantz, Actinide Removal from ICPP Waste, ICP-1106 (November 1976).
6. F. L. Moore, "New Extraction Chromatographic Method for Rapid Separation of Americium from other Transuranium Elements," Anal. Chem. 40(14), 2130 (1968).
7. D. W. Tedder and J. O. Blomeke (compilers), Actinide Partitioning and Transmutation Program Progress Report for Period April 1 to June 30, 1977, ORNL/TM-6056 (October 1977).

5. AMERICIUM-CURIUM RECOVERY USING INORGANIC ION EXCHANGE MEDIA

D. R. Tallant (Sandia Laboratories)

The objective of this study is to determine the usefulness of certain inorganic ion exchange media for separating the trivalent actinides and lanthanides. During the first year, feasibility will be determined. If successful, flowsheets will be developed during the second year.

5.1 Experimental

Studies were continued to determine the relative affinities of actinide and lanthanide ions for niobate, zirconate, and titanate ion exchange materials as a function of pH. Plots of distribution coefficients vs pH have been obtained for europium, gadolinium, and promethium by radioactive tracer analysis for all three ion exchange materials. A tracer equilibration of curium with niobate ion exchange material has been carried out.

Typically, the equilibration studies were performed by contacting 15 ml of a tracer solution, of pH 2, with 0.25 to 0.35 g (~1 meq of capacity) of ion exchange material in its hydrogen form at room temperature. Ion exchange loading factors varied greatly, but were never more than 1% of the sorptive capacity. The pH was adjusted by adding dilute nitric acid or sodium hydroxide solution. The mixtures were then equilibrated (~5 days) with reference solutions of the tracer adjusted to the same pH. The aqueous phase of each sample was counted and compared with the appropriate reference to determine the relative amount of tracer remaining in solution. Distribution coefficients were calculated from the formula:[1]

$$K_D = \frac{\text{(fraction of tracer on ion exchanger)}}{\text{(fraction of tracer in solution)}} \times \frac{\text{(ml of solution)}}{\text{(g of ion exchanger)}} .$$

Distribution coefficients with values much less than 1 could not be determined since the depletion of less than 1 to 2% of tracer from solution could not be measured. Likewise, the values of distribution

coefficients greater than 10^5 are subject to considerable uncertainty because of the difficulty of detecting small amounts of tracer radiation above background counts.

The results of these equilibrations are presented in Figs. 5.1-5.3. The data previously reported for lanthanum are also included in these figures. All the lanthanides investigated display approximately the same distribution-coefficient-vs-pH behavior for a given ion exchange material. Further, the (log) increase in distribution coefficient with pH is approximately linear, with a slope of $\sim$2(log) per pH unit for the niobate and titanate ion exchange materials and $\sim$1.5(log) per pH unit for the zirconate ion exchange material. On the other hand, the distribution coefficients for curium on the niobate ion exchange material (solid line, Fig. 5.1) are at least three times those of the lanthanides (dashed line, Fig. 5.1) in the pH range 1 to 2.5 (except for promethium at pH 1). No take-up of europium, gadolinium, or lanthanum by the niobate ion exchange material could be observed at a pH of 1. The discrimination between curium and the lanthanides shown in Fig. 5.1 suggests that elution of a mixture of these nuclides through a niobate ion exchange column with the pH controlled between 1 and 2.5 would produce actinide-lanthanide separation.

Additional experiments were carried out to determine whether the sorption of lanthanide ions by niobate, zirconate, and titanate ion exchange materials is reversible. From the equilibration experiments which provided the data of Figs. 5.1-5.3, samples were selected in which most of the tracer activity originally in solution (a known fraction) was on the ion exchange material. The remaining solution was filtered off the ion exchange materials, and 15 ml of a nitric acid solution with a concentration $\leq$0.1 M was added to desorb the lanthanide tracer ions. After equilibration, the solution was counted and the recovery calculated as the percentage of activity in solution as compared with that on the ion exchanger prior to the reverse equilibration. The results are presented in Table 5.1. Several experimental artifacts effectively prevented achievement of 100% recovery. First, it was extremely difficult to remove all the solution from the ion

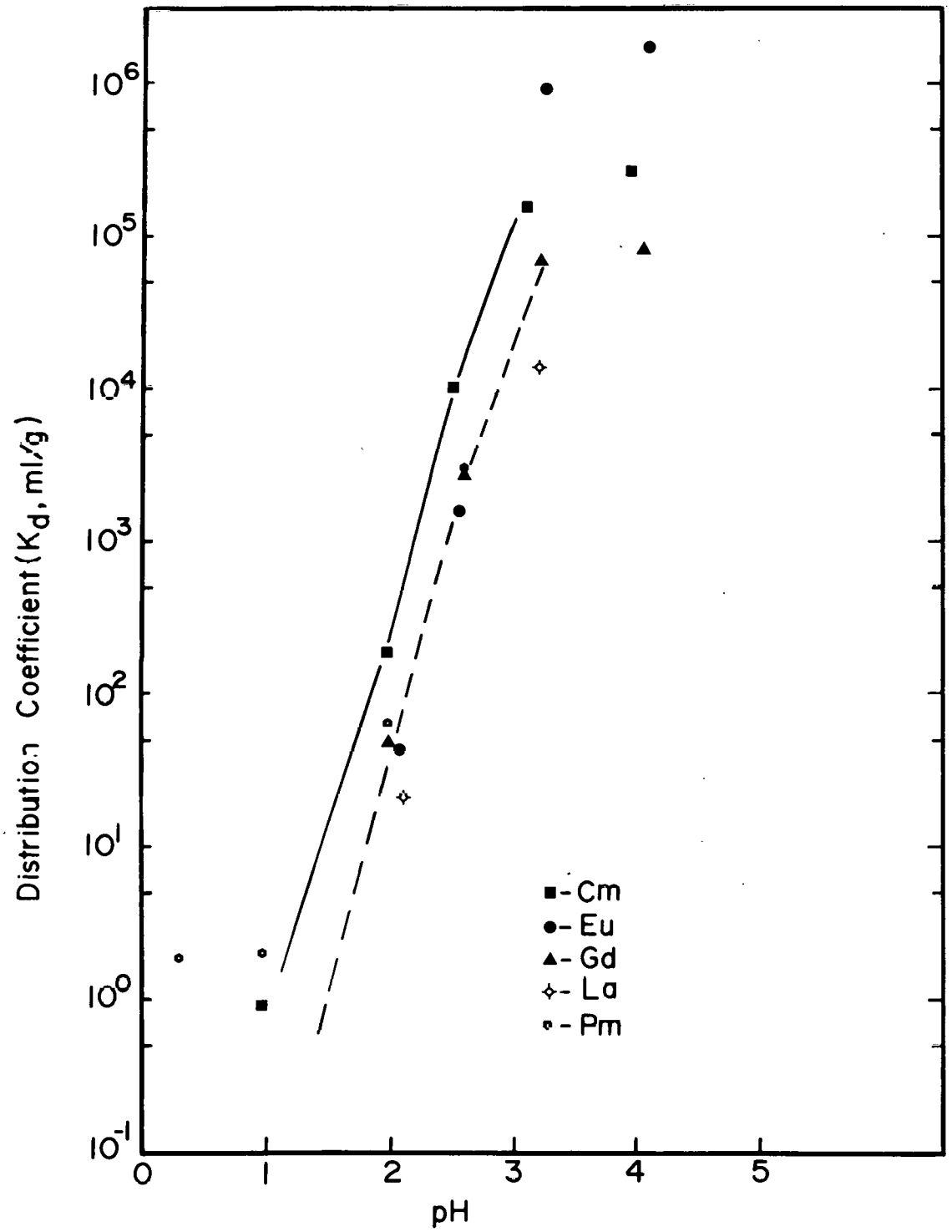

Fig. 5.1. Distribution coefficients of curium and some lanthanides on niobate ion exchange material as a function of pH.

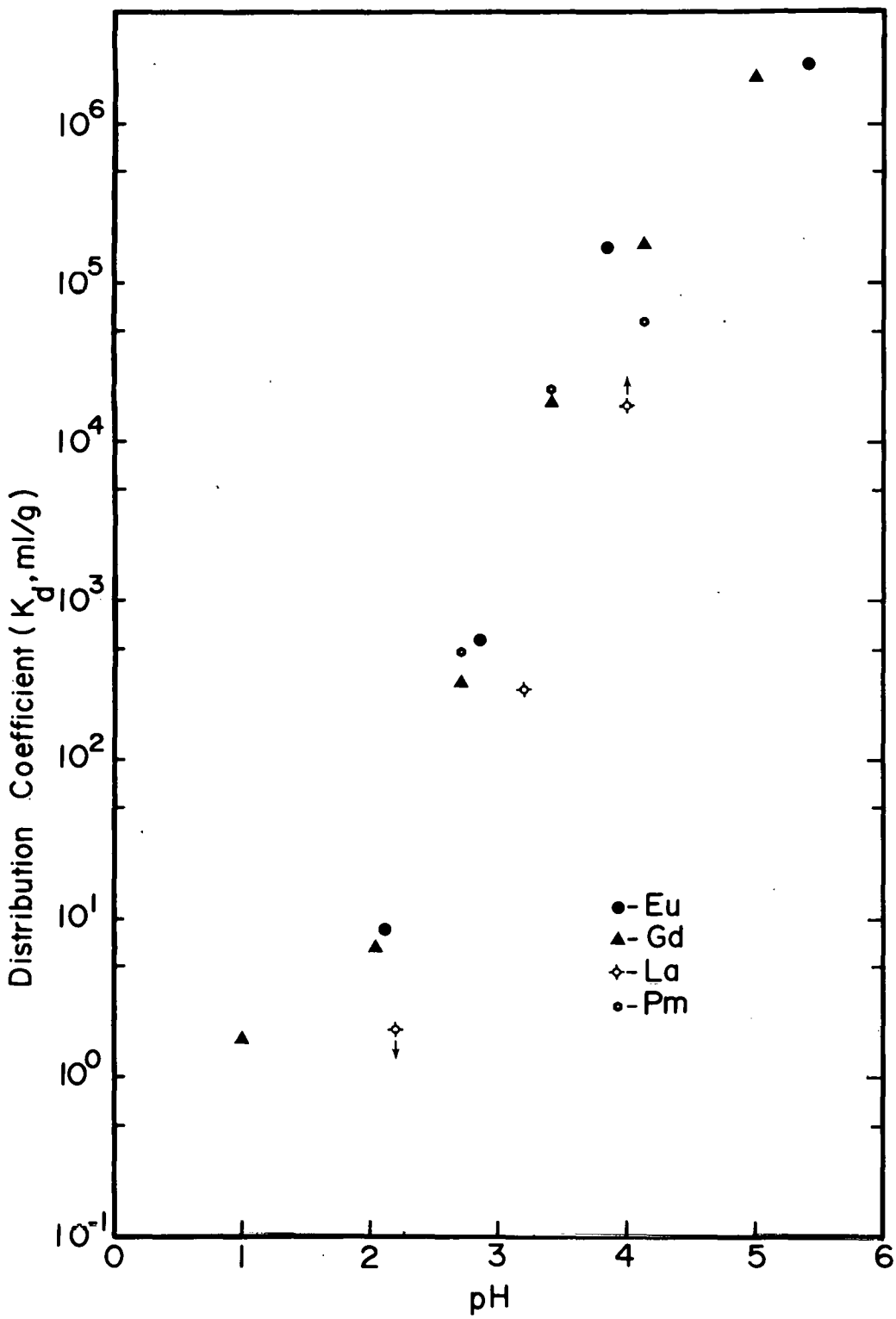

Fig. 5.2. Distribution coefficients of some lanthanides on titanate ion exchange material. The lanthanum data point at pH 4 (upward pointing arrow) is a lower limit. The lanthanum data point at pH 2 (downward pointing arrow) is an upper limit.

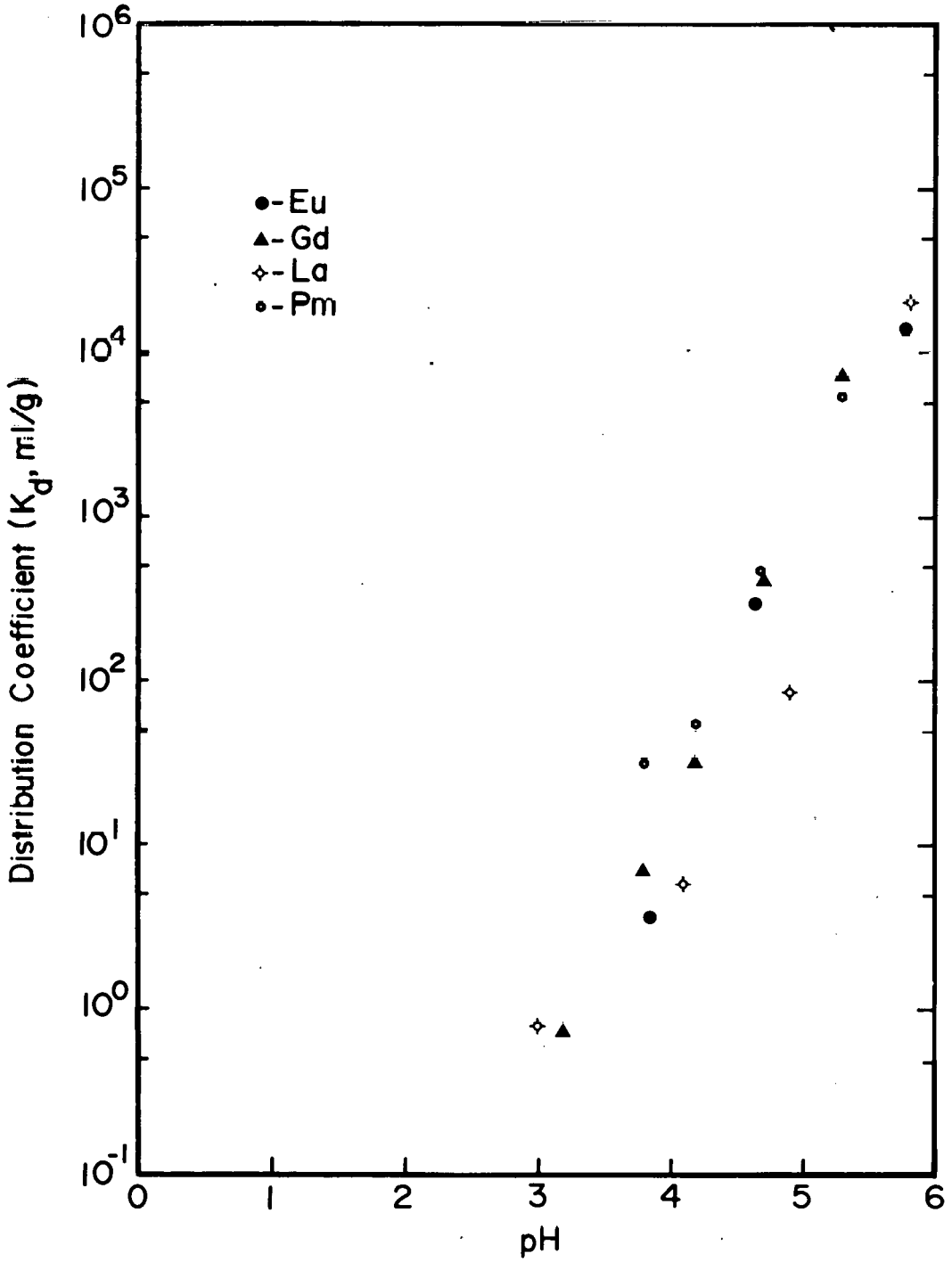

Fig. 5.3. Distribution coefficients of some lanthanides on zirconate ion exchange material.

Table 5.1. Observed percent recovery of nuclides sorbed on inorganic ion exchangers

Ion exchanger	Element		
	Europium	Gadolinium	Promethium
Niobate	91.9	99.9	90.6
	93.2	97.0	91.7
	86.6	98.1	87.2
Zirconate	95.1	100.0	79.9
	88.8	88.3	89.5
		92.3	89.3
Titanate	79.4	93.7	90.6
	80.5	92.1	84.0
		95.5	79.2

exchanger prior to the reverse equilibration, resulting in an unknown dilution of the specific activity of the reverse equilibration solution. Second, some of the ion exchange material was inevitably lost to the filter material (greatest loss for the titanate). These two factors alone could limit the maximum observed recovery to 90%. Further, loss of tracer activity to the walls of experimental apparatus has been observed. This might explain why the gadolinium recoveries (Table 5.1) are slightly better than those for promethium and europium, since the much greater carrier concentration in the gadolinium tracer minimizes the effect of small losses in gadolinium. Taking these possible loss mechanisms into account, desorption of tracer activity from the ion exchange materials must be considered to be nearly complete.

The data of Figs. 5.1-5.3 and Table 5.1 impute to niobate, zirconate, and titanate ion exchange materials some of the properties classically correlated with organic ion exchange resins. Separation of nuclear waste components on titanate ion exchange columns was observed in elution experiments carried out during work on the Sandia Solidification Process.[2] This suggests that the niobate, zirconate, and titanate ion exchange materials may be suitable for separative chromatography.

Adjacent rare earths may be separated on columns of organic ion exchange resins if the distribution coefficients are different by a factor of 1.2 or more.[1] As previously discussed, the distribution coefficients for curium on the niobate ion exchanger are greater than those for the lanthanides by a factor of 3. These results imply that a niobate ion exchange column could be used to perform an actinide-lanthanide separation.

As presently conceived, the niobate ion exchange partitioning of actinides from lanthanides would require that a mixture of actinides (americium, curium) and lanthanides essentially free of other fission product nuclides be partitioned from a nuclear waste stream, perhaps by an oxalate precipitation process as currently proposed.[3] After adjustment to a pH of 3, the mixture of nuclides would be applied to the top of a niobate ion exchange column. At this pH, both actinides and lanthanides would be strongly sorbed on the niobate ion exchange

material (see Fig. 5.1). Since no nonlanthanide fission products are present, there would be little danger of any components of the mixture precipitating at pH 3. Then the sorbed nuclides would be eluted with a nitric acid solution of pH 1 to 2. The components of the mixture would partition themselves along the column according to their distribution coefficients in Fig. 5.1, leaving the column in two main groups (lanthanides and actinides) which would be collected separately. This assumes, of course, that americium has distribution coefficients similar to curium on niobate. Residual nuclides on the column would be removed by increasing the nitric acid concentration in the eluent or through the use of a complexing agent at higher pH.[4] Additional experiments will be required to determine the degree of actinide-lanthanide separation possible and the volume of eluent required. However, flowsheets describing cation exchange chromatography using organic ion exchange resins[3,4] should be representative of the solution volumes required for a similar scheme involving inorganic ion exchange media.

Figures 5.1-5.3 also suggest an additional way in which inorganic ion exchangers may be applied to nuclear waste processing. The relatively large distribution coefficients observed for niobates, zirconates, and titanates in less-acid media suggest that they could be used as scavengers for lanthanides and actinides in low-level liquid waste streams. Conceptually, the ion exchangers would sorb nuclides from a large volume of waste solution at a relatively high pH until loaded near capacity; then the nuclides would be desorbed into a much smaller volume of low-pH eluent for recycle or disposal. Alternatively, the inorganic ion exchange media with its sorbed nuclides might be sent to disposal.

Work on inorganic ion exchangers is continuing at Sandia at a reduced level of effort. Distribution-coefficient-vs-pH data for americium on niobate ion exchange material, and americium and curium on zirconate and titanate ion exchange material, are still to be determined. It is possible that zirconate and titanate ion exchangers would also effect a lanthanide-actinide separation. Column elution

studies that would attempt a lanthanide-actinide separation are also planned. Finally, it would be interesting (but is not presently planned) to investigate the possible separation of a lanthanide-actinide fraction from other fission-product nuclides using inorganic ion exchangers.

5.2 References for Section 5

1. F. C. Nachod and J. Schubert (eds.), Ion Exchange Technology, p. 419, Academic, New York, 1956.
2. R. W. Lynch (ed.), Sandia Solidification Process—Cumulative Report, July 1974-January 1976, SAND-76-0105 (1976).
3. A. C. Croff et al., A Preliminary Assessment of Partitioning and Transmutation as a Radioactive Waste Management Concept, ORNL/TM-5808 (September 1977).
4. J. A. Kelley, Ion Exchange Process for Separating Americium and Curium from Irradiated Plutonium, DP-1308 (1972).

6. RECOVERY ALTERNATIVES APPLICABLE TO WASTE STREAMS

E. P. Horwitz, W. H. Delphin, G. W. Mason, and M. Steindler
(Argonne National Laboratory)

This task focuses on processing alternatives for recovering actinides and technetium from high-level liquid waste. Additional work will examine alternatives for separating the lanthanides from the trivalent actinides and for recovering actinides from salt wastes.

6.1 Introduction

The present program is directed toward the examination of the feasibility of recovering macro amounts of long-lived actinides, uranium, neptunium, plutonium, americium, and curium, from commercial high-level waste (HLLW), using dihexoxyethyl phosphoric acid (HDHoEP) and tricaprylmethyl ammonium nitrate (TCMA·NO_3). The process is divided into two distinct parts, each of which has been developed in sufficient detail to permit flowsheet construction and testing.

The first part of the process involves the extractions of uranium, neptunium, plutonium, americium, and curium from synthetic HLLW solution using 0.5 M HDHoEP in diethylbenzene (DEB). Zirconium, niobium, molybdenum, iron, yttrium, and the lanthanides are also extracted by the HDHoEP. The americium, curium, and lanthanides are back-extracted using 6 to 8 M HNO_3. An oxalate strip is then used to back-extract the neptunium and plutonium, together with the zirconium, niobium, molybdenum, and iron. The uranium, yttrium, and any remaining zirconium are back-extracted with 8 M H_3PO_4.

The second part of the process involves the purification of neptunium and plutonium from the zirconium, niobium, molybdenum, and iron and the oxalate strip solution using 0.25 M TCMA·NO_3 in DEB. Neptunium and plutonium are extracted into the organic phase and stripped with formic acid.

Work during this report period was focused primarily on flowsheet testing using batch countercurrent extraction and stripping. Feed

solution for the testing was prepared by spiking synthetic exhaustively-extracted waste (EEW) solution with the appropriate actinides or radioactive fission product mixture. Data are also presented on the extraction of ruthenium and palladium with 0.5 M HDHoEP in DEB and on the radiation stability of HDHoEP.

6.2 Experimental

The experimental procedure used for measuring distribution ratios was described last quarter.[1] Ruthenium-106 and palladium-103 served as tracers for measuring distribution ratios of ruthenium and palladium.

The batch countercurrent extractions were performed in six open-end 60-ml separatory funnels. Phases were stirred by means of motor-driven stainless steel centrifugal agitators. After phase disengagement, the separated phases were collected in centrifuge tubes and transferred manually in opposite directions. In the countercurrent extractions, the feed solution was introduced in stage 3 or 4, whereas the scrub and barren organic phases were introduced at opposite terminal (or end) stages. In the countercurrent stripping of loaded organic phases, the strip solutions and loaded organic phases were introduced at the opposite terminal stages. During the countercurrent extractions, the aqueous and organic phases, which were removed from the end stages, were assayed radiometrically to ascertain when near-steady-state conditions had been achieved. The concentrations of actinides in the end stages remained essentially constant (within ±5% for neptunium and plutonium and ±2% for americium) after the third or fourth effluent fraction.

Feed solution was prepared by spiking synthetic EEW waste with the appropriate actinides and fission product mixture. In order to simplify radiometric analysis, separate solutions of ^{239}Np plus ^{239}Pu, ^{241}Am, and a fission product mixture were studied. (The fission product mixture contained ^{134}Cs, ^{144}Ce, $^{152,154}Eu$, ^{95}Zr-^{95}Nb, and ^{106}Ru.)

A given nuclide or mixture of nuclides was always added to the synthetic EEW 24 hr prior to the extraction. The hydroxylammonium nitrate (HAN) and hydrazinium nitrate (which were used to adjust the

oxidation states of neptunium and plutonium) were introduced into the spiked EEW solution from 1 M stock solutions that were ∿0.1 M in HNO_3. After the reducing agent had been added, each portion of the feed solution was allowed to stand in a constant-temperature bath at 50°C for 10 min to facilitate reduction of NpO_2^+ to Np^{4+} prior to the countercurrent extraction. One-minute stirring times were used throughout the tests.

In the radiation damage studies, samples of a 0.5 M HDHoEP-DEB solution were exposed to gamma radiation from a ^{60}Co source that produced ∿1 x 10^4 rads/min at 6 cm. Distribution coefficients of Am(III) and Eu(III) were measured for each of the samples. In a few cases, samples that had received absorbed doses of 10 and 100 W-hr/liter were titrated with NaOH in 75 vol % ethanol-25 vol % H_2O in order to determine the quantity of H_2MHoEP produced. The titration was performed in 75 vol % ethanol-25 vol % H_2O.

6.3 Results and Discussion

6.3.1 Extraction of ruthenium and palladium by HDHoEP

The behavior of the trivalent nitrosyl ruthenium ion during its liquid-liquid extraction from HNO_3 solutions using HDHoEP is complex because of the various aquo, nitro, and nitrato complexes that may be present. Our investigations have shown that ruthenium forms both a moderately extractable and a poorly extractable species with HDHoEP. The poorly extractable form predominates in 2 M HNO_3 or in synthetic EEW solution. The extractable form has a K_d* of ∿2 from 2 M HNO_3, which is similar in magnitude to the K_d of Eu(III).

Since ionic species with charges less than 3+ are not readily extracted by dialkylphosphoric acids from 2 M HNO_3 (with the exception of UO_2^{2+}), the extractable form of ruthenium is probably $[RuNO(H_2O)_5]^{3+}$.

---

*The K_d is defined as the organic-phase composition divided by the aqueous-phase composition when the two phases are at chemical equilibrium.

After the extractable ruthenium has been removed, the K_d's for ruthenium are much lower and fairly constant (±25%). The K_d-vs-HNO_3 data for the poorly extractable form of ruthenium is shown in Fig. 6.1, together with K_d data reported last quarter. Possible ruthenium species which extract poorly are: $[RuNO(NO_3)(H_2O)_4]^{2+}$, $[RuNO(NO_3)_2(H_2O)_3]^{+}$, and $[RuNO(NO_3)(NO_2)(H_2O)_3]^{+}$. It is interesting to note that the K_d's for ruthenium shown in Fig. 6.1 are inversely hydrogen-ion dependent, yielding a curve with a slope of -1. These data were obtained from HNO_3 solutions that were 0.05 M in HAN, 0.017 M in iron, and 0.06 M in H_2N_4. A possible extraction equilibrium may be represented by the following equation:

$$[RuNO(NO_3)_2(H_2O)_3]^{+} + (HDHoEP)_2 \rightleftarrows$$

$$RuNO(NO_3)_2(DHoEP \cdot HDHoEP) + H^{+} + 3H_2O. \qquad (6.1)$$

The behavior of palladium during its liquid-liquid extraction from HNO_3 solutions using HDHoEP is also complex because of the formation of both slightly extractable and poorly extractable compounds with HDHoEP. As was the case with ruthenium, the poorly extractable form predominates in HNO_3. The K_d's of the poorly extractable form of Pd(II) as a function of HNO_3 are shown in Fig. 6.1. Palladium is present in 2 M HNO_3 solutions as a mixture of nitrato complexes; however, nitro groups can probably substitute for the nitrato group. In HNO_3 solutions with concentrations <2 M, H_2O substitutes for nitrate ions, thereby forming cations. For example, the cationic $[Pd(H_2O)_3NO_3]^{+}$ or neutral $[Pd(H_2O)_2(NO_3)_2]$ species are probably involved in the formation of the poorly extractable palladium compounds with HDHoEP. The resultant complex with the extractant may be, for example, $[Pd(H_2O)_2(NO_3)(DHoEP)]$. The more extractable palladium ($K_d \simeq 1$ at 2 M HNO_3) probably involves the extraction of neutral palladium nitrato complexes through the phosphoryl group of the HDHoEP.

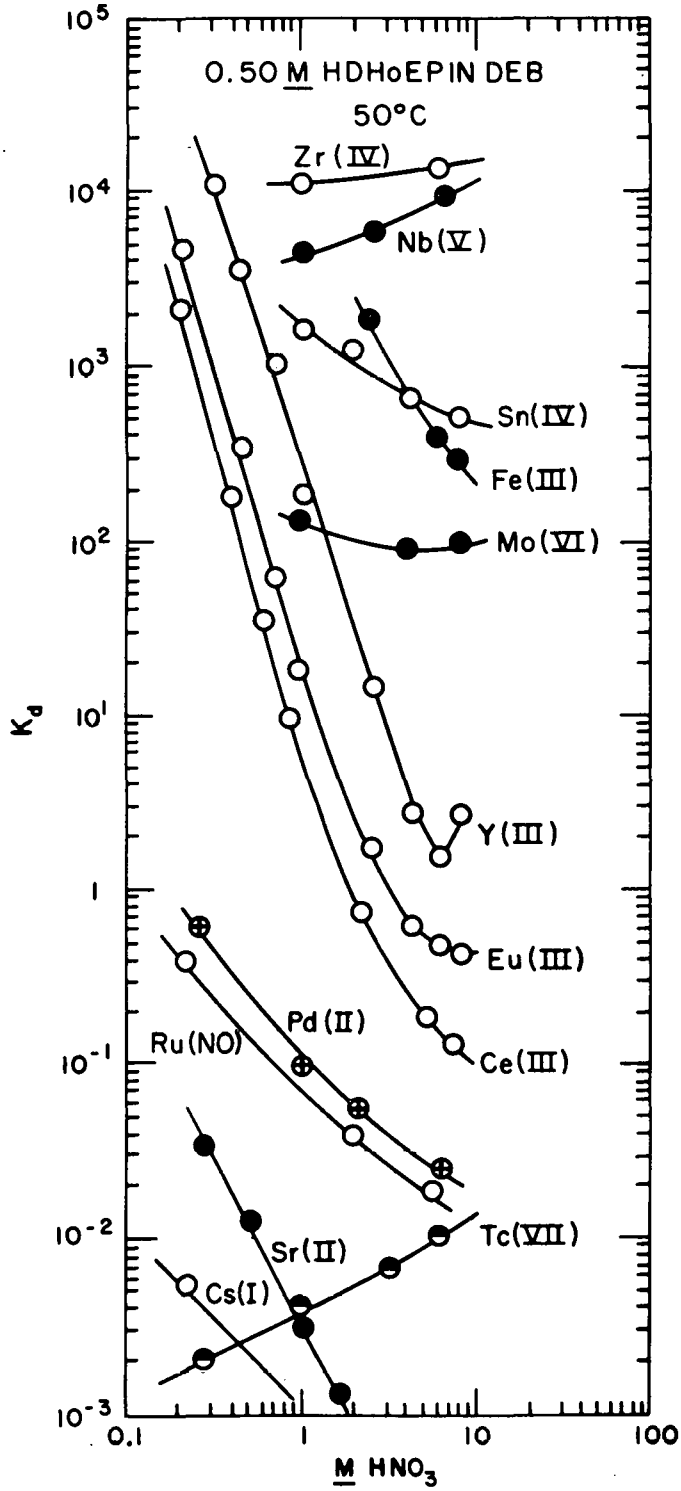

Fig. 6.1. Distribution ratios of selected fission products as a function of HNO_3 concentration. Organic phase, 0.50 M HDHoEP in DEB. Zr(IV), Nb(V), Mo(VI), and Fe(III) data obtained by back-extraction; RuNO(III) - (0.05 M HAN + 0.017 M Fe + 0.06 M N_2H_4 + HNO_3); Pd(II) - (0.05 M $NaNO_2$ + HNO_3).

6.3.2 Conceptual flowsheet and countercurrent extraction tests

A preliminary material balance flowsheet with calculated numbers of stages required to give an americium DF* of 10^3 was presented in the previous progress report.[1] This conceptual flowsheet was based on batch distribution coefficient measurements of actinides and selected fission products from synthetic EEW solution. The process involved the extraction of >99.5% of the uranium, neptunium, and plutonium and ∿30% of the americium and curium using 0.5 M HDHoEP in DEB at 50°C and a phase ratio,** R, of 0.25. The raffinate from the first extraction was diluted with H_2O to adjust the acidity to 2 M and then extracted a second time with 0.5 M HDHoEP in DEB at 25°C and R = 0.5. The two extractions with HDHoEP would give a combined DF for americium of $>10^3$.

The above processing sequence was tested using the batch countercurrent extraction setup. Experimental results are shown in Tables 6.1 and 6.2. The conditions are similar to those shown in the conceptual flowsheet,[1] except that the phase ratio used in the first extraction step was 0.5 (instead of 0.25) and the temperature was 25°C (instead of 50°C). An increase in R was necessary to improve the back-extraction of neptunium, plutonium, and zirconium with the tetramethylammonium hydrogen oxalate plus oxalic acid (TMA·HOx + H_2Ox) mixture. Increasing the phase ratio dilutes the $H_{4-x}Zr(DHoEP)_x$ complex, thereby facilitating the back-extraction of neptunium and plutonium. The data in Tables 6.1 and 6.2 demonstrate the feasibility of the extraction steps. The fluctuations in the percentage of neptunium extracted were expected because of the difficulty in maintaining the tetravalent oxidation state of this actinide. Phase disengagement required ∿30 to 45 sec; however, a small quantity of dark brown scum appeared at the interface,

---

*The DF, or decontamination factor, is defined as the number of moles of a species in the feed divided by the number of moles in the raffinate or stripped organic phase.

**$R = \frac{\text{organic volumetric flow rate}}{\text{aqueous volumetric flow rate}}$.

Table 6.1. Results of batch countercurrent tests of first HDHoEP extraction of feed

Organic phase: 0.5 M HDHoEP in DEB

Feed: EEW - 2.4 M HNO_3, 0.03 M HAN, 0.03 M N_2H_4

Scrub: 1.6 M HNO_3

Temperature: ∿25°C

Phase ratios: feed/organic/scrub = 0.86/0.50/0.14

Number of stages: 3 extraction, 3 scrub

Effluent fraction number	Percent of total in feed extracted		
	Np	Pu	Am
4	99.8	99.8	70.6
5	99.0	99.6	72.3
6	99.9	99.8	68.1
7	99.2	99.6	71.0
8	99.3	99.7	-
9	99.1	99.6	
Av.	99.4	99.7	70.5

Table 6.2. Results of batch countercurrent tests of second HDHoEP extraction of feed

Organic phase: 0.5 M HDHoEP in DEB

Feed: first raffinate diluted with H_2O to 2.0 M HNO_3

Scrub: 0.25 M HNO_3

Temperature: ∿25°C

Phase ratios: feed/organic/scrub = 1.0/0.75/0.50

Number of stages: 4 extraction, 2 scrub

Effluent fraction number	Percent of total extracted from first raffinate		
	Np[a]	Pu[a]	Am
5	80	98	95
6	-	-	94
7	-	-	94
8	-	-	93

[a]Calculated value based on batch K_d measurements made on feed solution.

particularly in the first extraction stage. This interfacial crud is probably a nitrosyl ruthenium-HDHoEP complex. (Batch extraction tests using EEW solution containing no ruthenium did not form the interfacial scum.) The brown scum partially dissolved during subsequent scrubbing and extraction steps.

The results of the countercurrent stripping of americium are shown in Table 6.3. Organic phase A contained macro quantities of zirconium, which increases the K_d of americium as described in the previous progress report.[1] The average K_d per stage is also shown in Table 6.3. These values are within 4% of the K_d's measured in single batch equilibrations. Performing the back-extractions at 50°C would lower the K_d's and improve the overall efficiency. Phase disengagement during the stripping step was very rapid (<30 sec).

Although the countercurrent liquid-liquid extraction tests have demonstrated the feasibility of the two-step-extraction process for removing the neptunium, plutonium, and americium from the EEW solution, a one-step-extraction process would be simpler and, perhaps, less expensive. It would, however, generate a larger volume of oxalate and H_3PO_4 waste solutions, as discussed in the previous quarterly report.[1] Figure 6.2 shows a conceptual flowsheet for the one-step-extraction process. Improved americium extraction is achieved by performing the initial extraction at 25°C instead of 50°C, using an organic to aqueous ratio of 1.0 instead of 0.5, and scrubbing with 1.0 M HNO_3 instead of 1.6 M HNO_3. The results of batch countercurrent extraction and stripping tests using the conditions described in Fig. 6.2 are shown in Tables 6.4 and 6.5. Distribution ratios were measured for individual stages. These K_d's were then used to calculate the quantities of actinides that would be extracted or stripped if additional stages were included. In the case of americium, the RK_d* for the first stage was 3.5; for all subsequent stages, it was 1.4. Using the equations described in ref. 1, ten extraction stages would remove 99.7% of the americium from the feed. The americium K_d for the back-extraction was essentially constant at 0.25. However, in the case of neptunium and

*The RK_d is the extraction factor.

Table 6.3. Results of batch countercurrent tests of HNO_3 strip of HDHoEP

Organic phase: (A) 0.5 M HDHoEP in DEB (from first americium extraction)
(B) 0.5 M HDHoEP in DEB (from second americium extraction)
Strip solution: 8 M HNO_3
Temperature: ~25°C
Phase ratio: organic/strip = 2.0/1.0
Number of stages: 3

Effluent fraction number	Organic phase (A)	Organic phase (B)
	Percent Am remaining in phase[a]	
4	20	8.4
5	22	8.1
6	22	8.4
	K_d of Am per stage	
	0.45	0.28

[a]The percentage of americium initially present in the organic feed to the column.

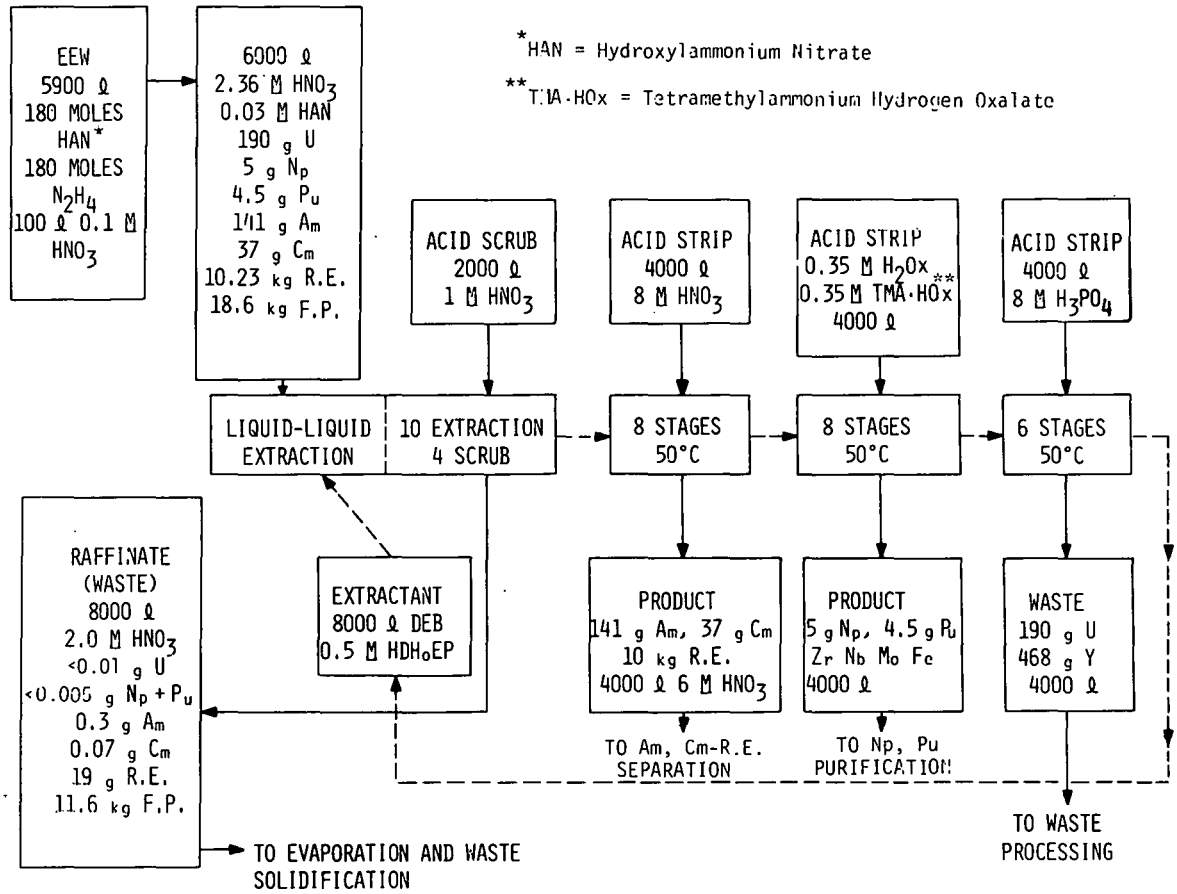

Fig. 6.2. Conceptual flowsheet for actinide extraction from HLLW using HDHoEP in DEB. Basis: 1 tonne heavy metal.

Table 6.4. Results of batch countercurrent tests for one-step-extraction of EEW

Organic phase: 0.5 M HDHoEP in DEB

Feed: EEW - 2.4 M HNO_3, 0.03 M HAN, 0.03 M N_2H_4

Scrub: 1 M HNO_3

Temperature: ~25°C

Phase ratio: feed/organic/scrub = 1.0/1.33/0.33

Number of stages	Percent extracted[a]		
	Np	Pu	Am
4 extraction; 2 scrub (experimental)	99.6 ± 0.2	99.8 ± 0.1	96.0 ± 1.0
10 extraction; 4 scrub (calculated)	>99.9	>99.99	99.7

[a]Errors are one standard deviation as calculated with five degrees of freedom.

Table 6.5. Results of batch countercurrent tests for back-extraction of neptunium, plutonium, and americium

Organic phase: 0.5 M HDHoEP in DEB (fission products, rare earths, and americium)
Acid strip: 6 M HNO_3
Temperature: ∿50°C
Phase ratio: organic/strip = 2/1

Number of stages	Percent back-extracted[a]		
	Np	Pu	Am
3 (experimental)	<0.1	<0.1	93.0 ± 1.0
8 (calculated)	<0.1	<0.1	99.8

Organic phase: 0.5 M HDHoEP in DEB (fission products, neptunium, plutonium)
Acid strip: 0.35 M H_2Ox + 0.35 M TMA·HOx
Temperature: ∿50°C
Phase ratio: organic/strip = 2/1

Number of stages	Percent back-extracted[a]		
	Np	Pu	Am
4 (experimental)	97.0 ± 2.0	99.7 ± 0.2	5 ± 1
8 (calculated)	99.8	>99.99	

[a]Errors are one standard deviation as calculated with five degrees of freedom.

plutonium, the K_d for oxalate strip fluctuates somewhat from one stage to another; therefore, an average of 0.25 (neptunium) and 0.14 (plutonium) per stage was chosen for the calculation.

Phase disengagement was rapid (∿30 sec) for all steps in the process. In addition, less interfacial scum was detected in the one-step-extraction process because of the larger volume of organic phase employed.

Countercurrent studies using synthetic feed spiked with ^{137}Cs, ^{144}Ce, $^{152,154}Eu$, ^{95}Zr-^{95}Nb, and ^{106}Ru were also carried out. The behavior of these fission products followed, in general, predictions based on the batch K_d data shown in Fig. 6.1 and in the previous progress report.[1] One exception, which is discussed below, was the behavior of zirconium during back-extraction with oxalate. As expected, ^{95}Zr and ^{95}Nb plus ∿10% of the ^{144}Ce [from Ce(IV)] were the only fission products (from the spike) that were detected in the neptunium-plutonium fraction. However, the TMA·HOx-H_2Ox strip did not remove zirconium as efficiently as predicted from the tracer-scale K_d measurements. Approximately 50% of the ^{95}Zr activity remained in the organic phase. This disparity in behavior between the tracer- and macro-scale concentrations of zirconium may be explained by the presence of a stable $H_{x-4}Zr(DHOEP)_x$ complex which forms at macro concentrations. This complex is a good extractant per se, as discussed in ref. 1, and is not readily dissociated by $C_2O_4^{2-}$. The fission product ^{95}Zr, ^{95}Nb, and ^{144}Ce are easily removed from the neptunium-plutonium fraction to undetectable levels using the TCMA·NO_3 extractant system, which was described in the previous progress report.[1] The overall DFs of fission products and americium and curium from neptunium and plutonium were: ^{134}Cs, $>>10^4$; ^{144}Ce, $>>10^4$; $^{152,154}Eu$, $>>10^3$; ^{95}Zr, $>>10^4$; ^{95}Nb, $>>10^4$; ^{106}Ru, $>10^2$; and Am-Cm, $>>10^4$.

Cerium and europium were the only radioactive fission products detected in the 6 M HNO_3 strip (i.e., the americium-curium fraction). The overall DFs of fission products in the americium-curium fraction were: ^{134}Cs, $>10^4$; ^{95}Zr, $>10^4$; ^{95}Nb, $>10^3$; and Ru, ∿10^2. The americium-curium fraction is also relatively free of neptunium and plutonium, the DFs of Np and Pu being $>10^3$.

The final step in the flowsheet involves an 8 M H_3PO_4 strip of the organic phase to remove yttrium, zirconium (which remained after the oxalate strip), and uranium. This step was not tested in a countercurrent mode but appears to be very effective, based on single batch extractions. During the stripping of the 0.5 M HDHoEP in DEB containing yttrium, zirconium, and uranium with 8 M H_3PO_4, no precipitate formed and phase separation was rapid. After stripping, the 8 M H_3PO_4 was diluted with H_2O to 2 M H_3PO_4, which caused zirconium phosphate to precipitate homogeneously from solution. Although ~99% of the zirconium precipitates from the phosphoric acid solution under these conditions, yttrium and uranium are not effectively carried by the precipitate. A method is needed for removing the yttrium and uranium from the phosphoric acid solution before evaporation and recycle. More importantly, a better method for stripping yttrium, zirconium, and uranium from HDHoEP must be found in order to avoid generating waste streams that are difficult to handle.

Two of the 200-ml portions of 0.5 M HDHoEP in DEB used in the countercurrent tests were stripped with six additional equal-volume portions of 6 M HNO_3 and, in the case where zirconium was present, with two equal-volume portions of 8 M H_3PO_4 in order to totally decontaminate the solutions from all tracer ^{241}Am and macro quantities of zirconium. The overall DF from ^{241}Am was $\sim 10^8$. Although the resultant solutions appeared yellow, titration with alcoholic NaOH and K_d measurements with ^{241}Am tracer showed no detectable change in the extractant.

6.3.3 Radiation damage studies

Radiation damage of HDHoEP solutions in DEB was studied by measuring distribution ratios of Am(III), Eu(III), and Pu(IV), as well as by standard pH titration of irradiated samples.* No significant change in the K_d's of Am(III), Eu(III), and Pu(IV) was observed when 0.5 M HDHoEP-DEB solutions received absorbed doses as high as 100

*Organic samples were preequilibrated with the aqueous phase and then irradiated.

W-hr/liter. Studies were performed both with HDHoEP solutions that were dry and solutions that had been preconditioned with 2 M HNO_3.

The titration of 0.5 M HDHoEP in DEB solutions that had received an absorbed dose of 100 W-hr/liter at 25 or 50°C showed that 2.9 or 3.9%, respectively, of the HDHoEP decomposed to H_2MHoEP (monohexoxyethyl phosphoric acid). This amount of degradation gives G values of 0.4 (25°C) and 0.5 (50°C) for conversion to H_2MHoEP. Any scission of the alkyl chain of the HDHoEP molecule at the ether oxygen would still give a monoacidic extractant and thus would not be readily detected by titration. After the irradiated HDHoEP solution had been scrubbed twice with an equal volume of 0.05 M HNO_3, the H_2MHoEP was no longer detectable. Titration of a 0.5 M HDHoEP solution which had received an absorbed dose of only 10 W-hr/liter showed no detectable (<0.5%) H_2MHoEP.

Radiation damage of the HDHoEP molecule does not appear to be a serious problem, although some degradation does occur. In all probability, the degradation products that form as a result of scission at CH_2-groups adjacent to the ether or ester oxygen are either weaker extractants than HDHoEP or are scrubbed out of the DEB during equilibration with HNO_3 solutions.

Additional studies are being carried out with the HDHoEP-DEB solutions containing gross amounts of actinides and certain fission products. The presence of such large amounts of complexed metal ions in organic extractants usually changes the G value; however, the types of degradation products are not likely to change. Thus, it is anticipated that radiation damage under actual processing conditions will not be a serious problem with HDHoEP in DEB.

6.4 Conclusions

An improved flowsheet has been developed for the extraction of uranium, neptunium, plutonium, americium, and curium. The process utilizes HDHoEP and TCMA·NO_3 as extractants. Batch distribution ratio measurements made on synthetic EEW solution were used in developing the flowsheet and in predicting the theoretical stages

required for the desired separation. A major portion of the flowsheet was tested by batch countercurrent liquid-liquid extraction experiments and appears to be functional. The DF of fission products cesium, cerium, europium, zirconium, niobium, and ruthenium and actinides americium and curium from neptunium and plutonium is $>10^4$. The DFs of fission products cesium, zirconium, and niobium, and of actinides neptunium and plutonium, from americium and curium are $>10^4$ and $>10^3$ respectively. The physical properties and radiation stability of HDHoEP are very good; however, extractant cleanup is still somewhat complicated by H_3PO_4 waste streams formed in stripping yttrium and uranium. Additional work on this problem is in progress.

6.5 Acknowledgments

The authors wish to thank C. A. A. Bloomquist, H. Griffin, and Dr. H. Lewis for performing many of the K_d measurements and Dr. George Vandegrift for assisting in the countercurrent extraction studies.

6.6 References for Section 6

1. D. W. Tedder and J. O. Blomeke (compilers), Actinide Partitioning and Transmutation Program Progress Report for Period April 1 to June 30, 1977, ORNL/TM-6056 (October 1977), pp. 108-39.

7. ACTINIDE RECOVERY FROM COMBUSTIBLE WASTE

G. H. Thompson, D. L. Cash, E. L. Childs, and L. J. Meile
(Rockwell International, Rocky Flats Plant)

The objective of this task is to determine the recoverability of actinides from incinerator ashes. During the second year, the distribution of actinides through the preferred recovery system will be measured.

7.1 Introduction

Combustible wastes produced during reactor fuel fabrication and reprocessing are comprised of paper, wood, plastics, rubber, cloth, spent solvent, activated carbon, and ion exchange resins. These wastes may be incinerated or "acid-digested" to reduce the volumes and organic contents and to facilitate actinide recovery. The objective of this project is to evaluate methods for recovering the actinides from incinerator residues. For a method to receive serious consideration, it must efficiently recover the actinides in a form suitable for recycle or transmutation and result in little actinide entrainment in the off-gas, but not materially increase final waste volumes or adversely affect processes for incorporation into final waste forms.

During the first report period, a preliminary literature survey was completed.[1] A preliminary evaluation of conventional leaching and fusion methods showed that fusion with commonly used reagents dissolves >60% of the ash from the fluidized-bed incinerator (FBI) process, while leaching with concentrated nitric dissolves 40 to 60% of the same ash. Preparation of plutonium-contaminated FBI ash was attempted.

During the second report period, the evaluation of leaching and solubilization methods was continued using ^{241}Am-traced high-fired PuO_2.[2] It was shown that fusion with commonly used fluxes solubilized $\geq$96% of high-fired plutonium-americium oxide. Acid digestion with 95 vol % H_2SO_4-5 vol % HNO_3 (concentrated acids) also solubilized the high-fired oxide, but lengthy refluxing was required.

The process for treating ash residues may be thought of as being comprised of three major steps: (1) treatment, (2) digestion, and (3) actinide recovery. All of these steps may consist of one or more unit operations, and several processing alternatives are still under consideration. The required treatment steps depend on the digestion step that follows and on the chemical interactions that result (e.g., silica interference). For example, if cerium oxidation in nitric acid is successful for leaching the ash, it may not be necessary to remove the silicates prior to treatment with the cerium. On the other hand, if a carbonate-nitrate fusion of the ash is required, a prior silica removal step is probably essential to avoid the subsequent formation of polysilicic acid when the salt mixture is acidified and digested. Some of the more important alternatives currently under consideration are summarized in Fig. 7.1.

In order to develop a working system, it is necessary to assess the alternatives in scoping studies. Many of the options examined during this past year have been unsuccessful; therefore, the scoping studies are still in progress. This section describes additional scoping evaluations of the most promising treatment and digestion systems that have been identified thus far. Initial results on silica removal are presented, along with some results on salt fusion and the digestion of ash with ceric ammonium nitrate.[3,4]

7.2 Experimental

7.2.1 Materials

The FBI system and the ash it produces were described previously.[1] This ash contains approximately 20 wt % carbon, 10 wt % aluminum, and 9 wt % silica, but no actinides or radioactive fission products since the system has not yet been used for contaminated waste.

The preparation of the ^{241}Am-traced high-fired PuO_2 was also described previously.[2] Briefly, the method consisted of dissolution of plutonium metal in HCl and subsequent recovery by the nitrate anion exchange method, denitration, addition of ^{241}Am tracer, oxalate

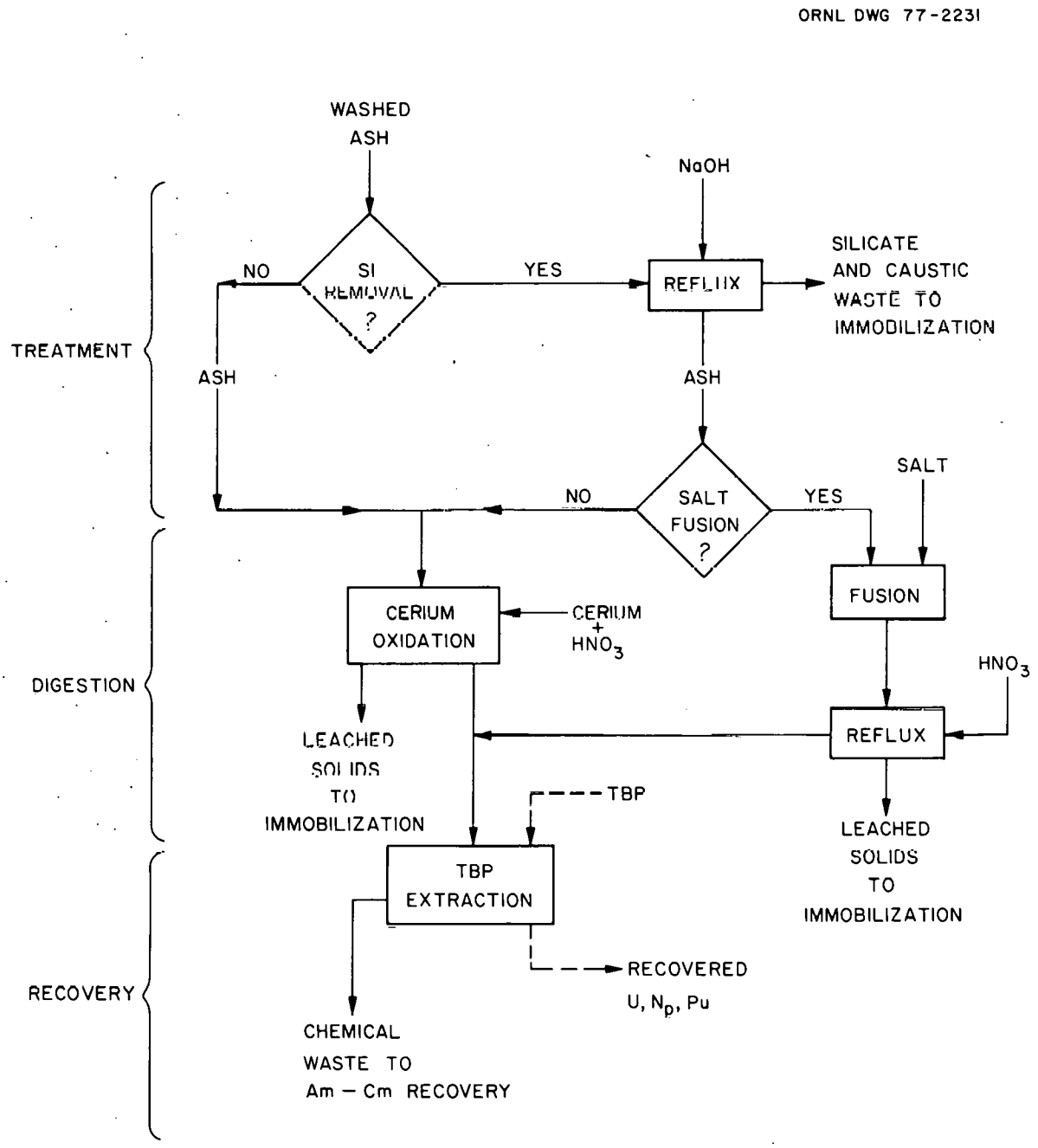

Fig. 7.1. Major alternatives for ash processing.

precipitation, and calcination to the oxide at 925°C. The americium concentration of the prepared oxide was determined to be 2.27×10^{-4} g per gram of plutonium.

The conventional incinerator ash was generated in the Rocky Flats Plant production incinerator. The production incinerator has a stationary grate and operates from about 800 to 1000°C.[5] Combustible wastes incinerated in this facility are plastics (polyvinyl chloride and polyethylene) and paper. Radiometric analysis of the conventional incinerator ash gave plutonium and americium concentrations of 0.053 g and 5.8×10^{-5} g, respectively, per gram of ash. Additional analysis of this ash is in progress. Analysis of "typical" conventional incinerator ash produced at RFP has shown 48 wt % SiO_2, 22 wt % carbon, 5.7 wt % Fe_2O_3, 4.6 wt % MgO, 4.0 wt % CaO, 3.3 wt % Al_2O_3, 2.8 wt % PuO_2, and other minor constituents.[6]

7.3 Procedure

7.3.1 Fusion

For fusion experiments, 10 g of flux was mixed with 1 g of conventional incinerator ash, or a combination of 0.9 g of FBI ash and 0.1 g of high-fired oxide (flux:solid ratio of 10:1). Seven fluxes were evaluated: Na_2CO_3, 90 wt % Na_2CO_3-10 wt % Na_2SO_4, 90 wt % Na_2CO_3-10 wt % $NaNO_3$, NaOH, 82 wt % $Na_3PO_4 \cdot 12H_2O$-9 wt % Na_2CO_3-9 wt % $NaNO_3$, 90 wt % $NaH_2PO_4 \cdot 7H_2O$-10 wt % $NaNO_3$, and 90 wt % $Na_2HPO_4 \cdot 7H_2O$-10 wt % $NaNO_3$. Since the water in hydrated salts was considered to be eliminated during fusion, the initial weights of salt were adjusted to provide the specified weight percent of "anhydrous" salt at the fusion temperature used. Most fusions were done in high-purity alumina crucibles. Fusions with 50 wt % Na_2CO_3-50 wt % $Na_2B_4O_7 \cdot 10H_2O$ required platinum crucibles. Fusions with $KHSO_4$ and $K_2S_2O_7$ were carried out in quartz crucibles.

Samples were mixed and fused at the desired temperature for times ranging from 1 to 2 hr. After being cooled, the samples were solubilized in 4 M HNO_3 and filtered to remove any residue; the filtrate was then

diluted to a known volume and sampled. The residues were solubilized by refluxing for 2 hr in 12 M HNO_3 solutions containing 0.1 M F^-. After being cooled and filtered, each of these solutions was also diluted to a known volume and sampled.

7.3.2 Dissolution with Ce(IV)

For these experiments, 0.15 M Ce(IV) in 4 M HNO_3 was reacted with samples at ambient and at reflux temperatures at a solid:liquid ratio of 125:1 or 250:1. Additional Ce(IV) was added as $(NH_4)_2Ce(NO_3)_6$ to replace the Ce(IV) reduced by carbon. In subsequent experiments, Ce(III) was reoxidized to Ce(IV) electrolytically. Solutions containing 0.05 M Ce(IV) in 4 M HNO_3 were reacted with samples at current-times ranging from 6 to 15 A-hr.

7.3.3 Removal of silica

Because silica interferes with both actinide recovery methods, procedures for removing silica were tested. Cold FBI ash samples were pretreated by refluxing for 3 hr with 2, 4, 6, or 8 M NaOH at a liquid:solid ratio of 100:1. After being cooled, the samples were filtered and the residues washed and dried. The residues were subsequently fused with 90 wt % Na_2CO_3-10 wt % $NaNO_3$ (flux:solid ratio of 10:1) for 2 hr at 900°C. After cooling, the mass was solubilized in 4 M HNO_3 and the residue removed by filtration. The residue was then dried and weighed.

7.4 Results and Discussion

These experiments were of a preliminary nature and designed to test many primary (dissolution) and secondary (recovery) methods. Therefore, a few tests were run on each method, and the mean standard deviation and numbers of tests are shown rather than the 90% confidence level. The most promising methods will be evaluated during FY 1978 using both conventional incinerator ash and contaminated FBI ash (see Sect. 7.5).

7.4.1 Fusion

Fusion methods that were evaluated last quarter on high-fired oxide were tested using mixtures of the oxide and FBI ash. The results of these tests (Table 7.1) show that fusion with basic fluxes (carbonate-nitrate, carbonate, carbonate-sulfate, and NaOH) gives poor recovery. Previously, excellent recovery (>99% plutonium, 97% americium) had been attained with carbonate-nitrate fusion and good recovery (>84% for both plutonium and americium) had been attained with NaOH fusion. The difference is attributed to the solubilization of silica in the ash by basic fusion. Upon acidification, the silicates form polysilicic acid, which is difficult to filter and entrains the solubilized actinides. Further attempts to improve filterability by using gelatin strikes, flocculating agents, evaporation and dehydration of the silica gel followed by dilute acid recovery of the actinide, and aging of the heated solution were unsuccessful.

Since carbonate-nitrate fusion gave the best results, attempts were made to solubilize the cooled melt in 0.3 M NaOH to enable removal of soluble silicates by filtration, followed by acidification of the residue to recover the actinide hydroxides. Unfortunately, substantial amounts of americium and plutonium were found in the filtrate, possibly the result of the formation of carbonate complexes in the basic solution. Consequently, it appears that a salt fusion step followed by a silicate removal step with caustic would probably result in significant actinide losses to the silicate and caustic waste. This is the opposite of the sequence shown in Fig. 7.1 (also compare with the results in Sect. 7.4.3).

Fusion of a mixture of 0.9 g of FBI ash and 0.1 g of oxide in 90 wt % NaOH-10 wt % $NaNO_3$ at 500°C for 2 hr, with subsequent water recovery instead of acid, was also used to remove silica as silicate and circumvent the carbonate complexation problem. After filtration, the residue was leached with 4 M HNO_3. However, actinide recovery averaged only 3.4 ± 2.9% in four tests. This anomalous behavior (NaOH fusion alone gives >84% recovery if no silica is present) cannot be explained. The silica should have been solubilized by fusion and removed in the water dissolution and filtration steps.

Table 7.1. Actinide recovery from fluidized-bed incinerator ash using fusion and 4 M HNO_3 leach

Flux:solid ratio of 10:1
Time: 2 hr
Sample: FBI ash plus mixture of Am-traced PuO_2 (2.27×10^{-4} g Am/g Pu) fired at 925°C to constant weight (90 wt % ash-10 wt % oxide)

Flux	Temperature (°C)	Actinide recovery[a] (%) Pu	Am
90 wt % Na_2CO_3-10 wt % $NaNO_3$	900	8.2 ± 6.1	28 ± 22
Na_2CO_3	900	15	15
90 wt % Na_2CO_3-10 wt % Na_2SO_4	900	10	24
$K_2S_2O_7$	500	97	94
$KHSO_4$	500	94	93
NaOH	500	2.4 ± 0.44	15 ± 5.8

[a]Results of single determination, except for carbonate, nitrate, and NaOH (mean % ± standard deviation for duplicate samples).

Fusion of 0.1 g of oxide in 1, 5, 10, and 20 g of $NaNO_3$ for 2 hr at 350°C with subsequent 4 M HNO_3 digestion and leach gave an average recovery of 0.32 ± 0.06% for the four runs. No trend was discernible for the different flux:solid ratios. Apparently, a high temperature is necessary for nitrate to be effective. (That nitrate, or some radical or ion formed from it, is present in carbonate melts at temperatures greater than the $NaNO_3$ decomposition temperature, 380°C, is shown by the evolution of NO_x at higher temperatures — see Sect. 7.6.)

Cold FBI ash and high-fired oxide were fused (separately) at 900°C with 50 wt % Na_2CO_3-50 wt % $Na_2B_4O_7 \cdot 10H_2O$ in platinum. The flux:solid ratios for ash and oxide were 10:1 and 100:1 respectively. The cold melt was solubilized in 4 M HNO_3. The weight fraction of the cold ash dissolved was calculated by simply weighing the starting material and the residual, while the weight fraction of actinide dissolved was calculated by radiometric analyses of the starting material and residual. The mean % ± standard deviation was 97 ± 3.4% (three tests) for ash solubilization. Duplicate tests on oxide alone gave 96 ± 2.8% recovery of actinides. Although this method provides good dissolution, filterability was again poor with ash because of polysilicic acid formation. Thus the method is no better than carbonate-nitrate fusion and, in addition, introduces boron into process streams.

The results of fusing cold ash with phosphate-carbonate-nitrate and phosphate-nitrate mixtures are presented in Table 7.2. They show that fusion with sodium orthophosphate-sodium nitrate mixtures solubilized the ash, but the presence of carbonate did not seem to affect solubilization. Fusion with sodium monohydrogen phosphate, either with nitrate or alone, did not adequately solubilize the ash. Solutions from the orthophosphate-nitrate fusions (which were effective in solubilizing ash) were difficult to filter. Solutions from the monohydrogen phosphate fusions (ineffective in solubilizing ash) were easy to filter. Fusion with sodium dihydrogen phosphate-sodium nitrate flux yielded a glassy material which was difficult to dissolve. Because the phosphate fusions offer no advantage over the carbonate-nitrate system, no work on the actinide oxide was done.

Table 7.2. Ash solubilization by fusion with phosphate, phosphate-nitrate, and phosphate nitrate mixtures

Flux:solid ratio of 10:1
Time: 2 hr
Temperature: 980°C
Sample: cold FBI ash

Flux	Ash solubilized (mean % ± standard deviation)
82 wt % $Na_3PO_4 \cdot 12H_2O$-9 wt % Na_2CO_3-9 wt % $NaNO_3$[a]	97
90 wt % $Na_3PO_4 \cdot 12H_2O$-10 wt % $NaNO_3$[b]	96 ± 1.4
90 wt % $Na_2HPO_4 \cdot 7H_2O$-10 wt % $NaNO_3$[a]	72
$Na_2HPO_4 \cdot 7H_2O$[c]	78 ± 2.3

[a]Single determination.

[b]Six samples.

[c]Duplicate samples.

7.4.2 Dissolution with Ce(IV)

The experiments with Ce(IV) were performed late in this report period; therefore, only a few results are available.

A preliminary experiment with 1 g of FBI ash in 125 ml of 0.15 M Ce(IV) in 4 M HNO_3 demonstrated rapid reduction of Ce(IV) to Ce(III) with evolution of CO_2. Additional ceric ammonium nitrate was added, and the mixture was refluxed until all the carbon had been oxidized; the total amount of reagent used, including the initial dissolvent, was 0.05 mole. The white residue (mainly SiO_2) was recovered and dried. Analysis showed that 70% of the ash had been solubilized. A second experiment used only the 125 ml of 0.15 M Ce(IV) in 4 M HNO_3 under reflux but included electrolysis of Ce(III) to Ce(IV). A total of 15 A-hr was delivered at the rate of 6 A for 1.5 hr and 3 A for 2 hr. At the end of this time, the carbon was gone and 64% of the ash had been solubilized.

In another experiment, 250 ml of 0.05 M Ce(IV) in 4 M HNO_3 was reacted with 1 g of cold FBI ash with electrolysis and refluxing during the entire period. A total of 6 A-hr was delivered at the rate of 2 A for 3 hr. At the conclusion of this period, carbon had been oxidized to CO_2 and 66% of the ash had been solubilized.

Additional work on this system is in progress. Preliminary results suggest that: (1) little solubilization of oxide occurs during the early reaction stage since Ce(IV) is rapidly reduced by carbon; and (2) the solubilization of the oxide is slow, even when the carbon is gone, under our present operating conditions [0.05 to 0.15 M Ce(IV) in 4 M HNO_3 with electrolysis at 0.5 to 6 A while refluxing].

7.4.3 Removal of silica

The data obtained for pretreatment of cold ash samples by refluxing with NaOH before fusion are plotted in Fig. 7.2. Refluxing with $\geq$6 M NaOH adequately removes silica, permitting subsequent fusion with 90 wt % Na_2CO_3-10 wt % $NaNO_3$ and actinide recovery with 4 M HNO_3. The cold ash residues were dried and weighed to determine the weight percent residue. Duplicate samples of 1 g of FBI ash containing 0.1 g of

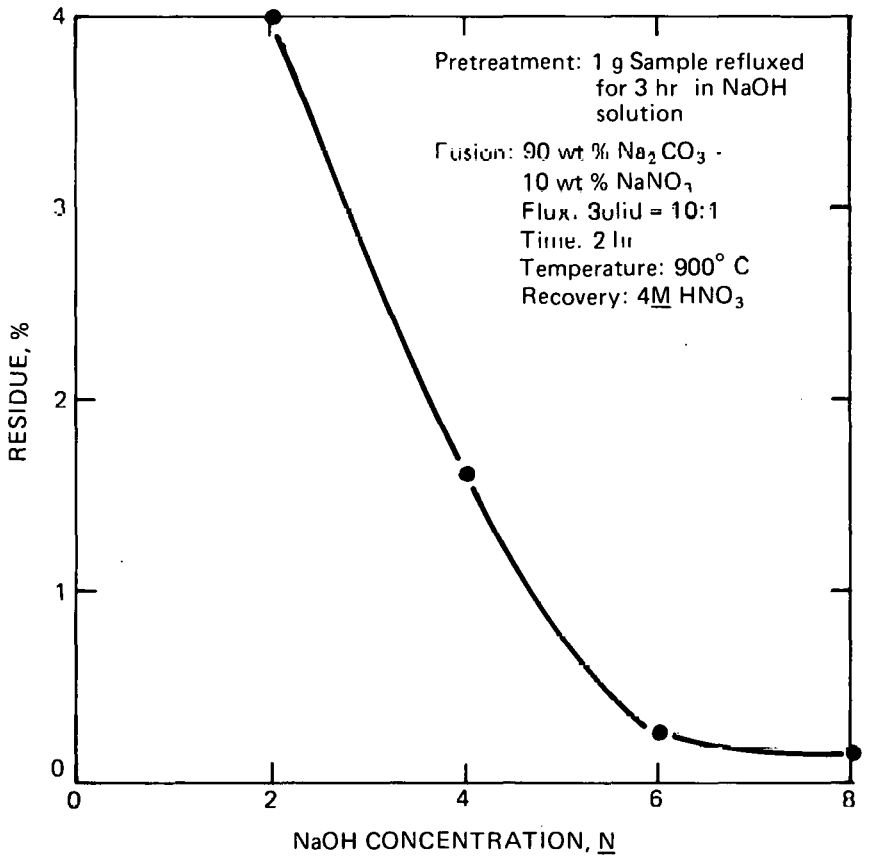

Fig. 7.2. Effect of sample pretreatment to remove SiO_2 on solubilization by fusion.

high-fired oxide gave 98 ± 1.7% recovery of the actinides. This result suggests that the silica treatment step followed by a subsequent salt fusion digestion, as shown in Fig. 7.1, may be feasible. The reverse sequence (i.e., fusion followed by silica removal) results in high actinide losses to the caustic stream under the conditions tested.

7.4.4 Future work

Work has begun on recovering plutonium and americium from conventional incinerator ash and from mixtures of FBI ash and high-fired oxide. The mixture of PuO_2 and FBI ash simulates contaminated FBI ash. Actual contaminated FBI ash will be prepared by adding plutonium to combustible waste and burning it in a laboratory-scale FBI system. Completion (including preliminary testing) of this system, which is currently being built, is scheduled for January 1, 1978. Combustible wastes to be burned in the FBI system include general trash, ion exchange resins, and spent solvents.

The most promising actinide recovery techniques evaluated to date are fusion with carbonate-nitrate mixtures after silica removal and dissolution with Ce(IV) in HNO_3. Fiscal year 1978 will be spent in investigating and documenting these primary and attendant secondary recovery methods. Pretreatment methods to remove silica will also be evaluated.

7.5 Appendix A: Fluidized-Bed Incinerator for Plutonium-Contaminated Waste

A quartz, laboratory-scale FBI system has been designed for burning plutonium-contaminated combustibles. The unit will be utilized to produce representative FBI ash samples for plutonium recovery studies. It will have the capacity to burn ∿1 lb of waste per hour, which represents a heat release of about 10,000 Btu/hr. Completion of assembly and testing of the quartzware, control instrumentation, and auxiliary equipment is scheduled for January 1, 1978.

7.5.1 Description of FBI process

The FBI process differs considerably from conventional incineration. Consequently, a dissimilar type of ash is produced. In the fluidized-bed system, combustion is carried out in two steps. Initial combustion takes place in a bed of fluidized sodium carbonate (Na_2CO_3) granules, which provides an active medium for uniform heat transfer. This characteristic of the bed permits controlled combustion at a relatively low operating temperature of approximately 550°C. The low combustion temperature produces a low-fired nonrefractory ash that cannot be obtained by conventional incineration methods. In addition to optimum heat transfer, the primary fluidized bed supplies Na_2CO_3 for immediate neutralization of chlorides or sulfates released during waste decomposition. This reaction converts a portion of the bed material to sodium chloride (NaCl) and sodium sulfate (Na_2SO_4).

An air-nitrogen gas mixture is used to fluidize the Na_2CO_3 bed. This mixture is controlled so that it provides only enough oxygen for the degree of combustion required to maintain an operating temperature of 550°C. In the absence of sufficient oxygen for complete burning, a portion of the waste is pyrolyzed into gaseous hydrocarbons. Afterburning of these unburned hydrocarbons is accomplished in a bed of fluidized oxidation catalyst granules. A catalyst of chromic oxide (Cr_2O_3) on alumina (Al_2O_3) support material is used for this application. Air is used for fluidization in the catalytic afterburner, which operates at approximately 550°C. The fluidization air also provides excess oxygen for complete combustion of the hydrocarbons entering the bed.

Dust is generated in both beds by particle abrasion during fluidization. Ash from waste combustion is also ground to a very fine powder in the fluidized beds. This fine particulate mixture, which is made up of Na_2CO_3, NaCl, Na_2SO_4, Cr_2O_3, Al_2O_3, carbon, and mineral ash is removed from the primary bed and afterburner by elutriation with the flue gas stream. The fines are removed from the flue gas by cyclone separation and sintered-metal filters. All ash is removed from the system in this manner; thus it is unnecessary to drain the beds for ash removal. Consequently, FBI ash is in the form of a fine particulate

mixture containing the sodium salts, catalyst, carbon, and mineral ash previously mentioned. The sodium salts and catalyst would not be present in conventional incinerator ash; however, the same sodium salts would be present in the aqueous wastes from conventional off-gas scrubbing systems.

7.5.2 Description of equipment

The laboratory-scale incineration system shown in Fig. 7.3 will be installed within a glove box for containment of contamination. Modular quartz construction was selected for the incinerator and afterburner vessels to facilitate modifications during installation and cold testing and to permit visual observation of the fluidized-bed process. The incinerator consists of two vessels, a lower primary reaction chamber and an upper afterburner chamber. The primary reactor is fabricated from 90-mm-diam quartz and is approximately 560 mm long. The afterburning section is 150 mm in diameter and about 813 mm long. The off-gas from the primary reactor will pass through a quartz cyclone separator to remove most of the entrained dust from the stream before being routed through another quartz cyclone separator for dust removal prior to the final filtration step. Six 38-mm-diam by 457-mm-long sintered-metal filters will perform the latter function. Clean off-gas leaving the metal filters is cooled by a water-cooled heat exchanger before being exhausted into the glove-box ventilation system. Motive force for the system will be provided by a small air ejector.

Fluidization gas will be preheated during start-up with a Chromolox electrical resistance heater and a tube furnace pebble-bed heater. A 32-mm-diam screw conveyor will feed preshredded waste into the primary reactor. Pneumatic controls will maintain gas flow rates and any air-nitrogen gas ratio that is desired for fluidization and combustion in the primary reactor. The ejector will also be pneumatically controlled to maintain a slight negative pressure throughout the system. Temperatures will be measured at various points within the system for control and data acquisition.

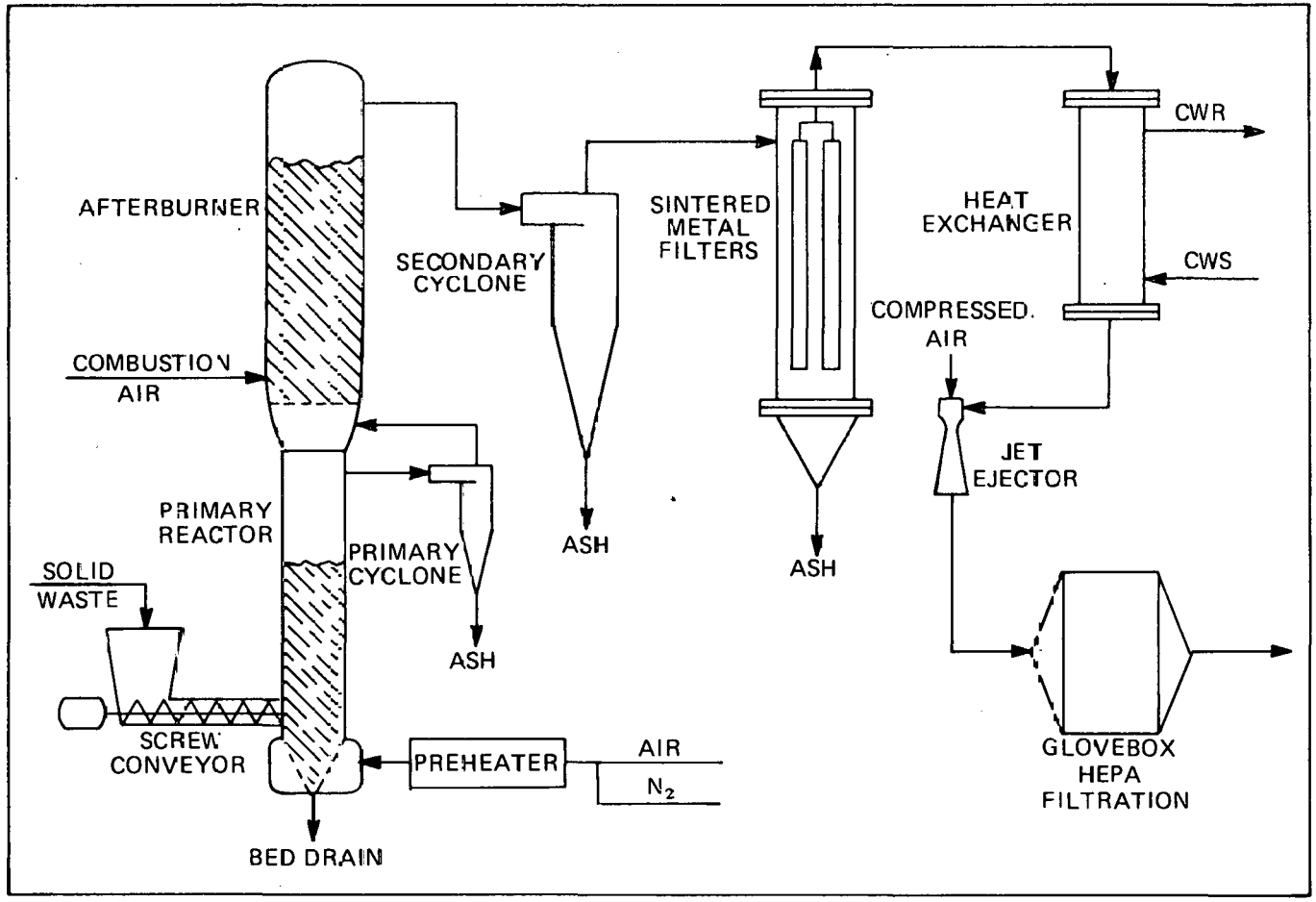

Fig. 7.3. Schematic of laboratory-scale fluidized-bed incineration system.

7.5.3 Planned operating procedure

Uncontaminated combustible waste samples of predetermined composition will be prepared and shredded outside the glove box. Waste will then be weighed and transferred into the glove box, where it will be spiked with a predetermined amount of plutonium. Plutonium can be added in any form that might be desirable for future ash leaching tests. The incinerator will be preheated to approximately 300°C before waste feeding is started. Waste will then be screw-conveyed into the incinerator at a rate sufficient to maintain an operating temperature of approximately 550°C in the primary cyclone, secondary cyclone, and sintered-metal filters, as is done on the larger FBI units. When a run is complete, ash and bed samples will be analyzed to compile a plutonium material balance. Work will then proceed to recover the plutonium from the ash samples.

7.6 Appendix B: Thermogravimetric and Mass Spectral Analysis of Volatiles Produced During Fusion Experiments

Fusion experiments have shown that Na_2CO_3 alone is not an effective flux for solubilization of ash and high-fired actinide oxides, at least not at temperatures less than 1000°C. However, fusion with 90 wt % Na_2CO_3-10 wt % $NaNO_3$ is very effective. Since $NaNO_3$ decomposes at 380°C, the question arose as to whether the $NaNO_3$ oxidation of ash constituents is complete at that relatively low temperature or whether NO_x species are present in the melt at higher temperatures. Thermogravimetric analyses (TGA) and mass spectral (MS) analyses were therefore made simultaneously on some fluxes and flux-ash mixtures to correlate weight loss and off-gas composition at temperatures up to 1200°C.

The programmed heating rate was 10°C/min. The volatile components were carried into the mass spectrometer inlet in a stream of helium carrier gas.

The weight percent loss and the temperature ranges in which the losses occurred are shown in Table 7.3, along with comments concerning the species being evolved. Table 7.4 shows the composition of the gas over the sample at the specified temperature. The results suggest that the carbonate-nitrate system is successful because nitrate decomposition

Table 7.3. TGA/MS results for fusion experiments

Sample	Temperature range (°C)	Weight loss (wt %)	Event
90 wt % Na_2CO_3-10 wt % $NaNO_3$	25-180	11.5	Desorption of H_2O
	180-500	0	
	500-900	9.2	Nitrate, carbonate decomposition
	900-1200	20.7	Carbonate decomposition; volatilization of sodium oxide, resulting in attack of quartz balance components
90 wt % Na_2CO_3-10 wt % $NaNO_3$ + 1 g FBI ash (flux:solid ratio = 10:1)	25-160	8.91	Loss of sorbed H_2O
	160-320	0.18	Further water loss
	320-500	1.78	Carbonate decomposition
	500-760	9.45	Nitrate decomposition
	760-980	2.14	Carbonate decomposition
90 wt % NaOH-10 wt % $NaNO_3$	25-350	6.2	Loss of sorbed H_2O
	490-960	41.8	Water evolved; nitrate decomposition above 800°C; volatilization of sodium hydroxide, resulting in attack of quartz balance components
90 wt % NaOH-10 wt % $NaNO_3$ + 1 g FBI ash (flux:solid ratio = 10:1)	25-210	6.19	Loss of sorbed H_2O
	210-410	2.03	Water evolved
	410-900	20.3	Water evolved; nitrate decomposition above 750°C; volatilization of sodium hydroxide, resulting in attack of quartz balance components
90 wt % $Na_3PO_4 \cdot 12H_2O$[a]-10 wt % $NaNO_3$	25-180	41.1	Loss of water of hydration
	180-250	2.84	Further loss of H_2O
	250-490	0	
	490-800	2.84	Decomposition of nitrate salt (N_2, NO, O_2)
	800-1030	1.42	Further decomposition; possible volatilization of sodium oxide
90 wt % $Na_3PO_4 \cdot 12H_2O$[a]-10 wt % $NaNO_3$ + 1 g FBI ash (flux:solid ratio = 10:1)	25-150	41.2	Loss of hydrated H_2O
	150-220	2.44	Further loss of H_2O
	220-380	0	
	380-660	2.82	Decomposition of nitrate salt (N_2, O_2, NO)
	660-1000	0	

[a]Original weight adjusted to provide specified weight percent of "anhydrous" salt after water of hydration has been expelled.

Table 7.4. Composition of gases evolved during fusion experiments

Sample	Temp. (°C)	Vol % of gas over sample								
		H_2O[a]	CO_2	NO	N_2O	O_2	N_2	H_2	Ar	H.C.[b]
90 wt % Na_2CO_3-10 wt % $NaNO_3$ + 1 g FBI ash	900	Trace	77.6	18.6	-	-	3.6	0.23	-	Trace
90 wt % NaOH-10 wt % $NaNO_3$ + 1 g FBI ash	500	34.5	-	0.54	2.0	2.4	19.5	40	0.06	1.0
90 wt % $Na_3PO_4 \cdot 12H_2O$[c]-10 wt % $NaNO_3$	950	49	-	0.66	0.82	38.0	3.3	7.3	0.04	1.0
10 g of 90 wt % $Na_3PO_4 \cdot 12H_2O$[c]-10 wt % $NaNO_3$ + 1 g FBI ash	950	5.7	16.1	59.5	1.4	0.3	13.5	3.1	0.04	0.43

[a] Because the sample was evacuated prior to heating, hydrated water may have been removed to some extent. Mass spectral values for water are less reliable.

[b] H.C. = hydrocarbons. The values reported are the total hydrocarbons in the volatile fraction, including methane, ethane, propane, butane, and benzene.

[c] Original weight adjusted to provide the specified weight percent of "anhydrous" salt after water of hydration has been expelled.

products (oxidizing species) are present in the melt at temperatures much higher than the decomposition temperature of $NaNO_3$, 380°C. Nitrate decomposition species are also undoubtedly present in the hydroxide-nitrate system at higher temperatures (as shown by the small amounts of NO_x at 500°C in Table 7.4 and nitrate decomposition at temperatures greater than 750°C, shown in Table 7.3). However, NaOH is sufficiently volatile at temperatures greater than 500°C that it wets the sides of the crucibles and "crawls out," carrying sample with it. Although we have not defined the mechanism, successful fusion with nitrate seems to require the presence of a flux which inhibits nitrate decomposition and loss at lower temperatures and acts as a stabilizing medium for the effective oxidizing species that are present at higher temperatures. A comparison of the phosphate-nitrate and phosphate-nitrate-ash data also shows that the evolution of NO_x is much greater when ash is present. This is probably the result of oxidation of carbon in the ash.

7.7 Summary and Conclusions

The program to determine the feasibility of actinide recovery from combustible waste is continuing. During this quarter, evaluation of leaching and solubilization methods using mixtures of ^{241}Am-traced high-fired PuO_2 and FBI ash or conventional (contaminated) incinerator ash showed that:

1. Refluxing with 0.15 M Ce(IV) in 4 M HNO_3 oxidizes the carbon present in all incinerator ash and solubilizes 75% of the ash.
2. Adequate actinide recovery will probably require dissolution of the silica present in ash to free encapsulated actinide oxide so that dissolvent may contact the oxide.
3. Fusion with 90 wt % sodium carbonate-10 wt % sodium nitrate solubilizes both silica and actinide oxide. However, attempts to recover the actinides in 4 M HNO_3 causes formation of polysilicic acid, which is difficult to filter and adsorbs the solubilized plutonium. Therefore, removal of silica is also necessary for this method.

4. Silica can be removed by refluxing with ≥6 M NaOH. The actinides can then be solubilized and recovered without interference from silica.

A laboratory-scale FBI system is being built for the combustion of contaminated waste. Actinide recovery methods will be evaluated using the contaminated ash produced in this system.

7.8 Acknowledgments for Section 7

The authors wish to thank D. L. Ziegler and A. J. Johnson of the Pilot Plant Development group of Chemistry Research and Development (CRD), F. J. Miner, Manager of CRD, and J. D. Navratil of the Chemical Research Group for their assistance in this program. Appreciation is also extended to the Analytical Laboratories, especially R. C. Nelson, E. D. Ruby, and K. J. Grossaint, for the analyses.

7.9 References for Section 7

1. J. O. Blomeke and D. W. Tedder (compilers), Actinide Partitioning and Transmutation Program Progress Report for Period October 1, 1976, to March 31, 1977, ORNL/TM-5888 (June 1977).
2. D. W. Tedder and J. O. Blomeke (compilers), Actinide Partitioning and Transmutation Program Progress Report for Period April 1 to June 30, 1977, ORNL/TM-6056 (October 1977).
3. H. D. Harmon, Dissolution of PuO_2 with Cerium(IV) and Fluoride Promoters, DP-1371 (October 1975).
4. D. E. Horner, D. J. Crouse, and J. C. Mailen, Cerium-Promoted Dissolution of PuO_2 and PuO_2-UO_2 in Nitric Acid, ORNL/TM-4716 (August 1977).
5. D. L. Ziegler, Fluidized Bed Incineration of Radioactive Waste, RFP-2471 (May 1976).
6. T. C. Johnson, Recovery of Plutonium from Incinerator Ash at Rocky Flats, RFP-2520 (December 1976).

8. ACTINIDE RECOVERY AND RECYCLE PREPARATION FOR WASTE STREAMS

J. D. Navratil, L. L. Martella, and C. M. Smith
(Rockwell International, Rocky Flats Plant)

The objective of this task is to determine the feasibility of removing actinides from secondary aqueous waste streams likely to be produced during reactor fuel fabrication and reprocessing. The waste streams are part of two flowsheets entitled "Salt Water Management" and "Acid and Waste Water Management." Evaluation of methods for the salt waste and waste-water streams and recycle preparation problems will be the major emphasis of this task.

8.1 Introduction

One of the more difficult aspects of this problem is the generation of feed material which is representative of the chemical species present in the actual salt wastes and the recycle streams. Real wastes cannot be generated without the operation of a hot pilot plant which allows the degradation products in the main purification cycles, for example, to build up and achieve a steady-state inventory. Consequently, synthetic feeds have been generated during this study primarily to examine the effects of those inorganic chemical species postulated to be present in the analytical and incinerator liquors produced by sampling and by the sodium carbonate fluidized-bed incinerator respectively. However, the third category of major salt waste, the sodium carbonate scrub solutions from the solvent extraction cycles, has not been included as a component in these salt wastes thus far. Since these scrub solutions contain larger quantities of actinides and significantly different chemical species from the other two sources of salt waste, they would probably be processed differently.

It should be recognized, however, that other chemical species may be present besides those included in the synthetic wastes thus far. Mono and dibutyl phosphate, for example, may prevent the use of TBP as a means of recovering uranium, plutonium, and neptunium from the scrub wastes. In the main process, the sodium carbonate scrub rate is typically 1 vol % or less of the organic volumetric flow rate.

Consequently, at steady state the concentrations of mono and dibutyl phosphates from the TBP systems are typically ≥100 times greater in the scrub solutions than in the main process streams. Moreover, the actinide concentrations in these salt wastes are orders of magnitude less than in the main process. Both of these concentration effects are unfavorable for actinide recovery since much of the uranium, for example, which reports to the salt waste may not be strippable even from the TBP organic phase.

Similar uncertainties arise when simulating recycle stream compositions. Typically, the probable contributions from the major reagents are known fairly well, but relatively little information is available about the trace contaminants or their most likely chemical form. Thus, these studies are fallible in that a significant chemical effect, perhaps causing irreversible actinide losses, may not be observable because the recycle stream or salt waste did not have the appropriate feed composition.

Nonetheless, the evaluation of recovery methods on a laboratory scale for the salt waste and waste-water streams as well as recycle preparation problems are the major emphasis of this task. Solvent extraction methods have been partly evaluated to determine their utility in the processing of some of the salt waste streams, and adsorption and membrane techniques should be evaluated for their application to treatment of waste-water streams. If the program is continued past FY 1977, the best methods for both waste streams should be tested further to obtain process information for flowsheet analysis.

During this report period, the evaluation of methods for the salt waste and waste-water streams was continued. Preliminary runs with a bidentate organophosphorus and a combined bidentate-TBP extraction process were made to remove actinides from salt waste. The former process effectively removed actinides but prevented efficient stripping of uranium. More satisfactory uranium stripping agents than water were not found.* The latter process appears to be more attractive for removing

*A 0.05 M HNO_3-0.05 M $H_2C_2O_4$ solution should effectively strip the uranium (see ref. 1, pp. 96, 102).

actinides from salt waste. The TBP removes most of the uranium and plutonium, while the bidentate extractant removes most of the remaining actinides.

Activated carbon, macroreticular resins, and polyurethanes were tested for their utility in removing detergents and corrosive anions from waste water. The preliminary results showed that an open-pore polyurethane (OPP) resin has the highest capacity for detergent, but a low capacity for anions.

8.2 Processing of Salt Waste

Prior work with impure dihexyl-N,N-diethylcarbamoylmethylenephosphonate (DHDECMP) showed high uranium distribution ratios (Ds)* in dilute HNO_3.[2] These earlier determinations were repeated using a different batch of purified[2] DHDECMP and an improved uranium analytical method. Table 8.1 shows the approximate compositions of the impure and purified extractants. Figure 8.1 shows D values of U(VI) obtained with DHDECMP vs HNO_3 concentration. The results show lower uranium D values at low acidities than obtained previously, indicating fewer uranium stripping problems.

Uranium stripping from 30 vol % DHDECMP in diisopropylbenzene (DIPB) diluent was compared with results obtained with 30 vol % TBP in dodecane, using water as the stripping agent. A 100-ml volume of each extractant was contacted with 20 ml of a 7 M HNO_3 solution containing 42 g of uranium per liter. The uranium-loaded extractants were then repeatedly contacted with water using an aqueous-to-organic (A/O) ratio of 5. The uranium concentrations in the aqueous strip solutions were determined by fluorometric techniques and used to construct the curves shown in Fig. 8.2.

Figure 8.2 shows a plot of the percent uranium stripped from the two extractant systems vs the number of contacts. The results show

*Defined as the organic-phase concentration divided by the aqueous-phase concentration when the phases are at chemical equilibrium.

Table 8.1. Gas chromatography-mass spectroscopy (GC/MS) analysis of impure and purified DHDECMP[a]

Component	Impure (%)[b]	Purified (%)[b]
Diethylamine	0.14	0
Decane	0.33	0
Undecane	0.33	0
Dichloro-N,N-diethylacetamide	0.71	0.3
α-diethylamino-N,N-diethylacetamide	2.38	0.2
Unidentified components	2.47	1.8
Hexylchloride	2.51	0.7
Chloro-N,N-diethylacetamide	2.98	0.5
Dihexylphosphite	4.09	0
Dihexylmethylphosphite	7.80	7.5
Trihexylphosphate	27.9	26.0
Dihexyl-N,N-diethylcarbamoylmethylene-phosphonate	47.0	63.0

[a]Purified by Amberlyst A-26 resin treatment.[2]

[b]Relative peak area of GC/MS.

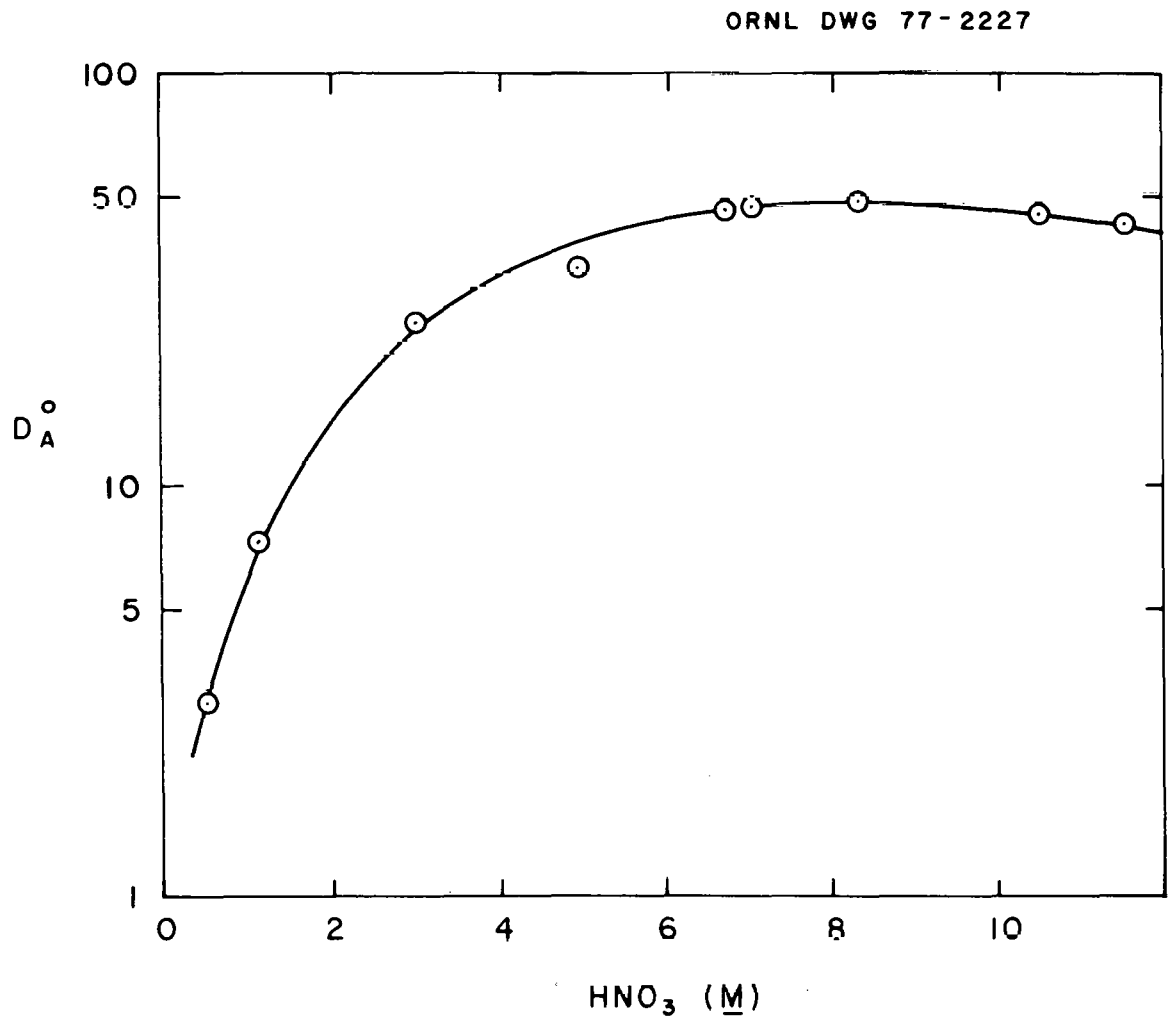

Fig. 8.1. Uranium D values vs HNO_3 concentration for 30 vol % DHDECMP in CCl_4. Feed = 6 g of uranium per liter; temperature = 22-24°C.

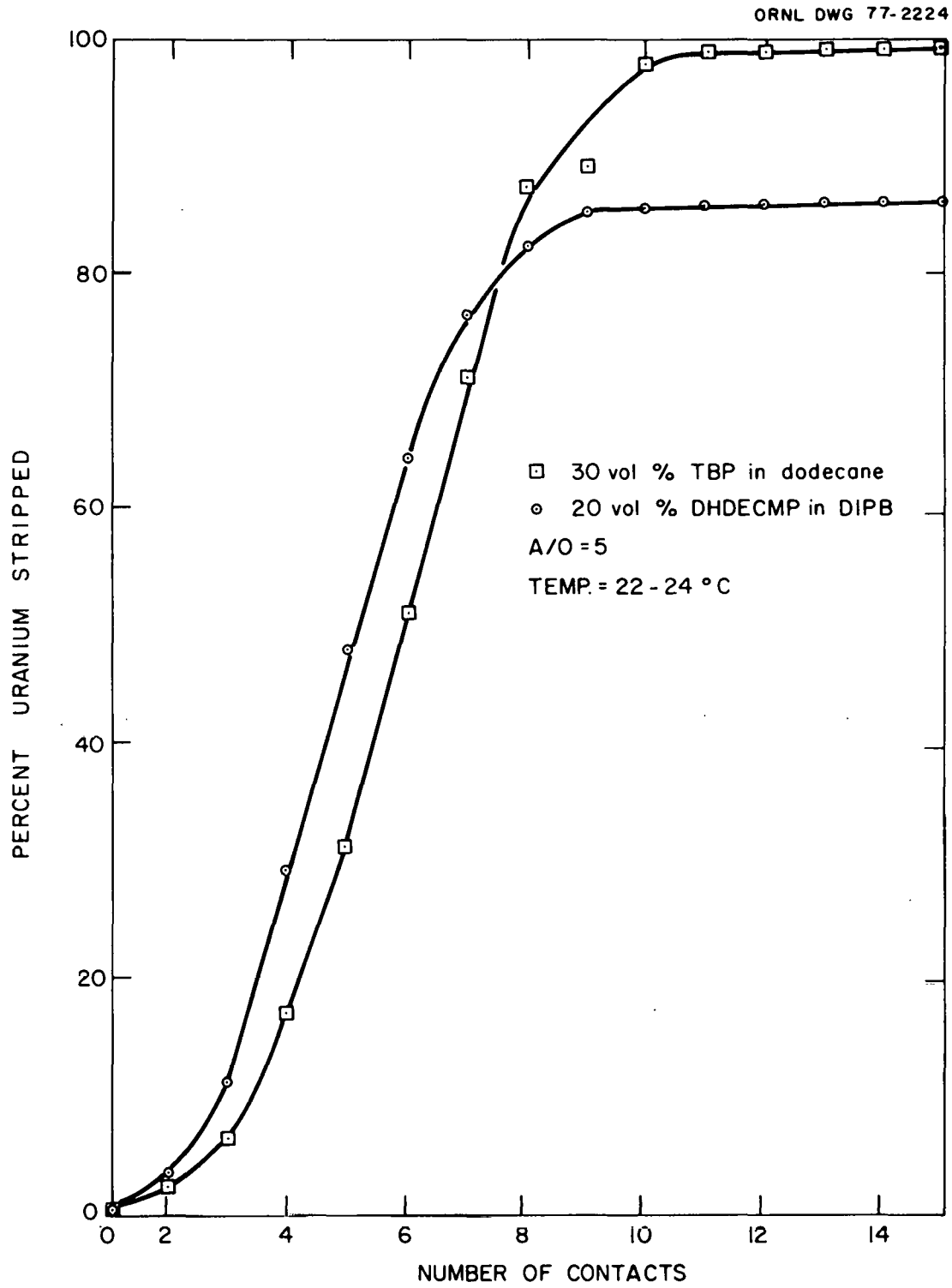

Fig. 8.2. Stripping of uranium from two extraction systems with water.

that the TBP-dodecane system permits uranium to be stripped more completely while the DHDECMP extraction system retains uranium. The leveling off of uranium removal with increased contact of the DHDECMP suggests the presence of an impurity in the DHDECMP which has a high affinity for uranium.

The extraction of plutonium from various acidified salt waste solutions was investigated. The synthetic waste solutions were prepared by adding plutonium nitrate to a basic salt waste* solution.[1] This solution was then acidified to a free acid concentration of 7 M and separated into four batches. One batch of acidified solution, which was not treated, was used as a control. A second batch was boiled for 1 hr. A third acidified solution was boiled for 1 hr, adjusted to 0.1 M Fe(II) with 3 M ferrous sulfamate, and sodium nitrite added. A fourth batch was adjusted to 0.1 M F^- with concentrated hydrofluoric acid, boiled for 1 hr, and adjusted to 0.1 M Al^{3+} with an acidified, concentrated solution of aluminum nitrate.

Each of the four acidified waste salt solutions was equilibrated seven times with a mixed extractant consisting of 20 vol % DHDECMP-30 vol % TBP-50 vol % DIPB (A/O = 5). After the fourth and seventh contacts, the aqueous phase was analyzed for plutonium. The results of these analyses are shown in Table 8.2.

The results show no difference between the acidified salt waste and the solution that was boiled. Compared to these two solutions, more plutonium was removed from the solution in which the valence of the plutonium was adjusted (Fe^{2+}, NO_2^-), and significantly more plutonium was removed from the solution treated with fluoride to destroy plutonium polymer.

These and previously reported data suggest the following tentative conclusions:[1,2]

1. A combined TBP-DHDECMP extraction system would be the best to remove actinides from combined analytical and incinerator salt wastes unless purified DHDECMP (99%) alone would permit efficient uranium back-extraction.

*This salt waste is representative of the analytical and incinerator liquors but excludes the TBP scrub solutions.

Table 8.2. Removal of plutonium from various acidified salt waste solutions with 20 vol % DHDECMP-30 vol % TBP-50 vol % DIPB

Initial plutonium concentration: 120 mg/liter
Temperature: 22-24°C
Estimated accuracy: ± 20%

Acidified waste treatment	Plutonium content after four contacts		Plutonium content after seven contacts	
	mg/liter	%	mg/liter	%
No treatment	0.10	0.08	0.05	0.04
Boiled	0.10	0.08	0.05	0.04
Boiled; Fe^{2+} and NO_2^- added	0.08	0.07	0.02	0.02
F^- added; boiled; Al^{3+} added	0.02	0.02	-	-

2. The DHDECMP extraction system will remove 99.98% of the plutonium and >99% of the americium from the acidified salt waste. The results shown in Fig. 8.3 verify the plutonium recovery.

8.3 Processing of Waste Water

The evaluation of various adsorbents to remove organics and anions from waste water was completed. The following six types of granular adsorbents were included in this study: Anasorb coconut carbon, Calgon bituminous coal carbon, Amoco carbon, Amberlite XAD-4 neutral adsorption resin, Amberlite IRA-93 anionic weak base exchange resin, and Amberlite IRA-900 anionic strong base exchange resin. Also, a nongranular adsorbent, in-situ formed OPP resin, was evaluated.

All of the adsorbents were dry-sieved to obtain a particle size between 40 and 50 mesh. The carbon samples from Amoco and Calgon had to be ground with mortar and pestle to obtain this mesh size. A weighed portion of adsorbent was poured into columns with an inner diameter of 0.6 cm to give a bed height of 10 cm. The bed volume (bv) for each granular column was 2.8 cm^3. Before use, the columns were washed with 20 bv's of methanol, 20 bv's of 1 M HNO_3, and, finally, 200 bv's of distilled deionized water.

The OPP columns were prepared by in-situ polymerization of 60 vol % toluene-40 vol % carbon tetrachloride solutions of an isocyanate and a polyol.[3] Each column, 10 cm long and 0.4 mm in diameter, was rinsed with 20 ml of heptane, 20 ml of methanol, and 200 ml of deionized-distilled water prior to use.

A 2.5-g/liter Pierce laundry detergent solution, adjusted to pH 5.0, was prepared for use as the synthetic waste stream. This solution was filtered through Whatman No. 42 paper prior to use. One-liter quantities of the detergent solution were pumped through each column at an average flow rate of 5.0 ± 0.3 ml/min. Forty-five fractions of 20 ml each were collected with an SMI drop-counting fraction collector. Selected fractions were analyzed for total organic carbon (TOC) and chloride ion to determine breakthrough capacities. The elution

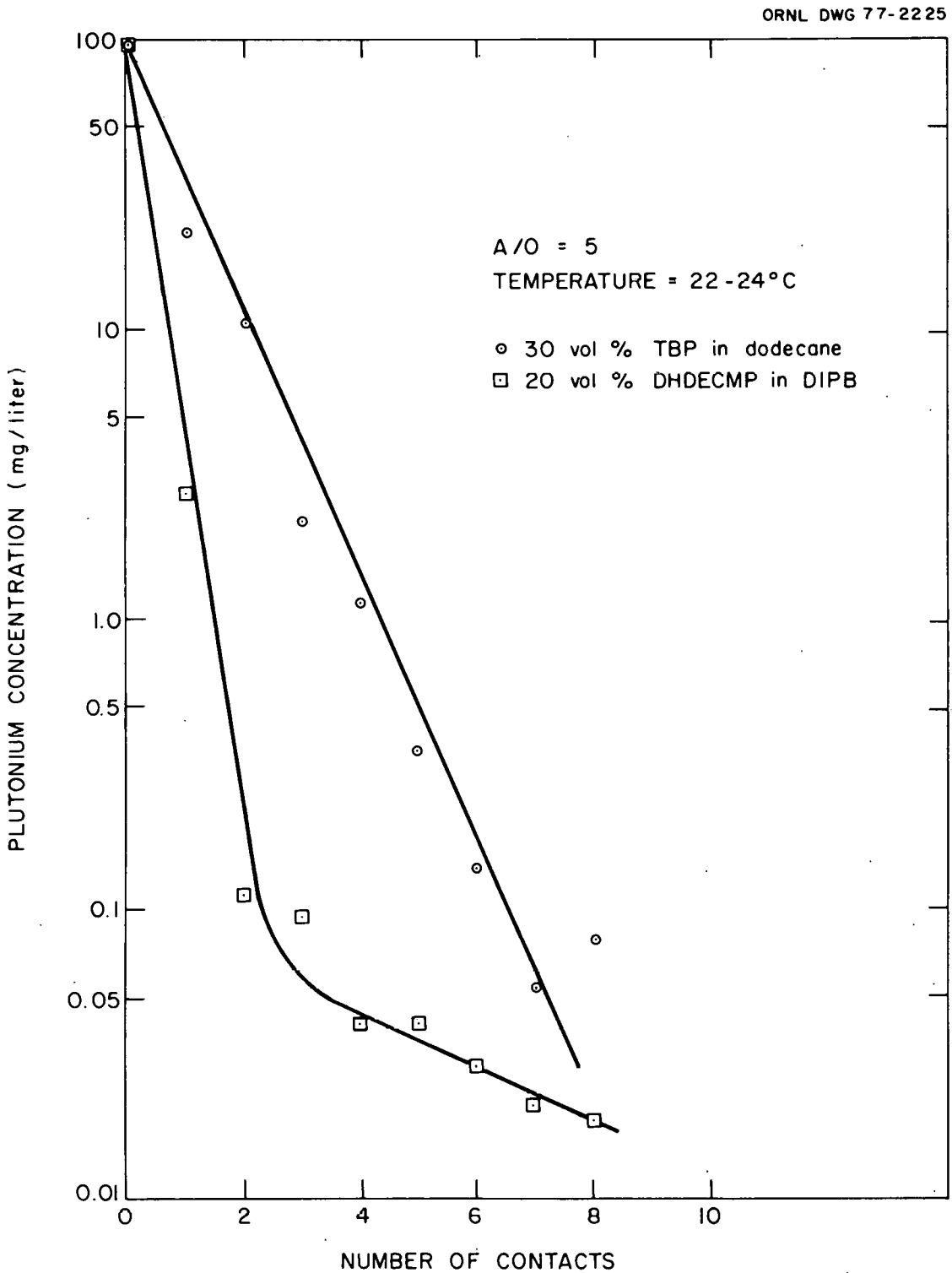

Fig. 8.3. Removal of plutonium from acidified salt waste with two extraction systems.

behavior of the materials was determined by pumping methanol through the columns at 1.5 ml/min. Fractions of the eluate were collected and analyzed to determine the elution behavior.

The results of the detergent and chloride breakthrough capacities and the elution behavior of the adsorbents are shown in Table 8.3. Amberlite XAD-4 has the highest capacity for detergent but no ionic capacity. Amberlite IRA-900 resin and OPP have the highest capacities for chloride; however, the former material would be better since the latter elutes the detergent poorly. The most rapid removal of detergent was obtained with Amberlite XAD-4. These results suggest that the use of XAD-4 and IRA-900 (mixed or in separate columns) should provide the most effective removal of organics and anions from waste water.

Figure 8.4 shows a conceptual flowsheet for removing organics and anions from waste water employing the two suggested resin schemes. The material balance is based on the assumption that the resins selectively remove the organics and anions, with the actinides following the effluents. The validity of this assumption needs to be determined with actinide-containing waste water.

8.4 Summary and Conclusions

A preliminary evaluation of methods for the salt waste and waste water streams and recycle preparation problems was completed. A feasibility study was conducted for removing actinides from synthetic salt waste using the following extraction systems: (1) 30 vol % TBP in dodecane, (2) 20 vol % DHDECMP in DIPB, and (3) 20 vol % DHDECMP-30 vol % TBP-50 vol % DIPB. The results indicate that the bidentate systems are the most efficient, providing removal of 99.98% of the plutonium and >99% of the americium.

The evaluation of adsorbents for removing detergents and anions from waste water was completed. The breakthrough capacities, with respect to total organics and chloride, were determined for six granular-type adsorbents. Results suggest the use of a combination of Amberlite XAD-4 (nonionic resin for organics) and Amberlite IRA-900 (strong base resin for anions) would be an effective preparatory step in the recycle of a waste-water stream.

Table 8.3. Breakthrough[a] and elution data on adsorbent materials

Adsorbent material	Breakthrough capacity		Elution
	ml det./g mat.[b]	mg Cl^-/g mat.[c]	(ml MeOH/g mat.)[d]
Anasorb	225	7	--
Amoco GX-31	240	--	>12
Calgon F 400	215	--	--
Amberlite XAD-4	250	--	1
Amberlite IRA-93	16	9	--
Amberlite IRA-900	11	47	--
OPP	100	48	8

[a]Breakthrough is defined as the concentration of solute in the effluent divided by the concentration of solute in the feed.

[b]Milliliters of detergent passed per gram of adsorbent at breakthrough of 0.30 TOC. TOC concentration in feed = 89 mg/liter.

[c]Milligrams of chloride passed per gram of adsorbent at breakthrough of 0.30. Cl^- concentration in feed = 1 mg/liter.

[d]Milliliters of methanol passed per gram of adsorbent when 30% of the material adsorbed on the column has been eluted.

ORNL DWG 77-2226

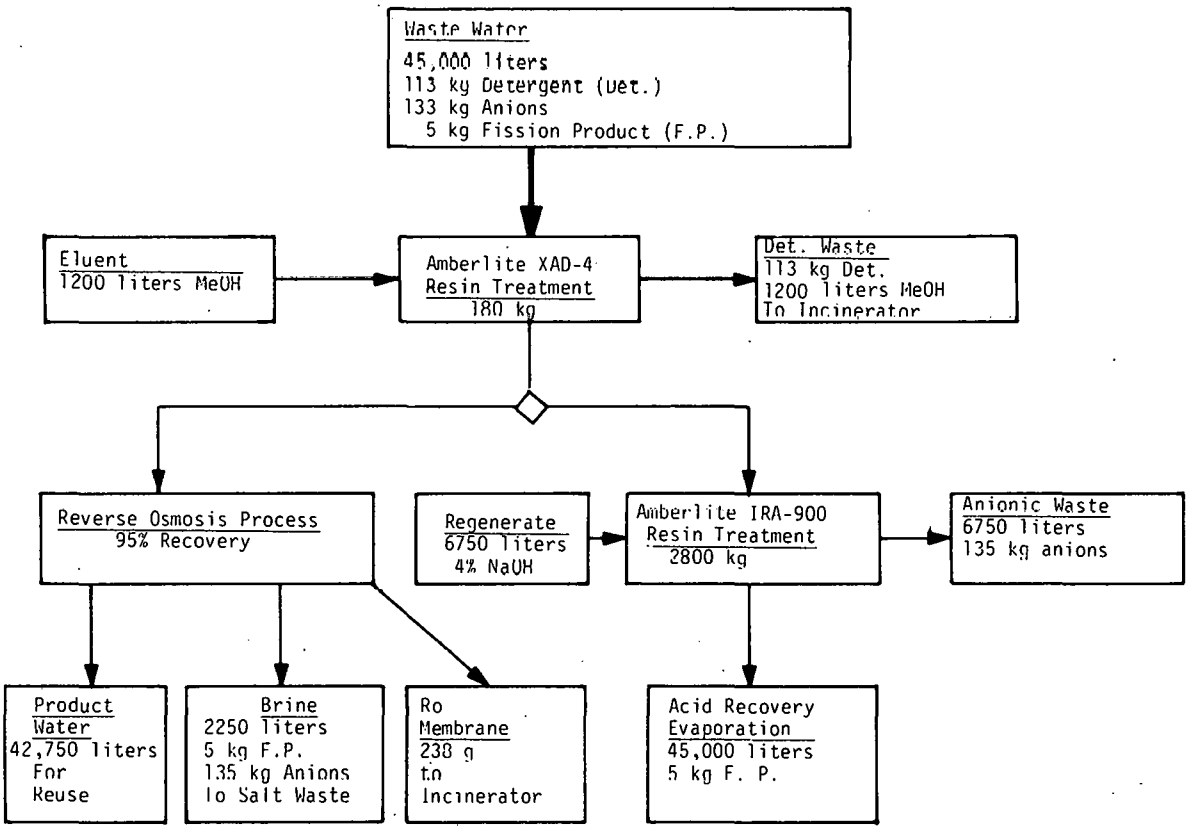

Fig. 8.4. Conceptual flowsheet for treatment of waste water.

8.5 References for Section 8

1. D. W. Tedder and J. O. Blomeke (compilers), Actinide Partitioning and Transmutation Program Progress Report for Period April 1 to June 30, 1977, ORNL/TM-6056 (October 1977).
2. J. O. Blomeke and D. W. Tedder (compilers), Actinide Partitioning and Transmutation Program Progress Report for Period October 1, 1976 to March 31, 1977, ORNL/TM-5888 (June 1977).
3. J. D. Navratil and R. E. Sievers, "Chemical Separations with Open-Pore Polyurethane," Am. Lab. 9(10), 38 (1977).

9. RADIATION EFFECTS

T. E. Gangwer, M. Goldstein, and K. K. S. Pillay
(Brookhaven National Laboratory)

This task examines the formation of radiation products in waste streams encountered in fuel reprocessing and refabrication plants which operate with a high degree of stream recycle. Analysis will provide methods of predicting the formation of chemical species which interfere with process operations or result in operating hazards.

The study of radiation effects on ion exchange materials is near completion, and the results will be published as a Brookhaven National Laboratory report.

10. FUEL AND TARGET FABRICATION STUDIES

(Oak Ridge National Laboratory)

This task identifies primary and secondary transuranic waste streams and evaluates waste treatment processing options for fabrication plants that are operated under the actinide partitioning concept. Chemical and equipment flowsheets will be prepared for use in a detailed cost estimate of these plants. The effects of alternate fuel forms are also examined.

This task was inactive during this report period.

11. LMFBR TRANSMUTATION STUDIES

M. L. Williams and J. W. McAdoo (Oak Ridge National Laboratory)

The objective of this task is to examine the in-reactor aspects of long-lived nuclide transmutation in projected commercial LMFBRs. During FY 1977, this subtask will be concerned with scoping studies leading to the determination of one or two preferred transmutation modes which will be examined in detail in FY 1978.

The LMFBR transmutation studies were terminated at the end of this quarter, and a final report of the work accomplished is in preparation.

12. THERMAL REACTOR TRANSMUTATION STUDIES

T. C. Gorrell (Savannah River Laboratory)

The objective of this subtask is to study the in-reactor aspects of long-lived nuclide transmutation in thermal reactors. Uranium- and plutonium-enriched LWRs will be the principal reactor types examined, although "CANDU" and high-power-density (SRL production type) thermal reactors will also be considered. During FY 1977, this subtask will be concerned with scoping studies leading to the determination of one or two preferred thermal reactor transmutation modes which will be examined in detail in FY 1978.

Transmutation studies for this quarter were made for four configurations of target material:

1. all actinides from one fuel assembly recycled into a new fuel assembly with ^{235}U added as needed for reactivity,
2. all actinides from five fuel assemblies recycled into a new assembly containing natural uranium,
3. waste actinides (excludes uranium and plutonium) recycled in a target irradiated in a D_2O reactor, and
4. waste actinides (excludes uranium and plutonium) from uranium and plutonium fuel assemblies recycled in a separate target assembly in a uranium-plutonium lattice.

A brief description of results for each configuration follows. Calculations were made using the Savannah River Laboratory's GLASS code, which computes multigroup neutron spectra and reaction rates for specified configurations of fuel and target assemblies.

12.1 All Actinides Recycled, with ^{235}U Added as Needed

In this mode of recycle, all actinides (including uranium and plutonium) were mixed with fresh fuel material, and the ^{235}U content was adjusted as needed for reactivity. This option could be used if the plutonium were not destined for future use in a breeder reactor. The irradiation time was 3 years (33,000 MWd/MT), while 1 year was

allotted for reprocessing and refabrication. After five recycle operations, the inventory of waste actinides in the spent fuel was 61% of that which would have been present without recycle (i.e., 39% of the waste actinides were fissioned).

Primary advantages of this recycle mode are that all operations associated with separate targets are eliminated and that plutonium is never fully separated from uranium, an important consideration in nonproliferation. The primary disadvantage is that special handling procedures are required for all fuel assemblies during fabrication and shipment operations because of high activity levels of the actinides.

12.2 All Actinides Except Uranium Recycled with Natural Uranium

All actinides except uranium were returned to the reactor, with the residues from five assemblies concentrated in one assembly of natural uranium. The initial reactivity for this case was the same as for the previous case. After five recycle operations, in which the waste actinides from five assemblies were added to the process stream each time, the inventory of waste actinides was 75% of that which would have been observed in the absence of recycle (25% of the waste actinides were fissioned). This case is impractical for any long-term operation because the new plutonium added from the five regular fuel assemblies at the start of each recycle far exceeded the plutonium burned in the target, and the plutonium content of the target increased to unacceptable values.

12.3 Waste Actinides Irradiated in D_2O Reactor

This case was included in the study to show that accelerated actinide depletion rates can be achieved in the SRP D_2O reactors. Target slugs containing waste actinides (no uranium or plutonium) from 100 LWR fuel elements were placed inside a tubular SRP fuel assembly containing enriched ^{235}U. After 1 year of irradiation, the remaining actinides were recovered and added to those from 100 other

additional elements for further irradiation in a new fuel assembly. Out-of-reactor time was 1 year. After five recycle operations, the inventory of waste actinides was 65% of that had there been no recycle. The total elapsed time was 10 years, as compared with 20 for five recycles in an LWR reactor. If a D_2O reactor were used for transmutation, a more efficient mode of operation would be to extend the irradiation of a given target from one to several fuel cycles, thus reducing the out-of-reactor time.

12.4 Waste Actinides Irradiated in Uranium-Plutonium Reactor

The reactor fuel loading for this case differed from previous ones in that one-third of the assemblies were plutonium-enriched. The remaining two-thirds were 3.2% ^{235}U-enriched. The process streams for the two types of fuel were kept separate during recycle operations. It was assumed that the required amount of plutonium was available initially, and that the initial composition of the two fuel types remained constant at the start of each cycle. Beginning and ending contents of the two assembly types are shown in Table 12.1. Neptunium-237 from a uranium-plutonium assembly was about one-third that from a uranium assembly because of the lower initial ^{235}U content and subsequent reduced ^{236}U production; however, a uranium-plutonium assembly produced larger quantities of americium and curium.

Waste actinides (excluding uranium and plutonium) were irradiated in separate target assemblies. Inner element locations, about 40% of the total, contained water rather than waste actinides to enhance the average thermal flux in the target assembly. Two actinide loadings were considered: a "light" loading, where waste actinides from 5 uranium assemblies and 2.5 uranium-plutonium assemblies were concentrated in single target assembly; and a "heavy" loading, where the contributing assemblies were increased to 20 and 10 respectively.

With the light loading, the thermal flux in the target was twice that in the uranium fuel, and there was little self-shielding of the actinide epithermal cross sections. Both conditions enhanced the actinide depletion rate. After five recycles, the inventory of waste

Table 12.1. Actinide contents of LWR fuel assemblies

Actinide	Actinide content (g/MT)			
	Enriched uranium		Uranium-plutonium mixture	
	Start of cycle	End of cycle	Start of cycle	End of cycle
^{234}U	0.289E03	0.154E03	0.265E03	0.178E03
^{235}U	0.320E05	0.814E04	0.658E04	0.305E04
^{236}U		0.401E04	0	0.707E03
^{238}U	0.968E06	0.943E06	0.948E06	0.927E06
^{237}Np		0.523E03	0	0.184E03
^{238}Pu		0.173E03	0.101E04	0.995E03
^{239}Pu		0.574E04	0.224E05	0.105E05
^{240}Pu		0.236E04	0.116E05	0.104E05
^{241}Pu		0.127E04	0.665E04	0.517E04
^{242}Pu		0.551E03	0.379E04	0.549E04
^{241}Am		0.111E03		0.652E03
^{243}Am		0.109E03		0.112E04
^{242}Cm		0.337E01		0.286E02
^{244}Cm		0.332E02		0.593E03
^{245}Cm		0.181E01		0.532E02
Total	0.100E07	0.966E06	0.100E07	0.966E06

actinides was 46% of that had there been no recycle. However, the specific power of the target assembly was only one-third that of the regular fuel assemblies, which constitutes inefficient use of lattice space for the target material irradiation.

With the heavy target loading (actinides from 20 uranium assemblies and 10 uranium-plutonium assemblies concentrated in one target), the specific power of the target assembly was about equal to that of the other assemblies. However, the accompanying decreases in thermal flux and epithermal cross sections from self-shielding resulted in a reduced transmutation rate. After five recycles, the inventory of waste actinides was still 75% of that had there been no recycle. During recycle 5, 10% of the actinides in the target assembly were fissioned.

12.5 Program for Next Quarter

The program planned for next quarter includes the following tasks:

1. completely assessing the actinide irradiation cases,
2. selecting the most favorable option,
3. planning the study program for FY 1978, and
4. writing the DP report describing FY 1977 studies in detail.

13. FUEL CYCLE IMPACT STUDIES

(Oak Ridge National Laboratory)

The objective of this task is to analyze the impacts of partitioning-transmutation that are not being considered by other subtasks. Examples of such impacts are the effects of the recycled actinide neutron activity on nuclear fuel cycle operations and determination of the recycled actinide inventories in the fuel cycle.

This task was not active during the July-September report period.

14. RISK/BENEFIT ANALYSIS OF CONCEPT

A. G. Croff (Oak Ridge National Laboratory)

The objective of this task is to estimate the additional risks that are incurred as a result of increased handling of the long-lived nuclides, and the long-term benefits that would accrue as a result of the biologically significant, long-lived nuclide content of fuel cycle wastes being significantly reduced.

Although this subtask was not formally active during this report period, planning activities have begun in an attempt to more accurately define the type of risk-cost/benefit analysis that might be obtained. As a first step in this direction, a discussion of the factors to be considered in the risk-cost/benefit analysis (Sect. 14.1) and how these factors might be used in making the risk-cost/benefit comparison (Sect. 14.2) is presented below. This discussion is concerned with the case where the waste actinides (neptunium, americium, and curium) are recycled separately in a target assembly, which is somewhat more general than the case where the waste actinides are homogeneously distributed in the reactor fuel.

14.1 Analysis of the Risks, Benefits, and Costs of Partitioning-Transmutation for Individual Fuel Cycle Operations

The evaluation of the partitioning-transmutation (P-T) concept is comprised of two distinct phases. The first phase is principally concerned with identifying potential partitioning and transmutation methods, experimentally or calculationally investigating these methods, analyzing the results of the investigations and selecting preferred methods for accomplishing P-T, and determining the probable performance of the selected methods and the uncertainty associated with this determination. The second phase of the overall evaluation of P-T involves (1) determining the impacts of the preferred P-T method on the risks, benefits, and costs of each individual nuclear fuel cycle operation relative to a fuel cycle without P-T; and (2) developing and

implementing a method for putting the individual risks, benefits, and costs of P-T on a comparable basis and establishing the incentives for P-T.

The purpose of this section is to discuss the determination of the individual fuel cycle impacts that would result from P-T relative to those in a fuel cycle without P-T. The fuel cycle operations that will be directly affected by P-T, and which must be considered when calculating the impacts of P-T, are: (1) fuel fabrication [(plutonium-enriched (MOX) and waste-actinide target fabrication)], (2) transportation of the waste actinides (fresh fuel, spent fuel, TRU wastes), (3) transmutation of the waste actinides, (4) reprocessing of spent targets and fuels, and (5) disposal of radioactive wastes. The indices of the impacts of P-T that will be used are: (1) the risk to the general population and operating personnel, (2) the benefit that would result from P-T, and (3) the changes in nuclear fuel cycle costs resulting from P-T.

Section 14.2 will consider how the incentives for P-T are to be established, assuming that the individual risks, benefits, and costs are known.

Before entering into a detailed discussion of the determination of risks, costs, and benefits, it is useful to define the premises upon which the following sections are based. As was noted earlier, the risks, benefits, and costs (R,B,&C) of P-T will be compared on a relative basis. Thus a "reference" fuel cycle without any provisions for P-T is needed as a starting point. The proposed reference fuel cycle contains only PWRs which use 70% uranium-enriched fuel and 30% plutonium-enriched natural UO_2 (MOX) fuel. The neptunium and transplutonium elements are assumed to be recycled in waste actinide targets (WATs), with a neutronically inert diluent being used to achieve the correct WAT specific power. The WATs are assumed to be irradiated in a PWR-Pu. The WAT and MOX fuels are assumed to be fabricated and reprocessed in separate facilities.

14.1.1 Fabrication of MOX fuel

Plutonium and ^{241}Am, which are present in MOX fuel fabrication plants, would have to be recovered from the plant wastes if P-T were implemented. Thus the parameters to be determined are the R,B,&C of MOX fuel fabrication plants with and without partitioning. It should be noted that, if the WAT irradiation were to take place in the PWR-Pu, the amount of MOX fuel required would decrease by 1.0 to 3.0%, depending on the specific recycle mode selected.

Routine risk to the general population. The routine risk to the general population that is imposed by a MOX fabrication plant is in the form of continuously released chemical, thermal, and radiological effluents. The implementation of partitioning, with the resulting increase in chemical processing, can be expected to increase the rate at which chemical, thermal, and radiological wastes are generated within the fabrication plant.

The increased thermal effluents must be released to the environment, since heat cannot be "captured" and disposed of otherwise. The only choice is whether it should be released to the atmosphere or to a body of water. An important question concerning thermal effluents is how to meaningfully quantify the risk represented by the heat. This aspect will be considered generically in Sect. 14.2.1.

The risk imposed by the increased generation of chemical and radiological wastes can be handled in two ways. First, it can be assumed that the application of additional off-gas treatment operations will reduce the effluent release rates to the same values as those in the fabrication plant without partitioning. This procedure effectively translates the potential risk increase into an increased cost. Alternatively, it can be assumed that the same chemical and radiological decontamination factors are experienced in both plants. Under this procedure, an increase in chemical and radiological effluents, and therefore in risk to the general population, would result in the plant with P-T. The magnitude of this increase should be readily calculable using existing environmental models after the source terms have been specified.

Routine occupational risk. The routine occupational risk imposed by a MOX fabrication plant results from the radiation emitted by the plutonium during processing. Application of sufficient amounts of shielding can generally reduce the dose rate per individual to a relatively low, constant value. However, an increase in total dose would be expected because the increased scope of a fabrication plant with partitioning, as compared with one without this capability, would require more operating personnel. Each of these additional people would (presumably) be exposed to the low, constant dose rate and would thus represent an incremental risk over that incurred with the nonpartitioning case.

Estimates of this risk can probably best be made by assuming an average dose rate per employee and estimating the total required number of operating personnel in fabrication plants with and without partitioning. However, the problem that still remains is how to compare occupational risk, where there is compensation, with risk to the general public, where there is usually no compensation. This point will be considered further in Sect. 14.2.2.

Accidental risk to the general population. The accidental risk imposed by a MOX fabrication plant is represented by the possibility that a significant fraction of the plant's inventory could be dispersed during upset conditions. The upset conditions that must be considered are criticality, explosions, fires, severe storms, earthquakes, and the impact of aircraft.

Analysis of these accidents is similar to the analysis of the risk to the general population from routine effluent releases. That is, the release rate of a particular effluent is calculated, and the risk from this release is subsequently determined by applying standard meteorological models. However, the determination of the appropriate effluent release rate is much more difficult in the accidental release case than in the routine release case because the probability of release in the routine case is unity, whereas the accidental case requires that release probabilities be estimated for relatively unlikely events in systems for which little or no experience has been

accumulated. The release probabilities for each accident situation are multiplied by the corresponding quantity of effluent released (which can also be difficult to calculate) and then summed to yield the effective effluent release rate.

Accident risk to occupational personnel. If certain types of accidents (e.g., an explosion) were to occur within a MOX fabrication plant, some of the operating personnel might be injured or killed or might inhale toxic species. Since the probability of an accident presumably increases due to the increased processing required in partitioning, this type of risk should be taken into account. The problems with this analysis are a combination of those present when attempting to determine the routine occupational risk and the accident risk to the general population. That is, it is necessary to establish how risk to the general public and occupational risk are to be compared and how the accident probabilities and consequences are to be determined. It is not evident whether the capability for conducting this type of analysis exists.

Costs. Determination of the costs of MOX fabrication plants with and without partitioning will involve (1) specifying a plant layout, and (2) applying existing cost estimation techniques based on the conceptual partitioning flowsheets developed at ORNL and a reference MOX plant flowsheet. Because of its greatly increased scope, the plant with partitioning is expected to cost considerably more than the plant without partitioning. Further cost increases could accrue if additional equipment were employed to reduce the effluent release rates to the same value as that in a plant without partitioning, as mentioned above.

14.1.2 Fabrication of waste actinide targets

It is currently anticipated that the highly radioactive waste actinides will be recycled in separate fuel assemblies so as to prevent dilution with the bulk of the fresh fuel. To minimize the number of these assemblies, a neutronically inert diluent, such as MgO, will probably be used instead of UO_2. Despite these differences, it is apparent that, for the purposes of the ongoing P-T program, the design

of the WAT fabrication plant would be similar to that of the MOX fabrication plant. This state of affairs will probably continue until waste actinides plus a diluent are actually fabricated to determine the adequacy of this assumption.

Given the above assumed similarity between WAT and MOX fabrication processes, it is evident that the methods used to determine the R,B,&C of MOX fabrication (Sect. 14.1.1) would also be applicable to WAT fabrication. However, even though the same methodology is used in each case, the significant differences in detail between the two plants must be taken into account.

The first difference is that the WAT fabrication plant would be much smaller than the MOX plant since it would only have to fabricate about 3% as much fuel. Thus it is entirely conceivable that one WAT plant could serve the entire United States. The second difference is the intense radioactivity of the waste actinides as compared with that of plutonium. The neutron activity of the waste actinides is three to six orders of magnitude larger than that from LWR plutonium. The decay heat of the waste actinides is roughly a factor of 7 larger than that of LWR plutonium. The third difference between MOX and WAT fuel is that the waste actinides are much more toxic than plutonium because they contain high concentrations of short-lived alpha emitters. However, even though these three factors will have a substantial impact on the detailed design and analysis considerations for the WAT fabrication plant, it presently appears that the methodology used to assess the R,B,&C of MOX fabrication with and without partitioning would be applicable to the WAT plant.

14.1.3 Transportation of fresh and spent MOX fuel

The characteristics of MOX fuel are unchanged by the presence or absence of partitioning. Therefore, the R,B,&C of MOX fuel transportation with and without partitioning are expected to be unchanged, except for a 1 to 3% decrease in the quantity shipped because the WAT irradiation takes place in the PWR-Pu.

Routine risk to the general public. The routine risk to the public imposed by the transportation of fresh and spent MOX fuels results from the dose imparted to the public by neutrons and gamma rays along the transport path. Quantification of this risk consists of calculating the dose rate at an appropriate distance from the shipping container (e.g., 10 mrem/hr at 6 ft), estimating the transport distance, and postulating the population density along the selected route. This risk has traditionally been one of the largest imposed by the nuclear fuel cycle.

Routine occupational risk. The routine occupational risk imposed by the transportation of fresh and spent MOX fuel also results from the radiation dose received by operators of the transport vehicle. Given the relatively fixed geometry involved, specification of the dose rate and exposure time should yield the risk in a straightforward manner. This risk, although expected to be small, should be easily calculable.

Accidental risk to the general public. The accidental risk imposed on the general public by MOX fuel transportation arises from the possibility that the fresh or spent MOX fuel might be dispersed in a collision or in a subsequent fire. Calculation of this risk involves determining the accident and dispersal probabilities as a function of fuel quantity released and then applying a standard meterological model to quantify dose. In the past, this risk has been calculated by several organizations and thus should be readily calculable for the cases of interest when considering P-T. It should be noted that the accidental risk from spent fuel transportation has been calculated to be on the order of a factor of 1000 smaller than the routine risk resulting from radiation.[1]

Accidental occupational risk. The accidental occupational risk imposed by the transportation of MOX fuel stems from possible dispersal and from the possibility of death or injury inherent in the operation of any moving vehicle. The former risk can be calculated using the same techniques described above. The latter risk can be determined from well-established statistical compilations related to death and

injury in collisions and hence should be relatively straightforward. This risk will probably be small because of the small population involved.

Costs. The total cost of transporting fresh and spent MOX fuels is comprised of operating costs (salaries, fuel, taxes, etc.) and amortization costs associated with the relatively large investment in the shielded fuel package. Since both fresh and spent uranium-enriched fuels have been transported in the past, the MOX transportation costs can probably be estimated quite accurately by adjusting the costs for uranium-enriched fuels. The transportation costs for fresh MOX fuels may be higher when compared with those for fresh uranium-enriched fuels because of the additional toxicity and neutron activity of the former. Transportation costs for the two types of spent fuels are expected to be nearly identical because the gamma radiation, which will be the controlling factor, will be roughly equal in both fuels for equivalent burnups.

14.1.4 Transportation of waste actinide targets

The considerations involved in transporting the WATs are the same as those (see Sect. 14.1.3) for transporting MOX fuel. Therefore, the general methodology used for MOX fuel can probably also be used for the WATs. The major significant difference between the two cases is that existing cask designs are not applicable to the transportation of WATs because of the high neutron activity. Therefore, a special shipping cask must be designed for this application. The problem of providing massive neutron shielding while still allowing for spent fuel heat dissipation promises to be quite difficult.

14.1.5 Transportation of normal radioactive waste

The quantity of radioactive wastes transported from the MOX fuel fabrication plant and all spent fuel reprocessing facilities can be expected to increase significantly with the implementation of partitioning. This increase can be expected to lead to larger waste transportation risks and costs which can be calculated using the methodology defined

in Sect. 14.1.3. It is likely that shipping package designs presently exist for these wastes, thus requiring little or no additional engineering design effort.

14.1.6 Transportation of wastes from target fabrication and reprocessing plants

The considerations involved in determining the R,B,&C of transporting wastes generated by WAT processing are exactly the same as those for transporting the WATs (Sect. 14.1.4). That is, the methodology for calculating the R,B,&C is the same as that described in Sect. 14.1.3; however, special conceptual transportation cask designs will be required for the neutron-active low-, intermediate-, and high-level TRU waste and cladding waste.

14.1.7 Transmutation reactor

According to the most recent guidelines from the Department of Energy, we are to consider only LWRs as irradiation devices for the WATs. Furthermore, as a result of their predominance and amenability to physics calculations, PWRs are preferred over BWRs. The presence of the WATs at a large nuclear power station could have many, diverse effects on the R,B,&C of reactor operation, which are discussed below. Although none of these impacts has been analyzed in detail, all except the cost impact appear to be small.

Routine risk to the general public. The incremental routine risk to the general public from the presence of WATs at the reactor site is expected to be nil. This is because the routine risk from a PWR results from its thermal, chemical, and radiological releases, and the character and magnitude of these releases should not be affected by the WATs. An exception could occur if there were fuel-clad compatibility problems with the WATs, causing a higher number of elements to release the volatile fission gases.

Routine occupational risk. The routine occupational risk imposed by the WATs during reactor operations can be expected to be somewhat larger than that resulting from normal reactor fuels because of the

increased neutron radioactivity of the WATs as compared with MOX fuel. However, it should be possible to reduce this risk to nearly zero by handling the fresh WATs in the same manner as spent fuel (i.e., underwater or in a shielded cask).

Accidental risk to the general public. There is no apparent reason why the presence of WATs at a nuclear power station should increase the accidental risk to the general public, assuming that the neutronic and physical characteristics of the WATs are such that the likelihood of an accident is not increased. The principal reason for this is that volatile fission product isotopes (^{85}Kr, ^{131}I, etc.) dominate the consequences of assumed reactor accidents because of their dispersibility. Thus, even though the WATs contain increased amounts of actinides with high specific toxicities (e.g., ^{242}Cm, ^{241}Am) as compared with the MOX fuel, their refractory nature produces a negligible impact on the overall consequences of an accident.

Accidental occupational risk. The accidental occupational risk at a nuclear power plant could increase slightly due to the presence of the WATs for two reasons: (1) the necessity for more frequent handling of large shipping casks; and (2) the greater decay heat generation rate of the WAT, which makes overheating in the absence of cooling a possibility. Since these effects should be small and are difficult to calculate, it is probably acceptable to neglect them.

Costs. The cost of operating the PWR transmutation reactor is expected to be significantly higher than that of a PWR fueled with MOX fuel alone. The principal cost increases that can be identified at present result from the increased fuel enrichment required to drive the subcritical WATs and are as follows:

1. additional enriching services (uranium-enriched fuel),
2. additional natural uranium (uranium-enriched fuel),
3. additional plutonium (MOX fuel), and
4. increased ^{235}U and fissile plutonium consumption because of decreased plutonium production in the fuel and the WATs.

These factors will be counteracted somewhat because (1) neither enriched uranium nor plutonium is required for the WATs, and (2) the

waste actinides fission and contribute to the reactor's heat production. However, a net fissile deficiency (which will result in a net cost increase) is still anticipated.

The intense radioactivity of the WATs could cause additional cost increases if it resulted in either increased personnel requirements for handling or increased reactor downtime (i.e., decreased capacity factor) for refueling, or both.

The cost effects of the increased fissile makeup requirements should be readily calculable after the reactor physics studies have been completed. The cost of increased personnel or downtime will probably be impossible to estimate accurately.

14.1.8 Reprocessing of spent reactor fuels

The considerations involved in determining the R,B,&C of MOX fuel reprocessing are the same as those for the MOX fabrication plant (Sect. 14.1.1) and thus will not be discussed in detail here. The only point to be noted is that the reprocessing plant should be assumed to be handling a mixture of 70% spent uranium-enriched fuel and 30% spent MOX fuel, instead of MOX fuel alone.

14.1.9 Reprocessing of the WATs

As with the MOX fuel reprocessing, the considerations involved in determining the R,B,&C of WAT reprocessing are expected to be the same as those for the WAT fabrication plant (Sect. 14.1.2). It may be possible to define the WAT reprocessing flowsheet more precisely than that of the WAT fabrication plant since the partitioning studies will be conducted as a part of the P-T program.

14.1.10 Waste disposal operations

Determination of the R,B,&C resulting from waste disposal operations with and without P-T is one of the most complex and important aspects of the entire R,B,&C analysis. Not only are the routine vs accidental and the general public vs occupational considerations present, but the

short-term vs long-term problem must also be considered along with the disposal of low-, intermediate-, and high-level wastes.

For the purposes of this program, a specific geologic repository will probably have to be assumed if the analysis is to be credible. The interconvertibility of waste types within the fuel cycle will probably require that all TRU wastes be emplaced in the same repository. The nuclide inventory in the repository must be known for cases with and without P-T.

Routine risk to the general public. By definition, all risk to the general public from a waste repository is accidental. Therefore, this risk is zero.

Routine occupational risk. The routine occupational risk imposed by waste management results from the routine radiation exposure during emplacement operations. If it is assumed that the dose per package is constant (for a given waste type), then the dose commitment resulting from waste management operations will be proportional to the waste volume and thus to the number of employees.

Accidental risk to the general public. Determination of the accidental risk imposed by a waste repository to the general public is one of the most important aspects of the R,B,&C analysis since the magnitude of the benefits (i.e., risk reduction), if any, will be defined here. Two factors are involved in determining this accidental risk: the short-term risk from emplacement mishaps, and the long-term risk from radionuclide release from the seabed repository.

Determination of the risk from waste emplacement operations includes consideration of the possibility that the waste package might be breached by physical or thermal forces after being removed from the shipping cask and the contents might be dispersed in some manner so as to reach the general public. Analysis of this scenario would be very difficult without access to a detailed repository design and the operational procedures for the repository, which are unlikely to be available before the end of the P-T program.

At any time after the repository has been sealed, there is a chance that it will be breached and the contents released. This breach can be natural or man-made, sudden or slow, large or small, or anywhere

between these extremes. The probability that a radionuclide release has occurred, although small initially, grows larger with time. On the other hand, the toxicity of the material in the repository generally becomes smaller with time.

The required determinations are: (1) the probability that a given release scenario (i.e., release pathway, quantity, and rate) has occurred as a function of waste decay time; and (2) the consequences of the release scenario in terms of, for example, man-rem. A sum over all possible accident scenarios will yield the probabilistic dose commitment as a function of time. Presumably, the lower actinide and ^{129}I inventories in the repository with P-T as compared with the same case without P-T will reduce the long-term risk imposed by the repository, thus supplying a calculated benefit for P-T. The difficulty in this procedure is in establishing the release-scenario probabilities for times far beyond human experience. While techniques are being developed to perform this type of analysis, the results of the analysis will be, at best, estimates. Even though the accident analysis of the long-term repository is very uncertain, it still must be performed since the calculated long-term risk reduction will constitute the major anticipated net benefit when the overall comparison of the risks, benefits, and costs of P-T is made.

Accidental occupational risk. The occupational risk from accidents in a repository derives from events such as mine explosions and cave-ins, dropping of shipping casks, rupture of waste packages due to overheating or improper packaging, etc. The frequency of these accidents can probably be expected to be larger in a fuel cycle with P-T because of the larger projected waste volumes. A reasonable assumption might be that risk is proportional to the waste volume handled.

Costs. Waste management costs in a fuel cycle with P-T are expected to be greater than those in a fuel cycle without P-T because the waste volume being handled is expected to be larger and the wastes from WAT fabrication and partitioning will have high neutron activities, requiring additional shielding during emplacement. A reasonable approximation might be to assume that cost is directly proportional to waste volume and ignore the higher neutron activity of the WAT wastes. It should be noted that this procedure may not be valid for high level wastes, where the heat generation rate may be the controlling factor.

14.2 Overall Considerations in Determining the Incentives for P-T

The purpose of this section is to discuss several aspects of the determination of the incentives for P-T that have an impact on several different fuel cycle operations. The first aspect considered (Sect. 14.2.1) is the quantification of risk. That is, if a given facility releases chemical, thermal, and radiological effluents, we need to know what units the risk is to be expressed in so that the effluent impacts can be determined on a comparable basis. The second aspect considered (Sect. 14.2.2) is how calculated occupational risk is to be incorporated into the overall incentives analysis with risk to the general public. The third aspect to be discussed (Sect. 14.2.3) concerns the specification of fuel cycle flowsheets with and without provisions for P-T. These flowsheets will form the basis for the incentives analysis. Section 14.2.4 discusses the comparison of the individual R,B,&C for each fuel cycle operation, leading to a determination of the incentives for partitioning. The final section (Sect. 14.2.5) summarizes the substances of Sects. 14.1 and 14.2.1-14.2.5 and attempts to assign priorities to individual tasks.

14.2.1 Quantification of the risks, costs, and benefits of P-T

The three principal sources of risk considered in Sect. 14.1 were radiological, chemical, and thermal. A particularly difficult question that must be resolved is how to quantify the risk from each source so that all of them are on a comparable basis.

Three different measures of risk are possible in the case of radiological effluents. The first is to calculate the dose commitment in units of man-rem. The second is to calculate the dose commitment and then convert it to health effects by assuming X cancers per man-rem. The third is to calculate the cost of reducing the routine radiological releases in a P-T fuel cycle to the same value as that in a fuel cycle with no P-T, thereby effectively converting man-rems to dollars. In the case of accidental radiological releases (including the waste repository), the maximum value of $1000 per man-rem equivalency would

probably have to be used since it may be impossible to determine the cost of reducing the radiological risk from an accident. Each of these measures of risk could likely be used in a P-T incentives analysis.

Consideration of the risk measure for chemical effluents is complicated because the toxicities of these effluents are not related to radioactivity. This lack of relationship effectively precludes the use of man-rem as a risk measure. One alternative would be to apply a factor that converts the chemical effluent concentration in air or water to health effects (e.g., Y deaths per ppm of increase in atmosphere NO_x). The availability and defensibility of such conversion factors are not presently known. A second alternative would be to calculate the cost of reducing the levels of chemical effluents in a fuel cycle with P-T to those found in a fuel cycle without P-T.

The quantification of risk from thermal effluents can be approached in much the same way as is done for chemical effluents, that is, either convert Btu's to health effects or calculate the cost of eliminating the risk. However, two additional complications are present in the case of thermal effluents. The first is that heat can be detrimental, neutral, or beneficial to the environment, depending on the circumstances of its release. The second complication is that it is impossible to "capture" thermal effluents in the same manner that radioactive and chemical effluents are captured. The only choice is whether the heat is to be released to a body of water (usually assumed to be detrimental) or to the atmosphere (usually assumed to be neutral).

Two risk measures, health effects and dollars, are common to all three effluent categories. Of these, the use of dollars would seem to be preferred over the use of health effects for two reasons. First, the conversion of chemical releases to health effects promises to be both controversial and difficult, while the conversion for thermal effluents would be almost impossible. The second advantage of using dollars as a measure of risk is that the risks and benefits would then be on the same basis as the costs of P-T, thus eliminating another compatibility problem in the risk-benefit-cost equation.

14.2.2 Incorporating occupational risk into the incentives analysis

The following discussion considers how occupational risk is to be placed on a comparable basis with risk to the general population, thus allowing it to be directly incorporated into the P-T incentives analysis. Two basic considerations make the direct incorporation of occupational risk difficult. First, because of their close proximity to the effluent sources and accident situations, and because allowable occupational doses are much higher than those for the public, the total occupational risk is much higher than the total risk to the general public. The second consideration is that the operating personnel have voluntarily chosen to accept this risk and are presumably fully compensated for it by their salaries. Thus, if occupational risk were directly incorporated into the incentives analysis, the voluntary, compensated risk would predominate over the involuntary, uncompensated risk to the public. Such a result would seem to defeat the purpose of a risk-cost/benefit analysis (viz., to ensure that the risk to the general population is reduced to the point where the incremental cost is greater than the incremental benefit). The only possible method for alleviating this situation would be to multiply the calculated occupational risk by an arbitrary weighting factor (e.g., 0.1 or 0.01).

The most straightforward solution to this dilemma is to assume that salaries fully compensate for occupational risk. This assumption would eliminate the need for considering the occupational risk since risk plus cost equals benefits (presumably) and an equality will not alter the overall risk-cost/benefit balance of P-T. The alternative of using an arbitrary weighting factor will be very difficult to justify unless the effect of the weighted occupational dose is made negligible by the weighting factor; in such an instance it would have been neglected initially.

14.2.3 Coprocessing fuel cycles with and without partitioning

The comparative analysis of the R,B,&C of P-T requires that two complete nuclear fuel cycles be examined: one with provisions for P-T, and a reference fuel cycle with no P-T. Both fuel cycles must be

identical in all respects, except those affected by the presence or absence of P-T operations, if a valid comparison is to be made. Furthermore, if P-T is to be justified, all the plutonium produced by the transmutation reactor must be recycled instead of being stockpiled. Finally, DOE guidelines obligate us to consider a coprocessing flowsheet for LWRs only. As a result of these considerations, the reference flowsheet selected uses a PWR fueled partially with self-generated-plutonium-enriched fuel and partially with uranium-enriched fuel. The uranium recovered during reprocessing will also be recycled. A schematic depiction of this fuel cycle with P-T operations included is given in Fig. 14.1. The transportation steps indicated are only those that might have to be considered in the R,B,&C analyses. Flow rates and compositions will eventually be developed for all of these streams for cases with and without P-T.

14.2.4 Determining the incentives for partitioning-transmutation

If it can be assumed that the changes in the R,B,&C of each operation affected by the implementation of P-T are known and quantified in compatible units (i.e., dollars), then determination of incentives for P-T is straightforward. The R,B,&C are summed over the time span where they are significant by using an appropriate discount rate. The controversy over the use of a discount rate in this application will probably require that both zero and nonzero discount rates be considered. The nonzero discount rate should reflect the "real" cost of money; it should be adjusted downward for inflation.

One matter that is not so straightforward is the upper time limit on the sum of the individual R,B,&C. If a nonzero discount rate is used, this limit could probably be assumed to be any value greater than 1000 or 10,000 years because the discount rate reduces the importance of the distant future events to nearly zero. However, in the zero discount rate case, a larger upper time limit will likely imply greater incentives for partitioning. Thus, it would be desirable to know how to select this limit so as to fairly account for the long-term benefits of P-T without unduly biasing the conclusions in a pro-P-T direction

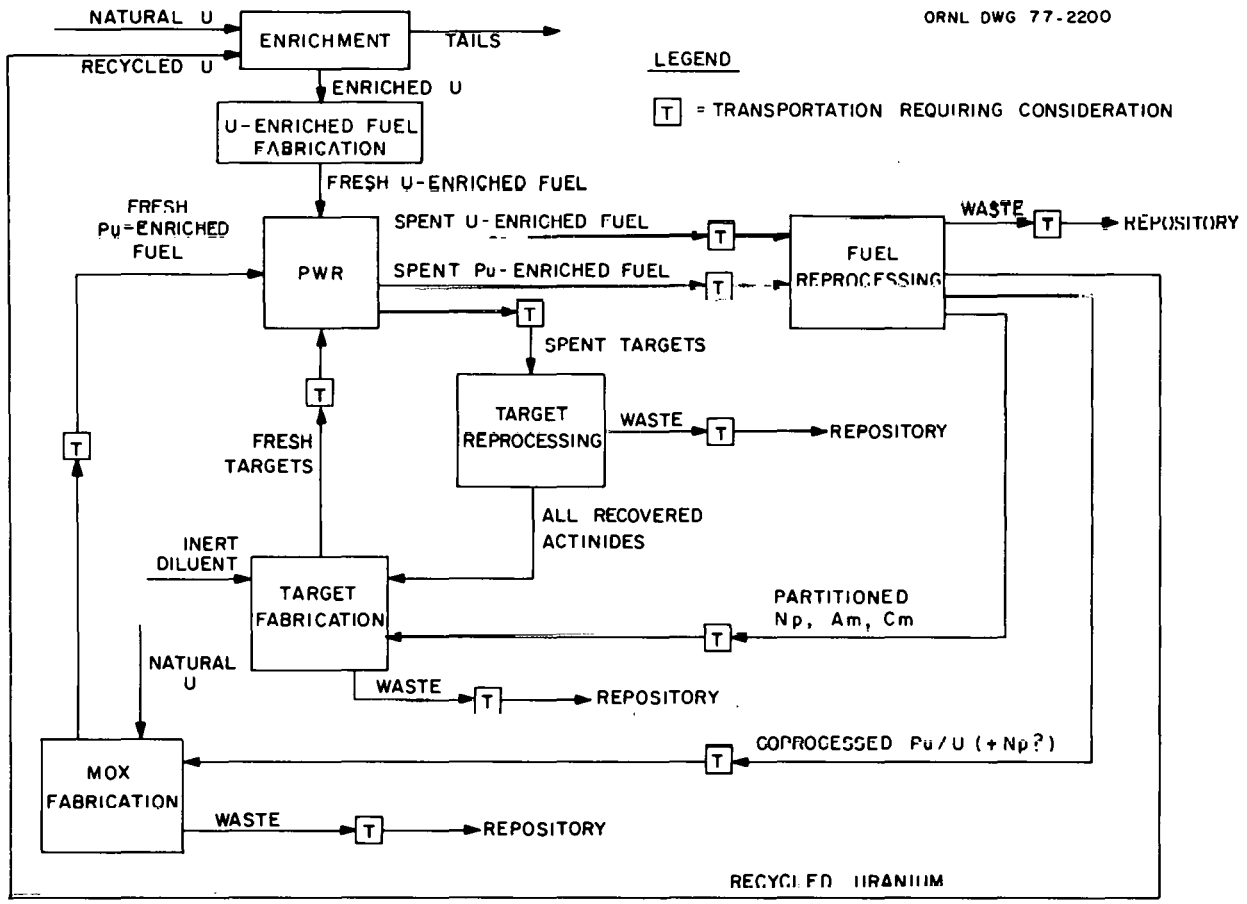

Fig. 14.1. Schematic of fuel cycle with actinide partitioning and transmutation.

with the use of a large time limit. Any solution to this problem is arbitrary, but an upper time limit of one million years does not appear to be unreasonable.

14.2.5 Summary of Proposed P-T, R,B,&C, and Incentives Analysis

Based on the previous discussion in this section, plus a considerable amount of intuition, each of the individual R,B,&C tasks has been assigned a priority of 1 through 4. These assignments are listed in Table 14.1, and the definitions of the priorities are in Table 14.2. As a general rule, the routine and accidental public risk effects and the cost effects of P-T have been given a high priority, while the occupational risk tasks have been given a low priority, principally based on the discussion in Sect. 14.2.2. Considering the importance of the tasks and that limited time and money are available, it appears reasonable to consider only those tasks with priorities of 1 or 2.

One of the most controversial aspects of striking the risk-cost/benefit balance discussed in Sect. 14.2 promises to be that of putting all of these factors on a common basis after they have been calculated. This involves consideration of (1) the conversion of dose or health effects to dollars, (2) the specification of a discount rate, and (3) the selection of a time limit for considering the in-repository benefits of P-T. Studies in these areas do not appear to be under way, although they will be required before a risk-cost/benefit analysis can be performed for any waste management system.

14.3 Reference for Section 14

1. D. R. Smith, R. E. Luna, J. M. Taylor, and A. R. DuCharme, Risk Assessment for the Transportation of Radioactive Materials in the U.S.A., SAND-76-5373 (1976).

Table 14.1. Individual R,B,&C task priorities

Fuel cycle operation	Task priority					
	Routine risk		Accidental risk			
	Public	Occupational	Public	Occupational	Cost	Comments
MOX[a] fuel fabrication	1	3	2	4	1	
WAT[b] fabrication	1	3	2	3	1	
MOX fuel transportation	3	4	3	4	2	
WAT transportation	1	3	3	3	2	
MOX waste transportation	1	3	2	3	2	
WAT waste transportation	1	3	3	3	1	^{129}I may be important
Transmutation reactor	3	3	3	3	1	
MOX reprocessing	1	3	2	4	1	
WAT reprocessing	1	3	2	3	1	
Waste management	4	3	1	3	1	

[a]MOX: plutonium-enriched natural uranium fuel.

[b]WAT: waste actinide (neptunium + americium + curium + progeny) assembly.

Table 14.2. Priority definitions for Table 14.1

Priority	Definition
1	(a) vital for incentives analysis, or (b) large change resulting from P-T
2	(a) large relative change because of P-T but small absolute effect, and/or (b) difficult to calculate
3	(a) small relative change because of P-T, or (b) not important in incentives analysis, but (c) of interest for completeness
4	(a) virtually no change because of P-T, or (b) very small absolute effect

15. DETAILED ECONOMIC ANALYSIS OF FABRICATION AND REPROCESSING PLANTS IN A PARTITIONING-TRANSMUTATION FUEL CYCLE

(Oak Ridge National Laboratory)

This task will provide detailed cost estimates of fuel reprocessing and refabrication plants operating with and without partitioning and transmutation. The analysis will show the economic impacts of this option on the fuel cycle.

This task is inactive during FY 1977.

16. PARTITIONING-TRANSMUTATION ANALYSIS, COORDINATION, AND EVALUATION

D. W. Tedder, A. G. Croff, and J. O. Blomeke
(Oak Ridge National Laboratory)

This task coordinates all other efforts related to the program. Integrated flowsheets are developed from the experimental evaluation of subsystems within the fuel and target reprocessing and refabrication plants. Alternative flowsheets are evaluated; options are chosen for detailed analysis. Constraints are defined which facilitate the integration of the concept to all aspects of the fuel cycle.

16.1 Solvent Extraction Analysis

16.1.1 Introduction

The numerical modeling of solvent extraction processes has been of general interest to the nuclear industry since the development of Purex. An accurate and reliable computer model is of significant value since it enables investigators to examine a wide range of process operating conditions and establish the sensitivity to various perturbations. By analogy, the simulation of unit operations in the hydrocarbon processing industry is a highly developed and widely used tool. On the other hand, the state of the art in modeling nuclear reprocessing operations is less highly developed for several reasons. First of all, the nuclear industry is not as extensive or mature as the hydrocarbon processing industry. Second, much of the pertinent information has either been lacking experimentally or classified and thereby unavailable for general use. Third, the systems to be modeled are much more nonlinear and nonideal than those simulated in hydrocarbon processing.

Nonetheless, there are at least two computer codes now in existence which attempt to model Purex-type solvent extraction. Although these codes, designated as SOLVEX[1] and SEPHIS,[2] incorporate significant advances in the art, they probably do not represent the ultimate model. SOLVEX, for example, can consider up to five components or more and has flexibility as far as introducing distribution correlations; however, it does not explicitly consider the competition of the various species for the

extractant or the other reagents such as aqueous nitrate. While SEPHIS considers the competition of the extractable species for the extractant and nitrate, it is limited to the examination of only three extractable components. It can be modified, but only with great difficulty.

Consequently, an effort is currently under way to develop a more versatile code (GENEX), which includes the desirable features of SOLVEX and SEPHIS but is also more generalized. GENEX has the capability of examining solvent extraction systems in which there is no competition for various reagents or of considering systems where much competition occurs. The assumed stoichiometries of the various competing reactions are defined as part of the input to the code; and different reactions can be examined without modifying the main code itself, although the distribution correlation subroutines must be changed according to the assumed stoichiometry. In addition, GENEX may consider any number of components and, although the current version models only steady-state, isothermal systems without consideration of redox reactions or kinetic effects, these effects could also be included at a later date.

GENEX is being developed as a generalized solvent extraction code which could be used to study the TBP system, the bidentate system, and possibly other solvent extraction systems that involve chemical reactions. The code works by solving a set of nonlinear, coupled matrix equations by trial and error. The equations are linearized by expansion into a Taylor's series, and the linearized equations are solved iteratively using the Newton-Raphson method to generate vectors of incremental changes in the variables until the residual sum of the squared errors in solving the original nonlinear equations is less than some specified tolerance.

16.1.2 Description of GENEX

In general, a countercurrent solvent extraction column may consist of M equilibrium stages and involve N aqueous chemical species which are in equilibrium with NR organic complexes. Figure 16.1 shows the possible inputs and outputs to the jth stage in such a sequence. Each stage in the countercurrent process may have an organic feed, an aqueous feed, or aqueous and organic side draws. Since the inventories are not defined

ORNL DWG 78-241

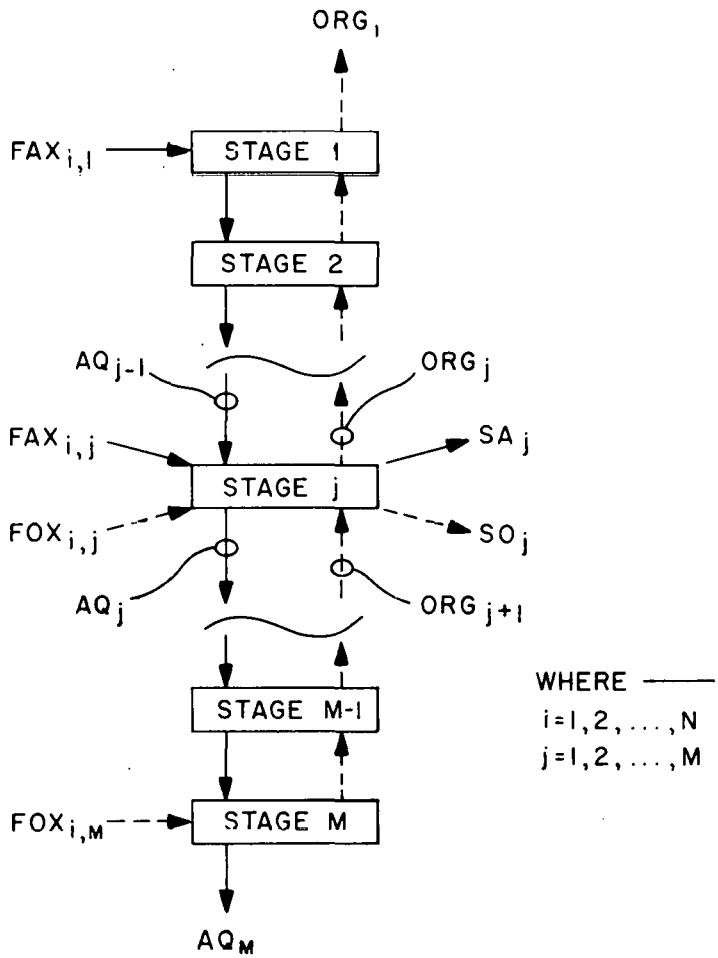

LEGEND

AQ_j = aqueous volumetric flow rate from the jth stage,
ORG_j = organic volumetric flow rate from the jth stage,
SA_j = aqueous volumetric side-draw rate from the jth stage,
SO_j = organic volumetric side-draw rate from the jth stage,
$FAX_{i,j}$ = aqueous molar feed rate of the ith species to the jth stage,
$FOX_{i,j}$ = organic molar feed rate of the ith species to the jth stage.

Fig. 16.1. General equilibrium stage model.

in a steady-state model, the system may be represented as shown in Fig. 16.1 without regard to details such as mixer-settler configurations or holdups.

In simple solvent extraction systems, the species distribute themselves between the two phases by physical attraction without chemical reaction. In this case, modeling is simplified since the material balance equations for any one chemical species do not involve the others. However, in the systems of interest, the chemical species interact to form extractable complexes. In this latter case, each organic-phase complex is comprised of some linear combination of the aqueous chemical species so that:

$$\sum_{k=1}^{N} Z_{i,k}\, MA_k \rightleftharpoons MO_i \,, \qquad i = 1, 2, \ldots, NR \tag{16.1}$$

where MA_k and MO_i designate molecules of an aqueous species and the organic complex, respectively, and $Z_{i,k}$ designates the stoichiometric relationship of the ith chemical equilibrium involving the kth aqueous species.

By this definition, the $\underline{\underline{Z}}$ matrix can be used to define systems where only physical distribution between the phases occurs or where extraction proceeds via chemical reaction. In the former case, only the diagonal elements of $\underline{Z}$ are nonzero, whereas in the latter case some of the off-diagonal elements of $\underline{\underline{Z}}$ are also nonzero, depending on the system under consideration. Table 16.1, for example, defines ten chemical species which have been modeled and are numbered as shown. Table 16.2 shows the $\underline{\underline{Z}}$ matrix corresponding to this system. All of the diagonal elements in $\underline{\underline{Z}}$ are nonzero, indicating that all of the extracted species participate in the chemical equilibrium leading to the formation of the corresponding organic complex. However, column 1 also contains nonzero, off-diagonal elements, indicating that TBP also participates in the extraction equilibria.

Although this version of the $\underline{\underline{Z}}$ matrix is square (N x N), this condition is not generally required; and $\underline{\underline{Z}}$ may take on dimensions (NR x N) to consider multiple equilibria for a single extractable species, where NR would equal the number of equilibrium reactions. For example, one may wish to consider two extractable forms of nitric acid.[3,4] In general, therefore, NR $\geq$ N since each aqueous species must participate in at least one type of phase equilibrium relationship.

Table 16.1. Chemical species modeled in example, along with their density parameters

i	Component label	β_i^a (g/g-mole)	β_i^o (g/g-mole)
1	Tributylphosphate	274.6	207.5
2	Nitric acid	31.2	301.30
3	Water	18.0	240.6
4	n-dodecane	170.6	170.0
5	$UO_2(NO_3)_2$	76.3	608.6
6	$Pu(NO_3)_4$	266.0	776.0
7	$NpO_2(NO_3)_2$	173.0	683.6
8	$Zr(NO_3)_4$	189.0	973.0
9	$Ru(NO_3)_4$	199.0	983.0
10	$(RE + TVA)(NO_3)_3$[a]	183.3	967.0

ρ_a = 1000 g/liter ρ_o = 748 g/liter

[a]This term denotes the total concentration of rare earths and trivalent actinides, which are modeled as a single species in this case.

Table 16.2. $\underline{\underline{Z}}$ matrix used in the ten-component example[a]

Extraction equilibrium i \ k	Species participation[b] 1	2	3	4	5	6	7	8	9	10
1	1									
2	1	1								
3	1		1							
4				1						
5	2				1					
6	2					1				
7	2						1			
8	3							1		
9	3								1	
10	3									1

[a]Blank spaces denote zeros.

[b]The species participating in the ith extraction equilibrium can be found by examining the table row-wise.

In principle, one can define NR linearly independent phase equilibria, each with a corresponding thermodynamic equilibrium constant, K, such that:

$$K_{i,j} = \frac{A^*_{i,j}}{\prod_{k=1}^{N} A_{k,j}^{Z_{i,k}}} \quad , \qquad (16.2)$$

$$i = 1, 2, \ldots\ldots, NR$$

$$j = 1, 2, \ldots\ldots, M$$

where $A^*_{i,j}$ and $A_{i,j}$ designate the activity of the ith chemical species on the jth stage in the organic and aqueous phases respectively. In practice, it is more convenient to define NR equilibrium correlations, $EQ_{i,j}$, involving the activity coefficients which can be used to calculate the organic molarities of the complexed species, $Y_{i,j}$, so that:

$$Y_{i,j} = EQ_{i,j} \prod_{k=1}^{N} X_{k,j}^{Z_{i,k}} \quad , \qquad (16.3)$$

where, in general,

$$i = 1, 2, \ldots\ldots, NR$$

$$j = 1, 2, \ldots\ldots, M$$

$$EQ_{i,j} = f(\underline{X}_j, \underline{Y}_j) \; . \qquad (16.4)$$

In these terms, $Y_{i,j}$ and $X_{i,j}$ designate the organic- and aqueous-phase molarities, respectively, of the ith species on the jth stage. Thus, there are N linearly independent material balance equations involving N aqueous, primary species and NR organic complex species, where NR $\geq$ N.

On the other hand, GENEX can be used to calculate the concentrations of aqueous species which do not extract per se, but coordinate with various cations. For example, the total aqueous nitrate concentration may be involved in the extraction equilibria for various extractable cations and yet not extract by itself without a cation. This effect can be modeled simply by setting the $EQ_{i,j}$ parameter equal to zero for the inextractable coordinating anion. The diagonal element in $\underline{\underline{Z}}$, as well as those off-diagonal elements involving the coordinating anion, would remain nonzero. The code would then calculate the desired total aqueous nitrate concentration profile and also consider the nitrate concentrations in the organic-phase complex.

The steady-state material balance equations are defined in terms of the stage inputs and outputs. Stages 2 through M-1 also involve the j-1 and the j+1 stages in their material balances. Hence the error associated with equations 1 through N is defined as follows using the nomenclature in Fig. 16.1:

$$e_{i,j} = \sum \text{Mass inputs to } j - \sum \text{Mass outputs from } j$$

$$= FAX_{i,j} + \sum_{k=1}^{NR} Z_{k,i}\ FOX_{k,j} + AQ_{j-1}\ X_{i,j-1}$$

$$+ ORG_{j+1} \sum_{k=1}^{NR} Z_{k,i}\ Y_{k,j+1} - (AQ_j + SA_j)\ X_{i,j}$$

$$- (ORG_j + SO_j) \sum_{k=1}^{NR} Z_{k,i}\ Y_{k,j} \quad , \qquad (16.4)$$

$$i = 1, 2, \ldots\ldots, N$$

$$j = 1, 2, \ldots\ldots, M$$

where $e_{i,j}$ is the residual error associated with solving the ith material balance on the jth stage.

The error associated with the aqueous-phase density balance is defined by:

$$e_{N+1,j} = \rho_a - \sum_{k=1}^{N} \beta_k^a\ X_{k,j} \quad , \qquad (16.5)$$

where

β_k^a = empirical density coefficient minus the molecular weight of the species in the aqueous phase (see Table 16.1),

ρ_a = density of pure water (a constant, see Table 16.1).

Similarly, the error associated with the organic-phase density balance is given by:

$$e_{N+2,j} = \rho_o - \sum_{k=1}^{NR} \beta_k^o\ Y_{k,j} \quad , \qquad (16.6)$$

where

β_k^o = empirical density coefficient minus the molecular weight of the organic-phase complex (see Table 16.1),

ρ_o = density of the organic-phase diluent (a constant, see Table 16.1).

Hence there are N+2 equations which must be solved for each stage to calculate incremental changes in the N aqueous-phase compositions and the volumetric rates of organic and aqueous material leaving that stage. Therefore, the model treats the two volumetric flow rates and the N aqueous-phase concentrations as linearization variables[5,6] which are adjusted to minimize the errors in the equations. The residual sum of the squared errors for the system, then, is defined as:

$$SS = \sum_{j=1}^{M} \underline{e}_j^T \underline{e}_j \quad , \tag{16.7}$$

where $\underline{e}_j^T$ is the transpose of the error vector, $\underline{e}_j$, associated with the jth stage which has N+2 dimensions.

The nonlinear equations are solved by linearization using the Newton-Raphson method of gradient search. With this method it is necessary to calculate the error vector, $\underline{e}_j$, for each stage as well as the Jacobian matrices $\underline{\underline{A}}_{j-1}$, $\underline{\underline{B}}_j$, and $\underline{\underline{D}}_{j+1}$, which correspond to the increment vectors $\underline{\delta}_{j-1}$, $\underline{\delta}_j$, and $\underline{\delta}_{j+1}$ for the stages j-1, j, and j+1 respectively. Of course, $\underline{\underline{A}}_{j-1}$ is identically zero for the first stage and $\underline{\underline{D}}_{j+1}$ is identically zero for stage M. Solving the normal equation for the vector $\underline{\delta}_j$, then, yields the expression

$$\underline{\underline{B}}_j^T \underline{\underline{A}}_{j-1} \underline{\delta}_{j-1} + \underline{\underline{B}}_j^T \underline{\underline{B}}_j \underline{\delta}_j + \underline{\underline{B}}_j^T \underline{\underline{D}}_{j+1} \underline{\delta}_{j+1} = - \underline{\underline{B}}_j^T \underline{e}_j \quad , \tag{16.8}$$

$$j = 1, 2, \ldots\ldots, M \quad ,$$

which can be solved by the subroutines[5,7] BAND(J) and MATINV to yield new values for the increment vector $\underline{\delta}_j$. As convergence is achieved, $\underline{\delta}_j$ goes to zero as does the sum of the squared errors defined by Eq. (16.7).

16.1.3 Sample results and discussion

Figure 16.2 summarizes the input feed data and resulting output streams calculated for one extraction column modeled by GENEX. In this example, ten components were introduced into the top and third stages of a five-stage extraction column as the aqueous feeds 1AF and 1AR. The extractant, stream 1AX, was introduced at the bottom stage. The streams

ORNL DWG 78-240

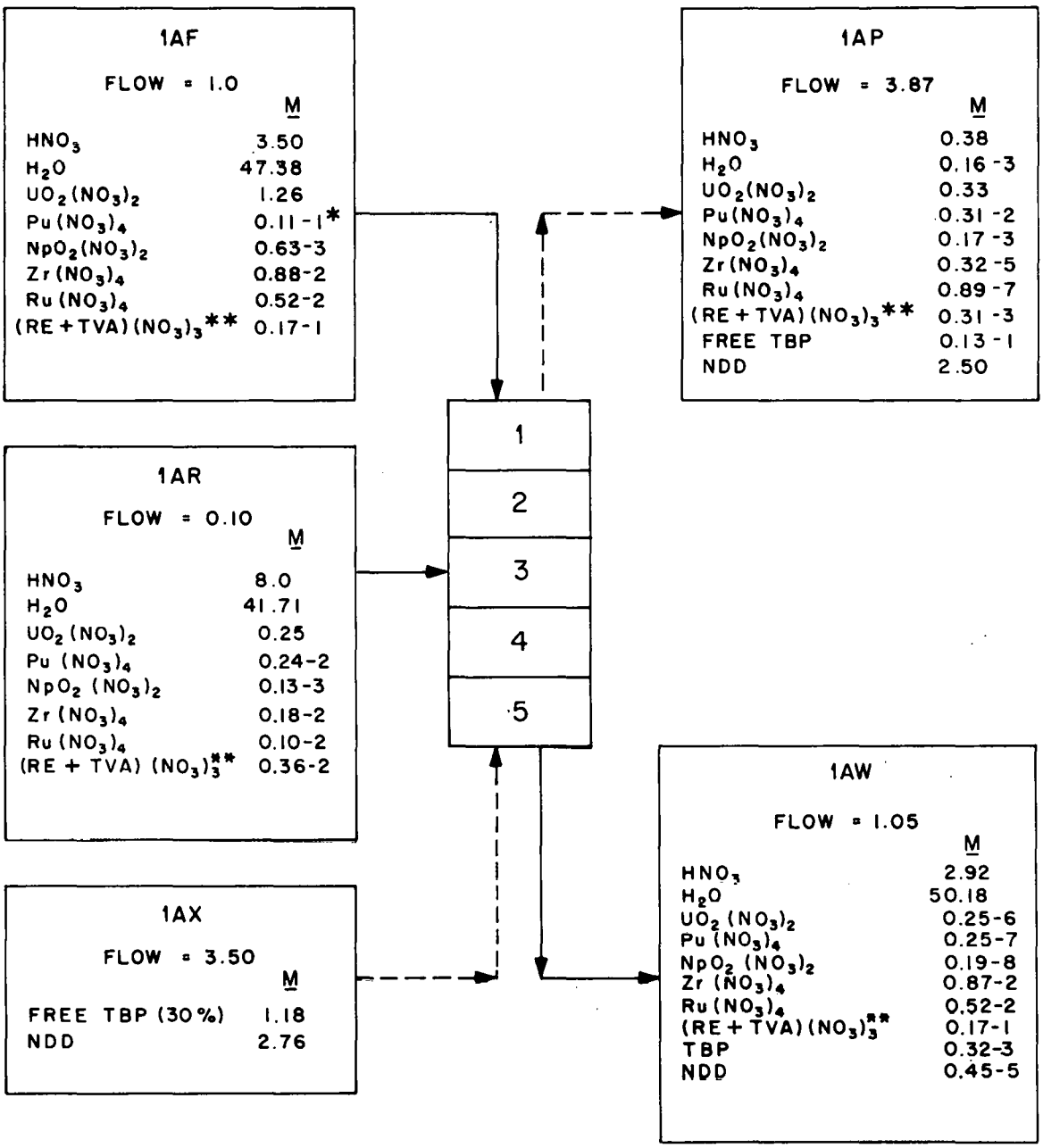

*Read as 0.11×10^{-1}.

**$(RE+TVA)(NO_3)_3$ is the total concentration of rare earths and trivalent actinides combined.

Fig. 16.2. Overall material balances produced by GENEX.

1AP and 1AW, as well as the internal column volumetric flow rates and concentrations, were then calculated by GENEX. In this example, the modified Richardson correlations[8] were used for the distribution functions of uranium, plutonium, and nitric acid. The neptunium was modeled by assuming that it exists only in the hexavalent state with a distribution coefficient equal to 0.47 times that value for U^{6+} as suggested by a recent study.[9] Additional printout, the phase volumetric flow rates, densities, and the stagewise extractant summary are reproduced in Table 16.3. Figure 16.3 shows selected distribution coefficients which were calculated using these correlations.

In addition to this information, GENEX also prints out the composition profiles for both phases, the molar extraction and raffinate product rates, and the overall mole balance errors for each component.

In summary, GENEX appears to be of potentially great value because of its generality and flexibility. It can consider more chemical species than other existing codes and can model them more accurately by including chemical competition for the extractant or other species as well.

Table 16.3. Summary of organic- and aqueous-phase profiles

	Organic		Aqueous		Extractant summary	
Stage	Rate (liters/time)	Density (g/ml)	Rate (liters/time)	Density (g/ml)	Mole % free extractant	% complexed
1	0.1232D 05	0.866	0.3341D 04	1.232	0.407	98.764
2	0.1226D 05	0.794	0.3331D 04	1.188	0.845	97.214
3	0.1225D 05	0.781	0.3649D 04	1.193	0.814	97.280
4	0.1222D 05	0.780	0.3569D 04	1.172	1.255	95.796
5	0.1189D 05	0.787	0.3281D 04	1.098	6.823	77.150

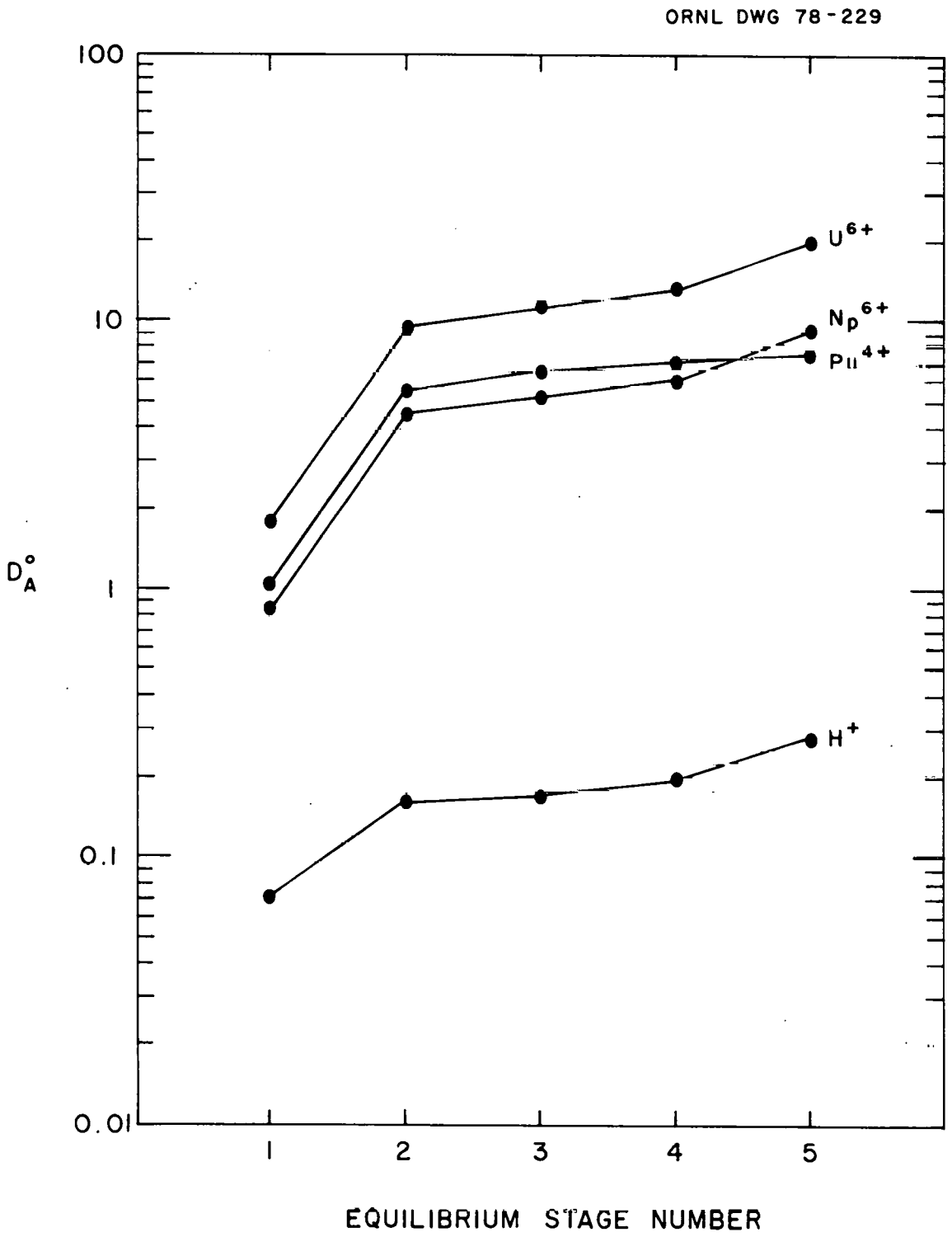

Fig. 16.3. Calculated distribution coefficients for selected species.

16.2 References for Section 16

1. W. C. Scotten, SOLVEX - A Computer Program for Simulation of Solvent Extraction Processes, DP-1391 (September 1975).
2. W. S. Groenier, Calculation of the Transient Behavior of a Dilute-Purex Solvent Extraction Process Having Application to the Reprocessing of LMFBR Fuels, ORNL-4746 (April 1972).
3. W. Davis, Jr., J. Mrochek, and R. R. Judkins, "Thermodynamics of the Two-Phase System: Water-Uranyl Nitrate-Tributyl Phosphate-Amsco 125-82," J. Inorg. Nucl. Chem. 32, 1689 (1970).
4. G. L. Richardson, The Effect of High Solvent Radiation Exposures on TBP Processing of Spent LMFBR Fuels, HEDL-TME 73-51 (June 1973).
5. J. S. Newman, Electrochemical Systems, p. 414, Prentice-Hall, Englewood Cliffs, N.J., 1973.
6. D. M. Himmelblau, Applied Nonlinear Programming, McGraw-Hill, New York, 1972.
7. John Newman, Numerical Solution of Coupled, Ordinary Differential Equations, UCRL-17739 (August 1967).
8. S. B. Watson and R. H. Rainey, Modifications of the SEPHIS Computer Code for Calculating the Purex Solvent Extraction System, ORNL-TM-5123 (December 1975).
9. D. Gourisse, "Laboratory Studies in Nitrous Acid and Neptunium Behavior in TBP Extraction Processes," Proceedings of the International Solvent Extraction Conference, The Hague, Netherlands, pp. 781-91, CONF-710417 (April 19, 1971).

THIS PAGE

WAS INTENTIONALLY

LEFT BLANK

ORNL/TM-6174

INTERNAL DISTRIBUTION

1-2. Central Research Library
3. Document Reference Section
4-6. Laboratory Records
7. Laboratory Records, R.C.
8. ORNL Patent Section
9. C. W. Alexander
10. R. E. Blanco
11-30. J. O. Blomeke
31. W. D. Bond
32. W. D. Burch
33. D. O. Campbell
34. A. G. Croff
35. D. E. Ferguson
36. B. C. Finney
37. L. M. Ferris
38. C. W. Forsberg
39. R. W. Glass
40. H. W. Godbee
41. G. H. Jenks
42. F. A. Kappelmann
43. S. Katz
44. O. L. Keller
45. R. E. Leuze
46. K. H. Lin
47. A. P. Malinauskas
48. W. C. McClain
49. J. G. Moore
50. E. Newman
51. J. P. Nichols
52. E. L. Nicholson
53. K. J. Notz
54. H. Postma
55. F. M. Scheitlin
56. C. D. Scott
57. R. R. Shoun
58. D. W. Tedder
59. L. M. Toth
60. D. B. Trauger
61. B. L. Vondra
62. B. Weaver
63. M. L. Williams
64. R. G. Wymer
65. G. R. Choppin (consultant)
66. E. L. Gaden, Jr. (consultant)
67. C. H. Ice (consultant)
68. L. E. Swabb, Jr. (consultant)
69. K. D. Timmerhaus (consultant)

EXTERNAL DISTRIBUTION

70-96. Technical Information Center, Oak Ridge, TN 37830

DOE-ORO, Oak Ridge, TN 37830
97. Research and Technical Support Division
98. J. J. Schreiber

DOE, Washington, DC 20545
99. J. L. Burnett
100. J. A. Leary
101. R. D. Walton

U. S. Nuclear Regulatory Commission, Washington, DC 20555
102. W. P. Bishop
103. R. Cooperstein

Allied Chemical Corp., P. O. Box 2204, Idaho Falls, ID 83401
104. L. D. McIsaac
105. C. M. Slansky

Atlantic Richfield Hanford Company, P. O. Box 250, Richland, WA 99352
106. H. Babad
107. W. W. Schulz

Battelle Northwest, P. O. Box 999, Richland, WA 99352
108. A. M. Platt
109. K. J. Schneider
110. E. J. Wheelwright

Argonne National Laboratory, 9700 South Cass Ave., Argonne, IL 62439
111. E. P. Horwitz
112. G. W. Mason
113. M. Steindler

Hanford Engineering Development Laboratory, P. O. Box 1970, Richland, WA 99352
114. R. Lerch

Sandia Laboratories, P. O. Box 5800, Albuquerque, NM 87115
115. R. L. Schwoebel
116. D. R. Tallent

George C. Marshall Space Flight Center, Marshall Space Flight Center, AL 35812
117. R. E. Burns

Mound Laboratory, P. O. Box 32, Miamisburg, OH 45342
118. E. L. Lewis
119. D. F. Luthy

Rockwell International, Rocky Flats Plant, P. O. Box 464, Golden, CO 80401
120. J. D. Navratil
121. G. H. Thompson

E. I. du Pont de Nemours and Company, Savannah River Laboratory, Aiken, SC 29801
122. T. C. Gorrell

Brookhaven National Laboratory, Upton, NY 11973
123. T. E. Gangwer

Los Alamos Scientific Laboratory, P. O. Box 1663, Los Alamos, NM 37544
124. W. J. Maraman

General Electric, Mail Code S-34, P. O. Box 5020, Sunnyvale, CA 94086
125. S. L. Beaman

Atomic Energy Research Establishment, Harwell, Didcot, Oxon., OX11 ORA, England
126. N. J. Keen
127. G. N. Kelly

Centre d'études nucléaires de Fontenay-aux-Roses, B.P. No. 6, Fontenay-aux-Roses, France
128. Y. Sousselier

OECD-Nuclear Energy Agency, 38, Boulevard Suchet, F-75016 Paris, France
129. M. Takahashi

International Atomic Energy Agency, P. O. Box 590, A-1011 Vienna, Austria
130. J. R. Grover

Institut für Heisse Chemie Kernforschungszentrum, Postfach 3640, 75 Karlsruhe, Germany
131. H. O. Haug

Lab. Teoria e Calcolo Reottori, C.N.E.N. - C.S.N. Casaccia, CP 2400 I-00100 Rome, Italy
132. L. Tondinelli

Commission of the European Communities, CCR Euratom, I-21200 Ispra, Italy
133. F. Girardi

Nuclear Research Institute, 25066 Rez, Czechoslovakia
134. L. Neumann

Chalmers University of Technology, Dept. of Nuclear Chemistry S-402 20 Göteborg, Sweden
135. J. O. Liljenzin

Arms Control and Disarmament Agency, Room 4951, U.S. Dept. of State, Washington, DC 20451
136. M. Moss

Battelle Columbus Laboratories, 505 King Avenue, Columbus, OH 43201
137. M. Pobereskin

☆ U.S. GOVERNMENT PRINTING OFFICE: 1979-748-189/388